Synthesis of Zr^{4+}/Ag^{+} metal oxides modified zeolite for application in fluoride and pathogens removal from water

By

Nemakanga Selby

Student number: 15008198

Submitted in fulfilment of the requirements for the degree of Masters in Environmental Sciences in the Faculty of Science, Engineering and Agriculture, Department of Geography and Environmental Sciences, at the University of Venda

Supervisors: Dr.Mudzielwana R.

Co-Supervisor: Dr.Ayinde W.B.

February 2024

Declaration

I, Nemakanga Selby, hereby declare that the dissertation for the Master of Environmental Sciences degree at the University of Venda titled "*Synthesis of Zr^{4+}/Ag^{+} metal oxides modified zeolite for application in fluoride and pathogens removal from drinking water*", hereby submitted by me, has not previously been submitted for a degree at this or any other university and that it is my work in design and execution and that all reference material contained therein has been dully acknowledged.

Full names : Nemakanga Selby

Signature : 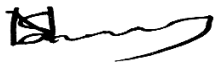 Date: 22/02/2024

Acknowledgments

I would like to express my gratitude to the NRF-Sasol sponsorship for their funding for my studies.

I would also like to thank the Water Research Commission (WRC) team for their support and effort in this project.

Also, my sincere gratitude goes to my supervisors DR Mudzielwana R and Dr Ayinde W.B for their dedication and guides in this work.

Lastly, my appreciation goes to the entire EnviReN group for their comments and assistance in my work.

Above all, I thank the Almighty God for the good spirit, strength, support, guidance and his blessings in my life.

Dedication

This endeavor is dedicated to my mother, Ms. Mbedzi Tshililo, two sisters Orifha and Netshedzo Nemakanga and my nephews Atshilaho and Rianze. May the Son of God, my Lord be with them always.

Abstract

People living in developing nations are challenged by acute water scarcity, hence they often rely on groundwater as their primary drinking water sources. Unfortunately, in most cases, groundwater is often contaminated with high levels of fluoride and pathogens, posing a significant health risk. This dissertation aims to synthesize Zr^{4+}/Ag^{+} metal oxides modified zeolite adsorbent for use in fluoride and pathogens removal from water.

The first section of this research aimed at optimizing the synthesis of zeolite from bentonite clay using the response surface methodology (RSM). The process involved alkali dissolution of calcined bentonite clay through ultrasonication, followed by hydrothermal treatment to obtain zeolite. The ultrasonication conditions were optimized by varying NaOH concentration (0.5 to 2.5 M) and aging time (10 to 120 minutes). Temperature (70 °C to 140 °C) and time (1.5 to 6 hours) were evaluated for hydrothermal treatment. The X-ray diffraction (XRD), scanning electron microscopy-energy dispersive spectroscopy (SEM-EDX) and Fourier transform infrared (FTIR) analysis were used to characterize the obtained materials, revealing that crystallinity of the obtained synthesized materials increased at higher hydrothermal temperatures and times. Furthermore, the XRD analysis indicated there was the formation of zeolite NaP phases at lower temperatures and times, while higher temperatures and times led to hydroxy sodalite mineral phases. Preliminary defluoridation experiments were conducted on all hydrothermally treated samples, with the sample prepared at 2 hours sonication, 105°C hydrothermal treatment, and 1 hour 30 minutes exhibiting a capacity for adsorbing fluoride of 0.19 mg/g hence, this zeolite was used subsequent experiments.

The second chapter of results presented the evaluated effectiveness of the synthesized zeolite NaP on fluoride and pathogen removal. Batch experiments were conducted to assess zeolite NaP's effectiveness in removing fluoride from water under various operating conditions while the well-assay diffusion method was used to study the antimicrobial potency of the zeolite. The optimum conditions for achieving maximum fluoride adsorption were identified as a contact time of 60 minutes, an initial concentration of 6.2 mg/L using a synthetic fluoride solution, an initial pH of 2, and an adsorbent dosage of 0.5 g/100 mL. Under these conditions, the maximum adsorption capacity reached 0.16 mg/g. Additionally, it was determined that the fluoride adsorption process followed a chemisorption mechanism, as evidenced by the fitting of experimental data to a *pseudo*-second-order kinetic model. Moreover, the adsorption isotherm data fitted well with the Langmuir model. This indicates that fluoride adsorption occurred on a surface in a single layer, with a limit on the number of active sites at any given time. Antimicrobial assessments revealed that zeolite NaP lacked

potency against gram-negative *E. coli* and gram-positive *S. aureus* strains. In conclusion, zeolite NaP demonstrated minimal defluoridation efficiency and no antimicrobial efficacy. The chapter suggests enhancing fluoride adsorption, antimicrobial potency, and material reusability through the introduction of cations into the zeolite frameworks.

The third chapter of results focused on the modification of zeolite NaP by incorporating zirconium/silver metal oxides to enhance its efficacy in removing fluoride and pathogens from water. The Zr^{4+}/Ag^{+} modified zeolite NaP was prepared using 0.5 M and 0.3 M $ZrCl_4$ and $AgNO_3$ respectively. The mixture of 10 g of calcined bentonite, 2 M of NaOH, and Zr and Ag solutions was subjected to ultrasonication for 2 hours followed by hydrothermal treatment at 105 °C for 90 minutes. The obtained material was therefore characterized using XRD, XRF, FTIR, Particle Distribution Analysis, and SEM-EDS. Defluoridation and antimicrobial potency were evaluated through batch adsorption experiments and well-assay diffusion method, respectively. Under optimal conditions, including a pH of 6 ± 0.5, a contact time of 270 minutes, an initial fluoride concentration of 6.2 mg/L, and an adsorbent dosage of 0.5 g/100 mL at an agitation speed of 250 rpm, the modified zeolite demonstrated a peak fluoride removal percentage of approximately 50%. The data fitted better to the *pseudo*-second-order kinetic model suggesting the dominance of chemisorption as the fluoride removal mechanism while adsorption isotherm data followed the Langmuir isotherm model suggesting that adsorption occurred on a monolayered surface for the Zr^{4+}/Ag^{+} modified zeolite. Antimicrobial studies revealed a 15 mm and 12 mm zone of inhibition against the gram-negative *E. coli* and gram-positive *S. aureus* strains, respectively.

In conclusion, the synthesized zeolite functionalized with zirconium and silver metal oxides exhibited improved fluoride removal efficiency and antimicrobial potency. Further research is recommended to improve the properties of synthesized zeolite for better removal of fluoride and pathogens from water.

KEYWORDS: Groundwater, Fluoride, Pathogens, Water treatment, adsorption, zeolite

Table of contents

List of Figures

List of tables

Chapter 1: Introduction

1.1 Background

In arid and semi-arid regions, communities depend mainly on groundwater for agriculture, domestic, and drinking purposes. Vargas-Solano et al. (2022) reported that drinking water sources, including groundwater contain excessive levels of contaminants, such as fluoride and pathogens. This is the case also in arid and semi-arid regions, fluoride and pathogens concentrations have been reported in groundwater at levels exceeding the permissible levels recommended by the World Health Organization of 1.5 mg/L and 0 colony-forming units per 100 milliliters (cfu/100 mL), respectively (WHO, 2019, Ed Butts, 2020, Potgieter et al., 2020, Khabo-Mmekoa et al., 2022). These high levels of fluoride and pathogens have been documented mainly in arid and semi-arid regions of Asia and African continents. Pathogens and fluoride contamination in groundwater sources is a worldwide phenomenon with countries such as China, Brazil, USA, Sweden, Norway, Korea, Thailand, Pakistan, Ghana, Nigeria, and South Africa reporting fluoride and pathogen levels of up to 10 mg/L and 100 cfu/100 mL, respectively (Onipe et al., 2020, Dong et al., 2023, Kumar et al., 2023).

In South Africa, elevated fluoride concentrations of up to 41.0 mg/L in Moretele Municipality of the North-West Province while in Siloam and Lephalale of Limpopo Province, fluoride concentration as high as 5.3 mg/L have been reported (Ntshephe, 2012, Odiyo and Makungo, 2012, Onipe et al., 2020). Moreover, pathogen concentrations in groundwaters of 1.87 cfu/100 mL in Vhuronga 1 Village of the Limpopo province and 579.4 cfu/100 mL in Magogoe village in the North-West province while 40.4 cfu/100 mL has been reported in Stinkwater community at the Gauteng province (Palamuleni and Akoth, 2015, Abia et al., 2017, Odiyo et al., 2020).

Exposure to fluoride concentrations surpassing 1.5 mg/L is associated with the onset of conditions such as skeletal and dental fluorosis (Habiyakare et al., 2021). Likewise, the presence of pathogenic contaminants at levels surpassing 0 cfu/100 mL has been linked to the potential occurrence of diseases such as fever, typhoid, cholera, diarrhea, and shigellosis (Ed Butts, 2020, Potgieter et al., 2020). Moreover, 200 million people suffer from endemic fluorosis whilst around 2 billion people drink water that is contaminated by feaces and 485 000 deaths occur each year due to pathogenic contaminated water (Yetis et al., 2021, WHO, 2022). Studies have indicated that both fluoride and pathogens can occur simultaneously in a single drinking water source, and this unfortunately can influence the occurrence of both fluorosis and pathogenic infections in the same region (Edokpayi et al., 2018, Madilonga et al., 2021). The United Nations Educational, Scientific and Cultural

Organization (UNESCO) has forecasted that, by the year 2025, approximately 1.8 billion individuals will reside in regions experiencing water scarcity (Sumalatha, 2021). The underlying cause could be climate change, which is causing a drop in rainfall in some regions, the rise in the global population, poor water management strategies, and contamination of water sources.

Fortunately, there are several water treatment strategies for improving water resources. This includes the membrane filtration which uses a porous layer in which certain fluids pass through depending on their size, ion exchange method which uses resins such as bone char and natural zeolites with ions exchange properties that bind with their respective unlike-charge ions in water, chemical precipitation which uses chemical reagents such as alum, lime or limestone which react with metal ions to form insoluble precipitants and the adsorption method which uses materials such as clay, charcoal, zeolite and activated carbon that permits water to pass through while immobilizing contaminants (Khairnar et al., 2015, Chakraborty et al., 2020).

However, limitations in their applicability poses doubts about their employability at households. For instance, the membrane filtration method is extensive, shows poor membrane strength, and easy clogging of the membrane, the chemical precipitation requires a flocculation process which uses a complicated mechanism, produces a slurry that is expensive to dispose and not eco-friendly, harsh conditions and low contaminants removal efficiency and the ion exchange method cannot be applied in large-scale treatment and synthetic resins are expensive as compared with the adsorption method (Feng et al., 2022). The adsorption method on the other hand has a high removal efficiency between 90-99%, uses natural resources that are acquired at low-cost materials, utilizes simple structures, consumes minimal energy, is environmentally friendly, and can be employed on a large scale, rendering it a practical method for water treatment even in remote areas (Chakraborty et al., 2020). This method uses less costly materials such as rice husks, red mud, clays, chitosan, and zeolites.

Among the materials used for adsorption, research indicates that zeolites show promise as effective adsorbents for simultaneously removing both inorganic and organic contaminants from water (Azizi et al., 2019, Obijole et al., 2019, Bu et al., 2020, Amin et al., 2021). Zeolites are defined as crystalline, microporous, hydrated aluminosilicates formed when volcanic rock or ash reacts with alkaline water which mainly contain SiO_4 and AlO_4 tetrahedra frameworks that are joined together (Król, 2020). They are occasionally distinguished as sieves at molecular levels pertaining to their capability to selectively filter certain molecules in water, making them well-suited as adsorbents. Moreover, the distinctive characteristics of zeolites,

including their high surface area facilitating interaction with a large volume of molecules, eco-friendliness, abundance in nature, insolubility in water, and cation exchange capacity (CEC), have captured the attention of scientists (Velazquez-Peña et al., 2017, Sivalingam and Sen, 2018). Due to their high CEC, reports indicate that zeolites functionalized with metal oxides offer an improved removal efficiency of organic and inorganic contaminants and higher regeneration capability showcasing the economic feasibility and sustainability of these materials.

Therefore, this study aims to utilize zeolitic adsorbents that are functionalized with zirconium and silver metal oxides to concurrently remove fluoride and pathogens from drinking water. In this study, zeolite will be synthesized from bentonite clay via the hydrothermal-ultrasonic assisted technique with the assistance of the Response Surface Methodology (RSM) for optimization of the synthesis conditions.

1.2 Problem statement

Residents living in poverty-stricken areas of South Africa depend on groundwater with elevated levels of fluoride and microbial contaminants sourced from groundwater (Edokpayi et al., 2018, Khabo-Mmekoa et al., 2022). Consequently, most suffer from fluorosis while others suffer from bacterial infections such as typhoid and cholera because of drinking water contaminated by pathogens and fluoride (WHO, 2019, Ed Butts, 2020, Potgieter et al., 2020). This has been evident in the Eastern Cape, Western Cape, Northern Cape, Gauteng, North West, and Limpopo provinces of South Africa (Kalule et al., 2019, Odiyo et al., 2020). (Odiyo and Makungo, 2012) investigated the effects of consumption of fluoride-contaminated groundwater in Siloam village, Limpopo province and reported that 50% of school learners aged 11-14 years old were affected by dental fluorosis which is associated with fluoride levels of 5.4 mg/L found in the groundwater of the area. Also, the National Institute for Communicable Disease (NICD) reported 37 prevalence cases of typhoid infections between July 2020 to January 2022 whilst 3000 and 561 cases of diarrhea and typhoid were reported respectively in South Africa (Monyatsi et al., 2012, NICD, 2022). Furthermore, reports indicate concurrent contamination of water sources by fluoride and microbial contaminants in rural regions of South Africa and both contaminants can pose life-threatening risks, potentially leading to fatalities (Alqahtany, 2021, Bhandari et al., 2021).

Available water treatment strategies include reverse osmosis, membrane techniques, ion exchange, and the adsorption method (He et al., 2020). However, these methods have limitations such as inapplicability in large-scale operations such as the ion exchange method whilst the precipitation method require advanced chemicals which are expensive and produce sludge after use with negative environmental impacts when compared with the

adsorption method (Mitiku, 2020, Yadav et al., 2021). The adsorption method on the other hand uses inexpensive material that is abundant in nature and eco-friendly, modifiable materials that meet application requirements and materials that are sustainable, feasible, and applicable in remote areas (Yadav et al., 2021). Furthermore, minimal work on multifunctional water treatment research efforts has been directed toward concurrently eliminating both fluoride and pathogens from water.

Adsorption materials such as zeolites have been adopted in the water treatment strategies for anions and pathogens removal in water due to their molecular sieve, high adsorption efficiency, and ease modification properties (Król, 2020). When functionalized with various cations or metal oxides, these offer an improved adsorption capacity towards anionic species in water. Moreover, functionalized metal oxide zeolitic adsorbent can serve as a multifunctional adsorbent designed to address both organic and inorganic contaminants, featuring enhanced properties like a high surface area, insolubility under normal water conditions, and the ability for regeneration. Hence this study seeks to develop a multifunctional pathogen and fluoride removal innovative method from water using modified Zr^{4+}/Ag^{+} zeolite synthesized from bentonite clay.

1.3 Objectives of the study

1.3.1 Main Objective

The main aim of this study is to synthesize Zr^{4+}/Ag^{+} modified zeolites from bentonite clay using an ultrasonication method for application in simultaneous fluoride and pathogen removal in water.

1.3.2 Specific Objectives

- To optimize conditions for the synthesis of zeolite from bentonite clay and further determine its physiochemical characteristics.
- To evaluate the effectiveness of the synthesized zeolite in pathogens and fluoride removal by evaluating the adsorption capacity, models and zone of inhibition.
- To modify zeolite using Zr^{4+}/Ag^{+} metal oxides and further evaluate its efficiency in fluoride and pathogen removal by evaluating the adsorption capacity, models and zone of inhibition.

To evaluate the regeneration potential of the modified Zr^{4+}/Ag^{+} zeolite by evaluating the change in adsorption capacity after each adsorption cycle.

1.4 Hypothesis

The synthesized Zr^{4+}/Ag^{+} modified zeolite can effectively remove fluoride and pathogens in water simultaneously.

1.5 Significance of the study

This study makes a substantial contribution to the body of science by providing a scientific understanding of the water treatment methods, and innovative and sustainable approaches to the global health crisis. In addition, the aims of this study align with the United Nations Sustainable Development Goals (SDGs) including SDG-6 of clean water and sanitation which support the provision of sustainable water treatment technologies. Moreover, the removal of both pathogens and fluoride in drinking water assists in meeting the World Health Organization's guidelines for contaminants in water and mitigation of waterborne diseases for the provision of clean drinking water. Furthermore, this study seeks to adhere to the Water Research Commission Act as well as the South African National Water Act 36 of 1998 for compliance and provision of clean water and the development of water resources.

References

Abia, A. L., Schaefer, L., Ubomba-Jaswa, E. & Le Roux, W. 2017. Abundance of pathogenic escherichia coli virulence-associated genes in well and borehole water used for domestic purposes in a peri-urban community of south africa. *International Journal of Environmental Research and Public Health,* 14.

Alqahtany, F. 2021. Chemical and bacteriological assessment of groundwater in tathleeth region of asir. *Egyptian Journal of Chemistry,* 0**,** 0-0.

Amin, Z., Waly, N. A. & Arshad, S. E. 2021. Biofilm inhibition and antimicrobial properties of silver-ion-exchanged zeolite a against vibrio spp marine pathogens. *Applied Sciences,* 11.

Azizi, L. M., Ehsani, A., Divband, B. & Alizadeh, S. M. 2019. Antimicrobial activity of titanium dioxide and zinc oxide nanoparticles supported in 4a zeolite and evaluation the morphological characteristic. *Scientific Reports,* 9**,** 17439.

Bhandari, P., Banjara, M. R., Singh, A., Kandel, S., Rawal, D. S. & Pant, B. R. 2021. Water quality status of groundwater and municipal water supply (tap water) from bagmati river basin in kathmandu valley, nepal. *Journal of Water, Sanitation and Hygiene for Development,* 11**,** 102-111.

Bu, N., Liu, X., Song, S., Liu, J., Yang, Q., Li, R., Zheng, F., Yan, L., Zhen, Q. & Zhang, J. 2020. Synthesis of nay zeolite from coal gangue and its characterization for lead removal from aqueous solution. *Advanced Powder Technology,* 31**,** 2699-2710.

Chakraborty, R., Asthana, A., Singh, A. K., Jain, B. & Susan, A. B. H. 2020. Adsorption of heavy metal ions by various low-cost adsorbents: A review. *International Journal of Environmental Analytical Chemistry,* 102**,** 342-379.

Dong, Y., Jiang, Z., Hu, Y., Jiang, Y., Tong, L., Yu, Y., Cheng, J., He, Y., Shi, J. & Wang, Y. 2023. Pathogen contamination of groundwater systems and health risks. *Critical Reviews in Environmental Science and Technology***,** 1-23.

Ed Butts, P. E. 2020. *Waterborne pathogens* [Online]. Water Well Journal. Available: https://waterwelljournal.com/waterborne-pathogens/#:~:text=The%20four%20groups%20of%20pathogens%20in%20water%20of,are%20different%20in%20both%20their%20structure%20and%20function. [Accessed 15 May 2022].

Edokpayi, J. N., Rogawski, E. T., Kahler, D. M., Hill, C. L., Reynolds, C., Nyathi, E., Smith, J. A., Odiyo, J. O., Samie, A., Bessong, P. & Dillingham, R. 2018. Challenges to sustainable safe drinking water: A case study of water quality and use across seasons in rural communities in limpopo province, south africa. *Water (Basel),* 10.

Feng, X., Long, R., Wang, L., Liu, C., Bai, Z. & Liu, X. 2022. A review on heavy metal ions adsorption from water by layered double hydroxide and its composites. *Separation and Purification Technology,* 284.

Habiyakare, T., Schurer, J. M., Poole, B., Murcott, S., Migabo, B., Mardochee, B., Amuguni, J. H. & Morgan, J. P. 2021. Dental fluorosis among people and livestock living on gihaya island in lake kivu, rwanda. *One Health Outlook,* 3**,** 23.

He, J., Yang, Y., Wu, Z., Xie, C., Zhang, K., Kong, L. & Liu, J. 2020. Review of fluoride removal from water environment by adsorption. *Journal of Environmental Chemical Engineering,* 8.

Kalule, J. B., Smith, A. M., Vulindhlu, M., Tau, N. P., Nicol, M. P., Keddy, K. H. & Robberts, L. 2019. Prevalence and antibiotic susceptibility patterns of enteric bacterial pathogens in human and non-human sources in an urban informal settlement in cape town, south africa. *BioMed Central Microbiology,* 19**,** 244.

Khabo-Mmekoa, C. M., Genthe, B. & Momba, M. N. B. 2022. Enteric pathogens risk factors associated with household drinking water: A case study in ugu district kwa-zulu natal province, south africa. *International Journal of Environmental Research and Public Health,* 19.

Khairnar, M. R., Dodamani, A. S., Jadhav, H. C., Naik, R. G. & Deshmukh, M. A. 2015. Mitigation of fluorosis - a review. *Journal of Clinical and Diagnostic Research,* 9**,** ZE05-9.

Król, M. 2020. Natural vs. Synthetic zeolites. *Crystals,* 10.

Kumar, R., Ali, S., Sandun Sandanayake, S., Islam, M. A., Ijumulana, J., Maity, J. P., Vithanage, M., Armienta, M. A., Sharma, P., Hamisi, R. & Kimambo, V. 2023. Fluoride as a global groundwater contaminan.

Madilonga, R. T., Edokpayi, J. N., Volenzo, E. T., Durowoju, O. S. & Odiyo, J. O. 2021. Water quality assessment and evaluation of human health risk in mutangwi river,

limpopo province, south africa. *International Journal of Environmental Research and Public Health,* 18.

Mitiku, A. A. 2020. A review on water pollution causes, effects and treatment methods. *International Journal of Pharmaceutical Sciences Review***,** 94-101.

Monyatsi, L., Onyango, M. S. & Momba, M. N. B. 2012. Groundwater quality in a south african rural community a possible threat to public health. *Polish Journal of Environmental Studies***,** 1349-1358.

Nicd. 2022. *Alert: Update on enteric fever in south africa* [Online]. National Institute for Communicable Diseases. Available: https://www.nicd.ac.za/update-on-enteric-fever-in-south-africa-18-feb-2022/ [Accessed 27-05-2022 2022].

Ntshephe, L. 2012. Marketing information needs of smallholder livestock farmers in the moretele area in the bojanala platinum district municipality of the north west province. *unisadspace*.

Obijole, O. A., Gitari, M. W., Ndungu, P. G. & Samie, A. 2019. Mechanochemically activated aluminosilicate clay soils and their application for defluoridation and pathogen removal from groundwater. *International Journal of Environmental Research and Public Health,* 16.

Odiyo, J. O. & Makungo, R. 2012. Fluoride concentrations in groundwater and impact on human health in siloam village, limpopo province, south africa. *Water SA,* 38.

Odiyo, J. O., Mathoni, M. M. & Makungo, R. 2020. Health risks and potential sources of contamination of groundwater used by public schools in vhuronga 1, limpopo province, south africa. *International Journal of Environmental Research and Public Health,* 17.

Onipe, T., Edokpayi, J. N. & Odiyo, J. O. 2020. A review on the potential sources and health implications of fluoride in groundwater of sub-saharan africa. *Journal of environmental science and health. Part A, Toxic/Hazardous Substances and Environmental Engineering* 55**,** 1078-1093.

Palamuleni, L. & Akoth, M. 2015. Physico-chemical and microbial analysis of selected borehole water in mahikeng, south africa. *International Journal of Environmental Research and Public Health,* 12**,** 8619-30.

Potgieter, N., Karambwe, S., Mudau, L. S., Barnard, T. & Traore, A. 2020. Human enteric pathogens in eight rivers used as rural household drinking water sources in the northern region of south africa. *International Journal of Environmental Research and Public Health,* 17.

Sivalingam, S. & Sen, S. 2018. Rapid ultrasound assisted hydrothermal synthesis of highly pure nanozeolite x from fly ash for efficient treatment of industrial effluent. *Chemosphere,* 210**,** 816-823.

Sumalatha, K. 2021. Water security: Imperative for national security.

Vargas-Solano, S. V., Rodríguez-González, F., Martínez-Velarde, R., Morales-García, S. S. & Jonathan, M. P. 2022. Removal of heavy metals present in water from the yautepec river morelos méxico, using opuntia ficus-indica mucilage. *Environmental Advances,* 7.

Velazquez-Peña, G. C., Olguín-Gutiérrez, M. T., Solache-Ríos, M. J. & Fall, C. 2017. Significance of fezr-modified natural zeolite networks on fluoride removal. *Journal of Fluorine Chemistry,* 202**,** 41-53.

Who 2019. Preventing disease through healthy environments inadequate or excess fluoride a major public health concern. *World Health Organisation*.

Who. 2022. *Drinking water* [Online]. World Health Organisation. Available: https://www.who.int/news-room/fact-sheets/detail/drinking-water [Accessed 31 May 2022].

Yadav, M., Singh, G. & Jadeja, R. N. 2021. Fluoride contamination in groundwater, impacts, and their potential remediation techniques. *Groundwater Geochemistry Pollution and Remediation Methods***,** 22-41.

Yetis, A. D., Yesilnacar, M. I. & Atas, M. 2021. A machine learning approach to dental fluorosis classification. *Arabian Journal of Geosciences,* 14.

Chapter 2: Literature review

2.1. Introduction

Communities in arid and semi-arid regions worldwide frequently sought groundwater for drinking water. Research has indicated that groundwater sources in these regions are frequently contaminated with fluoride and pathogenic contaminants (Mahagamage et al., 2020, Yadav et al., 2021, Ling et al., 2022). These contaminants have been found at high levels of 10 mg/L for fluoride and 100 cfu/100 mL for pathogens exceeding the recommended standards which are not safe for human consumption (Odiyo and Makungo, 2018, Mutileni et al., 2023). Nations like China, Ghana, India, Mexico, Ethiopia, and South Africa have been reported to experience elevated cases of both fluoride and pathogenic contamination in their groundwater (Vithanage and Bhattacharya, 2015, Liu et al., 2019, Onipe et al., 2021). The World Health Organization has mandated maximum acceptable levels of pathogens and fluoride of 0 cfu/100 mL and 1.5 mg/L respectively to mitigate their adverse health effects (WHO, 2019, Kothari et al., 2021, Munzhelele et al., 2021).

Drinking water with elevated fluoride levels can cause health implications such as skeletal and dental fluorosis, while pathogens in water can result in diseases such as fevers, cholera, and diarrhea (Yadav et al., 2021, Dong et al., 2023). Reports documented more than 200 million people are afflicted by fluorosis-related diseases while 3.4 million people have succumbed to death due to waterborne pathogenic diseases (Yadav et al., 2021, Izah et al., 2022, Li et al., 2024). According to Rai (2020), fluorosis persists in children under the age of 12 with 6 million children dying from endemic fluorosis worldwide. Tragically, over 1.4 million children lose their lives annually due to diarrheal diseases resulting from the consumption of water contaminated with pathogens (Mahagamage et al., 2020).

To tackle the issue of pathogens and fluoride contaminants in drinking water, various water treatment strategies, including precipitation, coagulation, ion exchange, membrane filtration, and adsorption methods, have been developed to purify water quality for human consumption. (Mitiku, 2020, Rai, 2020, Yadav et al., 2021, Solanki et al., 2022). Among these technologies, adsorption-based technologies are often preferred due to their simplicity in design and cost-effectiveness (Munzhelele et al., 2021, Gitari et al., 2023). Moreover, it uses materials such as rice husks, fly ash, and clays that are easy to source (Mukherjee and Singh, 2018).

This section presents a literature review of the fluoride and pathogens contaminants, their occurrence, factors affecting their distribution, health effects, and treatment technologies. This section also focuses on an overview literature on zeolite adsorbents as potential

fluoride and pathogens removal methods in water, their structural framework and properties, their synthesis routes, and their recent application performances towards fluoride and pathogens contaminants removal in water.

2.2. Occurrence of fluoride in groundwater

Occurrence of excess concentrations of fluoride in groundwater is a global concern as shown in Figure 2.1 (Gupta and Ayoob, 2016). Nations including China, India, Thailand, Uganda, Nigeria, Ghana, and South Africa have reported cases of fluoride levels surpassing 1.5 mg/L in the groundwater (Vithanage and Bhattacharya, 2015). High fluoride levels of 40 mg/l, 21 mg/L, 204 mg/L, 15.5 mg/L, 26 mg/L, and 11 mg/L have been reported in India, Pakistan, Ethiopia, China, Tanzania, and South Africa, respectively (Vithanage and Bhattacharya, 2015). Onipe et al. (2021) stated that 75% of people in the African continent use groundwater for drinking water as their primary source of survival and unfortunately some regions are contaminated with these elevated levels of fluoride. Furthermore, consumed fluoride in water is deposited in the calcified tissues of the human body mainly teeth and bones, hence these excessive concentrations of fluoride increase the risks of dental and skeletal diseases among communities (Gupta and Ayoob, 2016, Aloulou et al., 2021).

In South Africa, excessive levels of fluoride have been documented in the western and northern regions of the country. Concentrations of fluoride above 3 mg/L were reported in the Western Cape, Northern Cape, North west and Limpopo provinces (Onipe et al., 2020, Onipe et al., 2021, Elumalai et al., 2023). Ncube and Schutte (2005) emphasized that this is due to the presence of fluorite and fluorapatite minerals in the groundwater of these areas. Fluoride levels of 11 mg/L, 5.08 mg/L, and 6.08 mg/L were reported in Warmbath, Tshipise, and Siloam areas in Limpopo province respectively (Onipe et al., 2020). Furthermore, these areas are found in arid and semiarid climates which also favors evaporation and precipitation of fluoride ions in the groundwater.

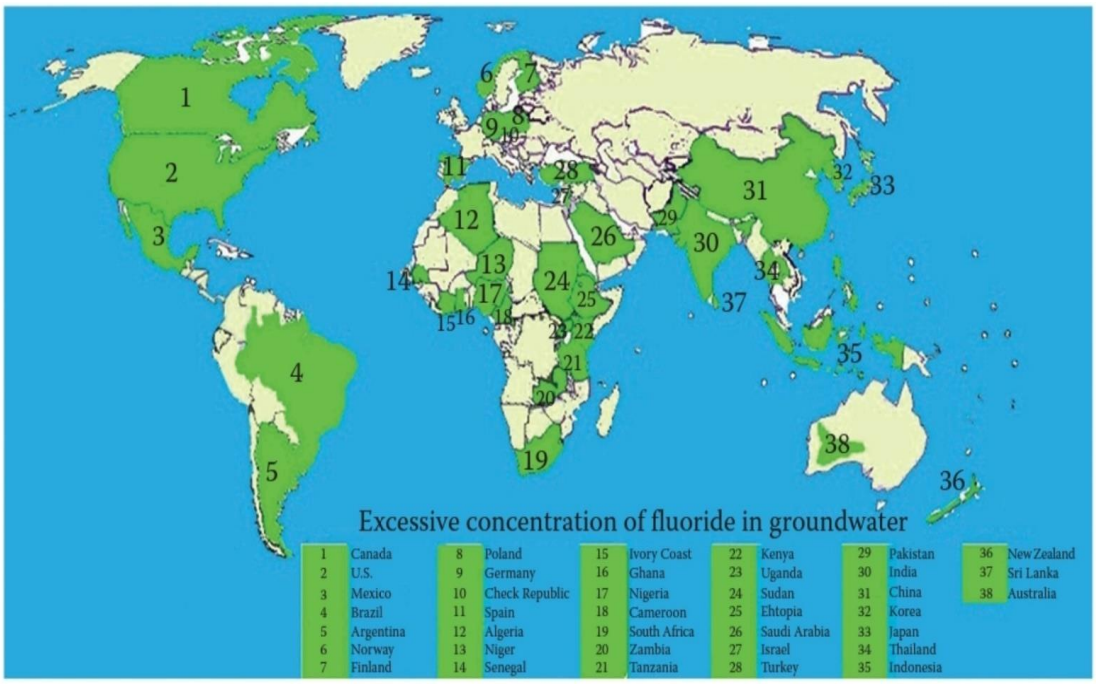

Figure 2.1: Reported occurrence of fluoride in groundwater across the globe (Gupta and Ayoob, 2016)

2.3. Factors affecting the occurrence of fluoride in groundwater

Studies revealed that some groundwater sources are contaminated by fluoride ions mainly in rural arid and semiarid regions from natural and anthropogenic sources (Khairnar et al., 2015, Gupta and Ayoob, 2016, He et al., 2020, Jayashree et al., 2020, Habiyakare et al., 2021). Contamination of groundwater by fluoride is governed by several factors such as the geological factor, temperature, water chemistry, and residence time (Xiao et al., 2022, Kumar et al., 2023).

2.3.1 Geological factor

The occurrence of fluoride in groundwater can be governed by underlying geologic rock minerals. These rocks minerals include fluorapatite, fluorite, and cryolite (McCaffrey and Willis, 2001). These rock minerals contain elemental fluorine which can then be released through weathering of these rock minerals which are in contact with the groundwater. In the periodic table, elemental fluorine is recognized as the most reactive and electronegative element, and it exists in an unstable form. This gives fluorine a high affinity towards positively charged elements and it forms anionic fluoride in aqueous solutions (Hossain and Patra, 2020). In addition, dissolution of the fluoride-bearing rocks induces the rate of fluoride formations in groundwater. Precipitation and ion exchange chemical processes influence the solubilization of rock minerals which contribute to elevated levels of fluoride in groundwater. During ion exchange, chemical constituents such as -OH in water may be exchanged with

fluorine in fluoride-bearing rocks. However, this condition is also pH dependent wherein groundwaters with alkaline pH favor the leaching of fluorine thereby elevating fluoride concentration in groundwater (Kumar et al., 2023).

2.3.2 Temperature

Environmental temperature has proportional effects on the increase in fluoride ions in groundwater. This mainly occurs in groundwaters with shallow depths as they are closer to the influence of surface temperatures (Xiao et al., 2022). The increase in temperature favors the solubility of fluoride minerals as they easily leach out fluorine during high temperatures (Odiyo and Makungo, 2012). During high temperatures, evaporation occurs causing water molecules to evaporate leaving high concentration of fluoride salts suggesting that water in arid and semi-arid areas exhibits higher fluoride levels as a result (Odiyo and Makungo, 2012, Xiao et al., 2022). In addition, high temperatures cause the solubility of carbonate minerals and form precipitates of calcium ions (Ca^{2+}) (Yan et al., 2020). These ions could then form complexes with fluoride ions thereby increasing fluoride ions in groundwater.

2.3.3 Water Chemistry

The presence of several chemical species such as hydroxides and bicarbonates influence the solubility of fluoride-bearing minerals. Groundwaters with high fluoride concentrations are characterized by high pH. This is due to chemical species such as bicarbonate (HCO_3^-) which favors the solubility and dissolution of fluorite minerals resulting in the leaching of fluoride ions as shown in equation 2.1. Moreover, alkaline water contains hydroxide ions (OH^-) which replace fluoride ions (F^-) in fluorine-bearing rock minerals (Chakraborty et al., 2020).

$$CaF^2_{(s)} + 2HCO^-_{3(aq)} \leftrightarrow 2F^-_{(aq)} + H_2O_{(aq)} + CO_{2(aq)} \quad (2.1)$$

2.3.4 Residence time

Prolonged exposure of groundwater with fluoride-bearing minerals increases fluoride levels in water (Xiao et al., 2022). This is due to a long period of contact with fluoride-bearing minerals which leads to the accumulation of fluoride ions as prolonged dissolutions and ion exchange take place without interference (Mukherjee et al., 2018, Kumar et al., 2023). Also, in groundwater with shallow depth, prolonged dry seasons influence fluoride levels in groundwater. This is due to high temperatures that influence further and further dissolution and ion exchange of chemical species including fluoride as the groundwater becomes overly saturated (Mukherjee and Singh, 2018). On the contrary, wet seasons cause interference through rain or groundwater recharge by surface water which imposes dilution effects in present fluoride ions in groundwater, thereby reducing fluoride levels. Moreover, as time

progresses, the mixing of groundwater from different sources with varying fluoride levels induces the increase of fluoride or dilutes its concentration in groundwater (Onipe et al., 2020).

2.4. Health implications of fluoride in drinking water

Exposure of the human body to elevated levels of fluoride exhibits varying health risks in the human body. Consumption of drinking water with fluoride concentrations lower than 0.5 mg/L causes dental caries which is a result of fluoride deficiency and it is characterized by the formation of plaque and tiny openings (Gupta and Ayoob, 2016). Fluoride levels between 0.5 and 1.5 mg/L have beneficial effects such as protection of teeth enamel which prevents tooth decay and sustains dental health. This is crucial, especially in building strong teeth hence citizens in countries such as the United States of America and Ireland receive fluoridated water specifically in areas without naturally supplied fluoride in water (Gupta and Ayoob, 2016).

Exceeding the World Health Organization's prescribed threshold of 1.5 mg/L for fluoride levels in water can lead to skeletal and dental fluorosis (WHO, 2019). To put it in perspective, human teeth are composed of hydroxyapatite substances of hydroxyl ions (-OH). When fluoride-rich water is ingested, these hydroxyl ions can be exchanged with fluoride ions from fluorapatite thereby causing these fluorosis diseases (Jha et al., 2013). Dental fluorosis is caused by drinking water with fluoride levels between 1.5 mg/L to 5 mg/L. This type of fluorosis is characterized by exceptional white spots in teeth which become more yellow, or brown-stained as the condition worsens.

Drinking water with fluoride concentrations exceeding 4 mg/L can cause skeletal fluorosis which favors the increase in bone density and result in crippling deformations as observed in Figure 2.2 (Gupta and Ayoob, 2016). Skeletal fluorosis is due to the deposition of fluoride ions in the bone tissues, and skeletal joints which can cause difficulty in locomotion. Other diseases linked to high fluoride levels in water includes Alzheimer’s disease, infertility, retarded growth, and cancer (Onipe et al., 2021). Also, Gupta and Ayoob (2016) emphasized that the detrimental impacts of excess levels of fluoride consumption have caused a decrease in children’s intellectual ability. This is due to 99% of consumed fluoride by humans is deposited in the bones and teeth (Kabir et al., 2019).

Figure 2.2: Pictorial view of dental (A) and skeletal (B) fluorosis (Bhowmik et al., 2019)

2.5. Fluoride treatment methods from water

There are several water treatment methods to improve water quality for safe and healthy drinking water. Several water treatment techniques such as reverse osmosis, Ion exchange, chemical precipitation, coagulation, membrane technique, and adsorption method have been employed to remove pathogens and anionic species such as fluoride in water (Chakraborty et al., 2020, Yadav et al., 2021). However, compared to the adsorption method, these water treatment techniques have limitations in their applicability such as low defluoridation efficiency, impractical in remote areas, production of sludge with negative environmental complications, and use of expensive materials (Chakraborty et al., 2020).

2.5.1 Ion exchange

The ion exchange technique uses synthetic chemicals or resins containing cation species for exchanging with anions in water. Resins such as bone char, carbon, quaternary ammonium selective ion-exchange resin, and natural zeolites are among the materials employed in the ion exchange method to selectively remove fluoride ions in water (Khairnar et al., 2015, Waghmare and Arfin, 2015, Chakraborty et al., 2020). A resin with chloride ions may be used to replace fluoride ions as shown in equation 2.2 (Pillai et al., 2021). The advantages of this method include a wide range of resin selections from manufacturers and has defluoridation efficiency of 90-95%. (Singh et al., 2020) investigated the efficiency of zirconium-impregnated exchanged resins in defluoridation studies and reported a percentage removal efficiency of 60%. The disadvantage on the other hand, is that it is induced by the pH of the solution, requiring longer reaction times, uses expensive resins that cannot be used in large-scale operations which makes it inapplicable in rural areas and lastly, it produces fluoride-rich solution which poses environmental complications if not properly disposed (Kumar et al., 2023). Furthermore, existing anions such as carbonate can cause interference with the ion exchange process.

$$Matrix - NR_3^+\ Cl_{(s)}^- + F_{(aq)}^- \rightarrow Matrix - NR_3^+ F_{(s)}^- + Cl_{(aq)}^- \quad (2.2)$$

2.5.2 Membrane filtration

This technique uses a semipermeable membrane to filter contaminants in pressurized water owing to the factor of the particle sizes of the contaminants in water (Yadav et al., 2021). The membrane technique is divided into three methods. These are the reverse osmosis method which uses a porous membrane to remove heavy metals, the nanofiltration method which uses membranes with larger pores compared to the reverse osmosis to filter contaminants with bigger particle sizes and the electrodialysis which removes ions with ion exchange membranes (Waghmare and Arfin, 2015, Chakraborty et al., 2020). The advantages include 45-95% defluoridation efficiency, can removal of multiple metal contaminants simultaneously, and filters contaminants in a wide range of pH (Kumar et al., 2023). A study by (Li et al., 2020) investigated the fluoride removal potential of fluorescent cellulose-based membranes and reported a maximum percentage fluoride removal of 90%. The disadvantages are that it uses electricity and high energy in water pumping which may be inapplicable in rural areas, it is costly, clogging the membrane which requires maintenance and the membrane might break which in turn compromises the effluent (Jayashree et al., 2020).

2.5.3 Coagulation

The coagulation technique uses coagulates as depicted in Figure 2.3 which are added to the contaminated water and force targeted ions to precipitate into insoluble salts which may then be filtered by employing a semi-permeable membrane. Coagulates used include alum and limes are rich in calcium ions prompting precipitation of fluoride ions in the water into calcium fluoride salt (Crini and Lichtfouse, 2018). However, this is contingent on the solution's pH. (Lacson et al., 2021) showcased fluoride removal equations using calcium and magnesium as coagulants as presented in equations 2.3 and 2.4. The advantages of this technique include applicability in large-scale operations, it is applicable in simultaneous defluoridation and bacterial inactivation, and it uses simple mechanisms and simple structures (Crini and Lichtfouse, 2018). A study by Qu et al. (2023) conducted fluoride removal by a zirconium-based coagulant and reported 96.8% of fluoride removal. The disadvantages include the rise in pH with the formation of salts which hinders further coagulation and generates sludge which may not be eco-friendly if disposed of carelessly (Yadav et al., 2021). In addition, this method requires highly concentrated dosages of coagulates which is costly and offers a defluoridation efficiency of 18-90% (Jha et al., 2013, Chakraborty et al., 2020, Kumar et al., 2023). Consequently, the method is not feasible in rural areas as the materials used are not reusable.

$$Ca^{2+}_{(aq)} + 2F^{-}_{(aq)} \leftrightarrow CaF_{2(s)} \quad (2.3)$$

$$Mg^{2+}_{(aq)} + 2F^{-}_{(aq)} \leftrightarrow MgF_{2(s)} \quad (2.4)$$

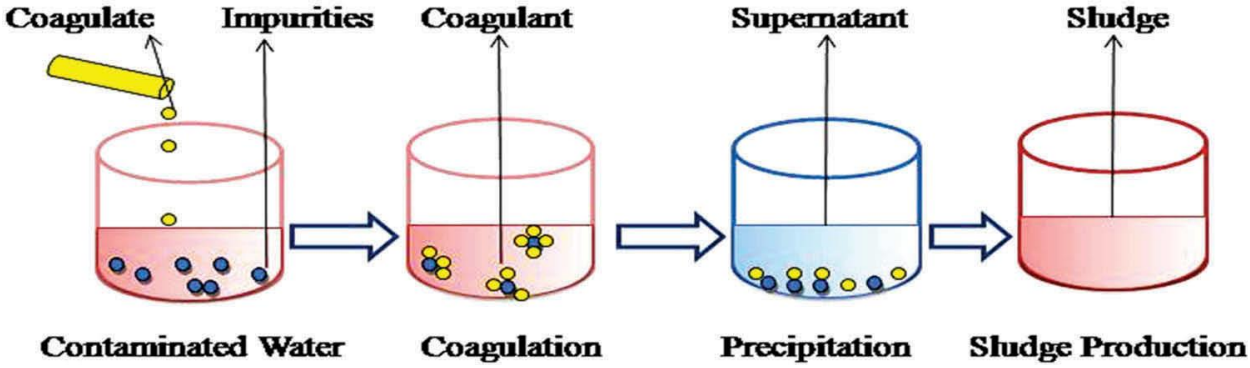

Figure 2.3: Set up of coagulation method in water treatment (Chakraborty et al., 2020)

2.5.4 Adsorption

The adsorption method involves binding or accumulation of contaminants on the surface of an adsorbent. Adsorbents used include fly ash, chitosan, clays such as red mud, and bentonite natural and synthetic zeolites (He et al., 2020). Adsorbents can act as both filtering and ion exchange medium. Cations and anionic species such as fluoride in an aqueous solution are removed by physical or chemical interaction with the adsorbent as water passes through and cations or anions are immobilized as shown in Figure 2.4 (Chakraborty et al., 2020). Studies reported that depending on the properties of the adsorbent, these materials can also be used to inactivate microbial activities in water such as *E. coli* pathogens (Crini and Lichtfouse, 2018). Such adsorbents can serve as multifunctional sorbents of ions and pathogens in water simultaneously. The advantages of the adsorption technique include the flexibility of adsorbents in integration with other chemical species to suit the required application, defluoridation efficiency of 90-99%, use of a wide range of materials including waste products which are also available in remote rural areas, and ability to remove a wide range of contaminants (Crini and Lichtfouse, 2018, Chakraborty et al., 2020). In addition, the used material has the capability of being regenerated making them sustainable and the treated water is of high quality (Kumar et al., 2023). Chen et al. (2022) documented a maximum defluoridation efficiency of 90% using aluminum hydroxide-loaded zeolite adsorbent. Disadvantages include non-selective ions removal in water including essential ions for human health and reduction in defluoridation efficiency (Jayashree et al., 2020).

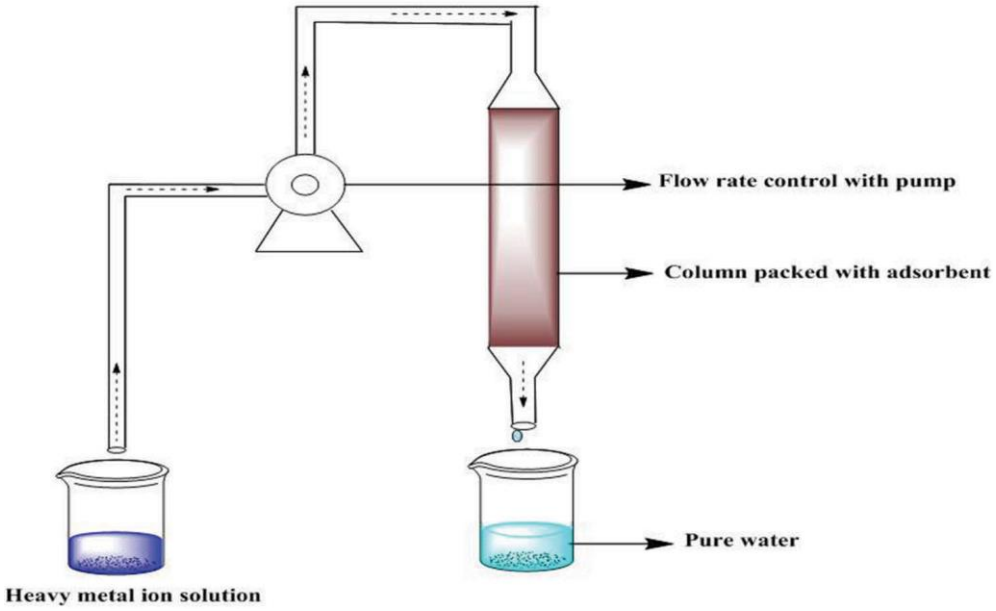

Figure 2.4: Water purification set up for the adsorption process (Chakraborty et al., 2020)

2.6. Microbial contaminants

2.6.1 Microbial contaminants in groundwater

Human perception regards groundwater as a safe and healthy water source but sadly this is not the case. Bradford and Harvey (2016) indicated that statistics show that 76% of waterborne disease outbreaks are linked to groundwater. Sources such as leakage of sewage, landfills, and municipal and industrial waste discharge play a major role in increasing contamination of groundwater by pathogenic contaminants (Khan and Ahmad, 2012, Lugo et al., 2021). Among these sources of contaminants, leaking sewers and septic tanks have the highest influence on microbial development in groundwater (Lugo et al., 2021).

Several pathogenic contaminants have been reported in groundwater sources such as *Escherichia coli, shigella spp, vibrio cholera, giardia lamblia, and Salmonella typhi* (Bradford and Harvey, 2016). Pandey et al. (2014) elucidated that pathogens such as *E. coli*, *salmonella,* and *S faecalis* are stable in groundwater conditions making matters worse. Depending on the current levels of pathogens in groundwater, reports indicate that groundwater can transport these contaminants onto rivers and wells through groundwater discharge and these risks are high where shallow aquifers exist (Pandey et al., 2014). Also, the same can be emphasized on contaminated surface water bodies that are in contact with shallow groundwater which enriches the groundwater with microbial contaminants.

2.6.2 Global distribution of microbial contaminants in groundwater

The presence of pathogenic microorganisms in groundwater is a worldwide concern. Studies indicate that approximately 1.6 million children of age 5 and below succumb to pathogenic infections each year due to the consumption of groundwater containing microbial contaminants (Dong et al., 2023). These cases are more prominent in the rural outskirts of several countries. Countries in the Asian continent such as India, Thailand, and Indonesia have reported microbial infection cases after exposure to groundwater sources. Furthermore, almost all countries in the African continent have reported cases of pathogenic infections including Ghana, Nigeria, Tanzania, Zimbabwe, and South Africa (Lugo et al., 2021). Pathogenic infections can occur through ingestion or contact with an open wound on the skin (Pandey et al., 2014). Microbial infections in humans depend on several factors such as age, previous exposure, nutrition, concurrent infections, immune status, and overall health (Khabo-Mmekoa et al., 2022). Children and elderly people are highly susceptible to microbial infections and around 700 000 children die worldwide due to diarrheal disease (Khabo-Mmekoa et al., 2022).

Various studies confirmed the presence of microbial contaminates in different groundwaters located in South Africa. Khabo-Mmekoa et al. (2022) reported 347 cfu/100 mL of bacterial contamination in the groundwater found in Ugu district municipality in KwaZulu-Natal. Another study by Enitan-Folami et al. (2019), reported a high level of *e coli* microbial species with concentrations around 700 cfu/100 mL in the Thulamela municipality, Limpopo province. Such levels of pathogens are widely reported in privately owned and traditional boreholes wherein there are no water treatment strategies in place resulting in the consumption of pathogenic contaminated water in the community (Pandey et al., 2014, Enitan-Folami et al., 2019). The most challenging and emerging issue of concern is that bacterial pathogens have been developing resistance to some available treatment methods (Enitan-Folami et al., 2019). Furthermore, Edokpayi et al. (2018) emphasized that the co-occurrence of microbial contaminants and fluoride ions in the same groundwater increases health risks as chances of contracting fluorosis and microbial infections are eminent.

2.7. Pathogen removal methods

2.7.1 Filtration method

This technique is one of the most commonly regarded and relied on for the removal of pathogens and contaminants. This method allows water to pass through a medium such as a membrane or sand gravel and sieve pathogens from water based on their particle size (Habibi-Yangjeh et al., 2020). The filter medium has tiny pores which exclude particles in water due to their size (Wang et al., 2021). In this method, inexpensive materials such as

sand gravel or clays are used (Bahri et al., 2009). In addition, water passes through slowly with the force of gravity and therefore this method is viewed as a low energy demand and sustainable technique. However, issues such as saturation and clogging of the medium become a problem as it reduces the efficiency of the method.

2.7.2 Chemical disinfection method

This approach utilizes chemical agents such as chlorine, ozone, and detergents to inhibit the growth of pathogens and reduce their concentration. This method is widely used and preferred as it has high efficiency against a significant range of pathogens and can be applied in large-scale water treatment plants (Dandie et al., 2019). Parameters including the type of disinfectant, pH, contact time, and temperatures are responsible for the effectiveness of the chemical agents used. Major concerns of this method are the by-products produced i.e. trihalomethanes which have carcinogenic effects (Grzegorzek et al., 2023). These compounds can accumulate in water and exposed to the human circulatory system through drinking (Latif et al., 2022).

2.7.3 Coagulation

This method operates similarly to the disinfection method. Coagulants such as alum and lime are added to water and react with the targeted particles to form aggregates that settle on the bottom of the water container (Bahri et al., 2009, Dayarathne et al., 2021). The targeted particles include microbes and organic matter which do not settle naturally. In general, these particles are negatively charged, and addition of coagulates neutralizes them and causes them to combine and form flocs which are heavier and then filtered (Dayarathne et al., 2021). Hence, pathogens containing water-soluble proteins that are positively charged can be neutralized and disassociated to prevent their growth in water (Mitiku, 2020). The drawbacks of this method include disintegration of aggregates during flocculation, high alkalinity of filtrate water, sludge disposal costs, and residuals of coagulant in filtrate which can cause diseases such as Alzheimer's disease after prolonged consumption (Ciobanu et al., 2022).

2.7.4 Ultraviolent Irradiation Method

This is one of the physical methods of removing pathogens in water through ultraviolet exposure from a UV lamp. The UV radiation destabilizes the genetic materials of the exposed pathogens thereby disturbing the reproduction of pathogens (Pullerits et al., 2020). This method offers advantages such as the inactivation of pathogens in a very short time and no sludge production (Delorme et al., 2020). In addition, this method does not involve handling of chlorine gases which could be unsafe and have low maintenance costs (Bhatt et al., 2020, Delorme et al., 2020, Habibi-Yangjeh et al., 2020). However, issues including

industrial or commercial applications persist due to high starting cost, low penetration depth, and recontamination (Yemmireddy et al., 2022).

2.8. Simultaneous/Multifunctional removal strategies

Methods such as integrated coagulation-filtration, membrane-filtration, and adsorption-filtration technology have been widely utilized as multifunctional water treatment strategies. Numerous materials have been fabricated to facilitate the simultaneous removal of both fluoride and pathogens from water. These include materials such as iron doped poly composite by Munzhelele et al. (2021), bifunctional biopolymer nanocomposite by Nehra et al. (2020), zirconium-silver nano bimetallic network composite by Gupta et al. (2021), silver-magnesium nanohydroxyapatite cellulose composite by Ayinde et al. (2022) and mechanochemically activated aluminosilicate clay adsorbent by Obijole et al. (2019). However, studies on multifunctional fluoride and pathogens treatment are few hence this study will explore zeolite adsorbent as a multifunctional water purification adsorbent for the removal of pathogens and fluoride in water.

2.9. Zeolites

Zeolites adsorbents are known as porous and molecular sieving sorbents that can be found in abundant (Reeve and Fallowfield, 2018, Król, 2020). The discovery of their molecular dimension properties, high ion exchange, and surface area has led to their diverse application ranges in ion-exchange processes, catalysis, and gas and metals adsorption studies in water (Price et al., 2021). Studies depict zeolitic materials as eco-friendly and sustainable materials as they can be obtained at low cost from natural abundant sources of materials. Examples of such sources include clays and waste products such as coal fly ash and rice husk. Their abundance in nature makes zeolites versatile as they can also be utilized in remote regions.

2.9.1 Structure of zeolites

Generally, the matrices of zeolites are composed of alumina (AlO_4) and silica (SiO_4) tetrahedra joined together by an oxygen atom (Johnson and Arshad, 2014, Kumar et al., 2019, Król, 2020). These materials are crystalline, and they are composed of open pore channels, and cavities of molecular dimensions that contain cations and water molecules. The presence of cations is facilitated by the net negative charge found within the alumina tetrahedra of the zeolite (Król, 2020). Cations such as magnesium (Mg^{2+}), potassium (K), and sodium (Na^{+}) balance out the negative charges in the alumina network of the zeolite (Abdullahi et al., 2017, Reeve and Fallowfield, 2018). Abdullahi et al. (2017) emphasized that it is this cation exchange morbidity that enables the ion exchange of zeolites and its

catalysis ability. The following formula denotes the basic structure of zeolites. Equation 2.5 shows the chemical configuration of the zeolite framework.

$$M_{X/n}\,[(AlO_2)_x(SiO_2)_y].wH_2O \qquad (2.5)$$

Where M represents an alkali or alkaline metal cation, n is the valence of the cation, x, and y are the total number of aluminum and silicon tetrahedra per unit cell, respectively and w is the number of water molecules per unit cell (Mgbemere et al., 2017, Kumar et al., 2019, Khaleque et al., 2020). The ratio value of y/x (Silica to Aluminum) is used to distinguish different types of zeolites. This value can range from 1 to 100. Zeolites with silica-to-aluminum ratios of 1 to 1.5 are defined as zeolite A and have the lowest ratio (Cataldo et al., 2021). Intermediate zeolites have silica to aluminum ratio of 2 to 5 and they a categorized as zeolite Y. Lastly, zeolites with the highest silica-to-aluminum ratio range from 10 and above and they are categorized as ZSM-5 zeolite or mordenite (Ayoola et al., 2018, Cataldo et al., 2021). The increase in the Silica-Alumina ratio of the zeolite induces a decrease in the cation exchange capacity of the zeolite (Dutta and Wang, 2019).

2.9.2 Natural and Synthetic zeolites

Zeolites occur both naturally and as-synthesized materials. Naturally occurring zeolites are found as sedimentary minerals originating in alkaline environments. However, they are scarcely found in their pure state, instead, they are found with other impurities such as quartz and metals (Cataldo et al., 2021). Mordenite, clinoptilolite, and chabazite are among the naturally occurring zeolites (Król, 2020). These types of zeolites can be employed in several applications including waste treatment, gas adsorption, and metal adsorption in water. Also, their abundance in nature offers a cost-effective approach to water treatment strategies in developing nations (Baek et al., 2018, Król, 2020). Although these crystalline materials are used in various applications, they have limitations in their applicability which is due to their channel diameter, silica to aluminum ratio, and impurities. Both the channel diameter and ratio of natural zeolites are limited compared to their synthetic counterpart. Furthermore, natural zeolites have a finite silica-to-alumina ratio which affects their reaction with polar and non-polar molecules (Wang et al., 2019). In the water purification industry, cations impurities present in the naturally occurring zeolites compete with ions in wastewater making it difficult for efficient ion exchange and adsorption to take place.

On the other hand, zeolites can also be obtained artificially through various synthesis methods. Unlike naturally occurring zeolites, synthetic zeolites have an immense range of applications including agricultural additives, acting as catalysis in petroleum processing, and as water purification adsorbents. In water treatment processes, synthetic zeolites are preferred as they can be modified to suit the user's preference (Jia et al., 2022). Also,

synthetic zeolites are highly preferred as they are synthesized in their purest form with improved properties such as uniformity of particle sizes, high surface areas, and high Cation Exchange Capability (CEC) (Khaleque et al., 2020). The unique properties of synthetic zeolites have led to their high demand compared to their natural counterpart (Ojumu et al., 2016). Furthermore, natural zeolites are found in natural deposits which could be inaccessible to humans and their production time scale can reach up to a decade whilst synthetic zeolites can only take hours or a few days to synthesize (Khaleque et al., 2020).

Synthetic zeolites are produced in the laboratory using raw natural sources such as clays or diatomite and waste materials including rice husk and coal fly ash. In addition, synthetic sources such as sodium aluminate and silica and aluminum gels may also be used to improve the ratio silica to aluminum ratio of the synthesized zeolite (Abdullahi et al., 2017). Research indicate that natural and waste sources used in synthetic zeolite have an economic advantage over synthetic sources due to their abundance in the environment (Obijole et al., 2019). However, the purity of adsorbent sources in the environment is questionable and pre-treatment steps such as acid leaching and calcination to remove impurities may be required (Messing, 2021).

2.9.3 Synthesis of zeolite

2.9.3.1 Hydrothermal synthesis

The conventional hydrothermal synthesis approach has been widely utilized in the production of synthetic zeolite products including zeolite A, Y, X, NaP, and Faujasites. This procedure includes the use of high-temperature and pressure systems such as autoclave reactors, a mineralizing agent, and water to decompose silica and alumina-rich materials and recrystallize the mixture to produce zeolitic materials (Campoverde and Guaya, 2023). Also, regarded as the earliest duplicate synthesis technique of the natural production of zeolite, the hydrothermal synthesis approach offers advantages such as ease of control of the mixture and stability of the zeolite, the high reactivity of the reactants, crystal size, shape and surface area manipulation and low air pollution (Khaleque et al., 2020, Patuwan and Arshad, 2021, Suvaci and Özel, 2021, Sazali et al., 2022). Several parameters such as dihydroxylation, dissolution, aging time, and crystallization conditions such as temperatures and times are considered during the conventional synthesis of zeolite to produce the desired zeolite (Abdullahi et al., 2017, Collins et al., 2020).

2.9.3.1.1 Dihydroxylation

According to Salahudeen (2022), natural and waste sources of alumina and silica used in zeolite synthesis contain unreactive tetrahedral layers which hinders the yield of zeolite products. Hence, raw materials are heated at high temperatures to obtain reactive phases

which are ready for transformation into zeolite products. This process of making zeolite sources reactive is known as dihydroxylation (Abdullahi et al., 2017). In this process, these materials are converted to their oxide form through heating below their melting point in the absence of air. Dihydroxylation eliminates hydroxyl groups and other volatile substances present in the clay minerals making them more reactive (Corma et al., 2010).

An important note is that a higher calcination temperature greater than 950 ˚C may lead to decomposition and loss of the material whereas lower temperatures below 400 ˚C result in less reactivity of the material (Guozhi et al., 2019). Studies indicated that the optimal conditions for the activation of these materials revolve around the optimum temperature range of 400˚C to 900˚C (Abdullahi et al., 2017, Guozhi et al., 2019). The study of Le et al. (2023) reported the effect of temperature during the calcination process of kaolin clay into meta kaolin which is the activated and reactive phase of kaolin clays. The study reported that during calcination, at 300°C, water molecules are removed while the matrices of kaolin clay start to break at 500°C. The disintegration in the clay's structure continues until the metakaolin phases are formed at 900°C. A study by Mahima Kumar et al. (2021) investigated the influence of calcination temperature and reported similar results. The study indicated that calcination temperatures below 450°C do not affect the activation of kaolin clay whilst temperatures above 450°C are effective. However, the study hinted that 1000°C leads to the development of mullite and spinel phases which are non-reactive.

2.9.3.1.2 Dissolution

In zeolite synthesis, enough alumina and silica from various sources such as fly ash, rice husks, and clays are required for the production of zeolitic material. These Si and Al are extracted through the dissolution process in the presence of an alkaline medium (NaOH or KOH) or acidic medium (HCl) to form the zeolite framework. Studies emphasized that an alkaline medium or acidic medium leads to the solubility of silica and alumina from clay sources and eases up the extraction of Si and Al as the alkalinity increases. In addition, the alkaline medium speeds up the polymerization of aluminate and silicate ions decreases nucleation time while accelerating the crystallization of zeolites, and reduces the particle size and distribution of zeolites (Johnson and Arshad, 2014).

Intensive studies have been conducted on the dissolution of zeolite sources in an alkaline medium. Among various dissolution agents, sodium hydroxide (NaOH) is highly favored and used as it yields higher amount of Si and Al compared to other agents such as potassium hydroxide (KOH) (Panagiotopoulou et al., 2006, Akkoca et al., 2013). In some cases, hydroxides are widely used as mineralizers for zeolites. However, it is crucial to note that higher concentrations of hydroxides can result in zeolite being too soluble thus preventing

the crystallization of the zeolite whereas too little amount of hydroxide results in less solubility of the material thus there will be little or no crystal growth resulting in the formation of amorphous materials (Corma et al., 2010, Kumar and Jena, 2022). Therefore, the right concentration ratio between the hydroxide and the raw clay in use must be optimized (Corma et al., 2010). In addition, these agents will solubilize the precursor material and convey ionic species into forming a new zeolite framework.

Sazali and Harun (2022) investigated the influence of the concentration of NaOH on the synthesis of zeolite LTA from kaolin clay at constant hydrothermal conditions. The study conducted the effect of dissolution using 0.5 to 3 Molar concentrations of NaOH of which the study concluded that 1 Molar of NaOH was the optimum concentration in the production of a highly crystalline zeolite LTA structure. In contrast, Ryu et al. (2020) argued that NaOH concentrations lower than 3M do not produce the required zeolite product while concentrations of 5 Molar and higher lead to the formation of the hydroxy sodalite phases which have lower surface area and are not required. However, an important note is that the article used a higher solid-to-liquid ratio during the dissolution of silica and aluminum which could have impacted in the effectiveness of NaOH concentrations lower than 3M.

A study by Dabbawala et al. (2020) investigated the influence of the NaOH concentration in the synthesis of zeolite Y at constant crystallization conditions of 24 hours at 100°C. The study varied the alkali concentration from 6 to 9 Molar and reported that lower concentrations lead to the formation of amorphous structures whereas concentrations higher than 7M produced pure zeolite Y phases. The level of alkali needed in the dissolution of Al and Si species is influenced by the nature of the precursor material and crystallization conditions.

2.9.3.1.3 Aging

Aging is the process of generation or formation of crystals/ nuclei through nucleation and crystal growth over an extended duration for maturation of the zeolite matrices (Nguyen et al., 2023). The aging process reduces the stimulation period and the time for crystallization of the materials. This is also known as homogenization and it is carried out prior to crystallization. According to Mohd et al. (2020) aging induces reduction or increase in crystal size depending on the temperatures used. The effect of aging also extends to the fabrication of pure zeolite phases as prolonged aging time provides enough time for solubilization of the precursor material. According to Lv et al. (2020), the effect of aging is also observed in the increase in stability of the zeolite structure, porosity, and surface area.

Studies indicate that exposure of clay in use to higher temperatures increases the growth of crystals and particle sizes in a short time (Corma et al., 2010). However, an important note

is that prolonged exposure to such high temperatures may result in loss of crystallinity (Abdullahi et al., 2017). This can cause disintegration of the zeolite matrices hence aging and temperature must be controlled.

Mohd et al. (2020) conducted a study on the synthesis of the zeolite NaX from sodium silicate and aluminate while investigating the effect of aging duration. The aging duration varied from 4 to 168 hours. The study reported that zeolite NaP and NaX phases were obtained after 4 hours of aging while pure zeolite NaX phases were obtained after 24 hours. Hence, the study hinted that aging can have a suppression effect in other peaks of the zeolite wherein less aging time can result in impure zeolite with more than one phase, and more duration of aging can result in a pure zeolite phase structure. The reduction of peaks from X-ray-diffraction analysis was also documented in Arni et al. (2020) and Nguyen et al. (2023) wherein the peak intensities decreased with an increase in aging time. Ibsaine et al. (2023) reported that an increase in aging time and temperature leads to the fabrication of more nuclei needed for the crystallization of the zeolite during hydrothermal treatment, thereby reducing the crystallization process. The study reported optimum aging time and temperature conditions of 8 hours at 75°C.

Studies have also reported other notable effects of aging treatment from the properties of the zeolite produced. Campoverde and Guaya (2023) reported that an increase in aging duration leads to the formation of small-sized particles confirming the effect of crystal size reduction. Kumar and Jena (2022) added that prolonged aging time leads to the formation of a more thermodynamically stable zeolite product. When subjected to extended aging duration, the molecular rearrangement within the zeolite structure progresses further, resulting in the formation of a crystalline framework with enhanced thermal stability. This increased stability arises from the optimization of intermolecular interactions, ultimately yielding a zeolite product with superior resistance to structural degradation. However, Zhang et al. (2020) reported that aging time has a negligible effect on the structure of zeolite produced.

2.9.3.1.4 Crystallization time and temperature

In hydrothermal synthesis, crystallization temperature and time play a major role in the crystallization of the zeolite. These conditions are employed in an in-situ environment to prevent water, heat, and pressure loss (Nguyen et al., 2023). Studies urged that the quality of the zeolite produced depends solely on the crystallization time and temperature conditions. The effect of time can be distinguished by two stages provided the crystallization temperature remains constant. The earliest time during crystallization is defined as the first stage wherein nucleation induction occurs, and only amorphous structures can be observed

at this stage (Patuwan and Arshad, 2021). The later time of crystallization or the last stage is distinguished by the detection of zeolite crystals during morphological and phase observation. Pei et al. (2022) observed that amorphous phases were detected between crystallization time of 0.5 to 1 hour and crystalline zeolite phases were observed between 2 to 4 hours at a constant crystallization temperature of 82°C.

A similar effect of crystallization time was observed by Nakhaei and Mohammadi (2021) during the synthesis of zeolite Y & P at a constant crystallization temperature of 90°C. The study documented that after 24 hours of crystallization time, only amorphous structures were observed emphasizing that the crystallization was in the early stage. After 30 hours of crystallization time, fewer peaks associated with zeolite Y were observed. However, zeolite Y peaks were completed and consumed after 66 hours, and new peaks of zeolite P were observed. These results were consistent with several studies (Hong and Um, 2021, Kumar and Jena, 2022, Ibsaine et al., 2023). In addition, a study by Kumar and Jena (2022) reported that zeolite purity is also influenced by the duration of crystallization. The study reported that after 40 hours of crystallization time at a constant temperature of 150°C, Xray-diffraction analysis showed that zeolite Na-P1 peaks were observed along other peaks of quartz and mullite phases. However, pure zeolite Na-P1 was observed after 60 hours of crystallization time.

Crystallization temperature is a critical parameter during the synthesis of zeolite. A study by Kumar and Jena (2022) conducted the effect of crystallization parameters in zeolite Na-P1 synthesis. The study optimized the crystallization time from 24 to 48 hours and temperature of 100 to 200°C. The study hinted that an increase in temperature and time to 200°C and 48 hours produces the targeted zeolite Na-P1. In addition, lower crystallization temperatures showed that no peaks attributed to the zeolite were observed. Furthermore, Lee et al. (2022) reported that an increase in crystallization temperature from 80 to 100°C produces the desired zeolite A at a constant hydrothermal time of 24 hours. However, the study documented that a further increase in temperature to 120°C led to a decrease in the crystallinity of the zeolite produced. This decrease is the transition stage of the transformation of the zeolite produced to a highly stable zeolite phase such as hydroxy sodalite. This phenomenon can also be observed under prolonged crystallization time.

The influence of the crystallization temperatures also extends to the structural framework of the zeolite produced. Studies indicate that higher temperatures lead to further solubilization of silicate species causing a hierarchical assortment of metastable spherical particles of sodalite phases (Lee et al., 2022). However, Liu et al. (2020) added that an increase in temperature causes agglomeration of particles hence irregular particles are observed at

higher temperatures. Therefore, the type of zeolite produced is based on the hydrothermal parameters employed during the synthesis process, and synthetic silica and alumina sources are required.

2.9.3.2 Other methods

From time to time, the application of conventional hydrothermal synthesis methods has been improving as researchers find ways to synthesize zeolites at a much more efficient time and temperature. However, alternative methods such as alkali fusion, microwave, and sonochemistry have been explored to reduce the cost of zeolite synthesis while producing a higher yield (Suvaci and Özel, 2021).

2.9.3.2.1 Fusion method

Unlike the conventional hydrothermal synthesis method, this process involves the pre-treatment of silica and alumina materials in the presence of heat and an alkali agent. During the pre-treatment process, the raw materials are fused with alkali under high temperatures to decompose silica and alumina salt constituents required to produce zeolitic products (Khaleque et al., 2020). This procedure takes place in the absence of water and an inorganic compound such as an aluminosilicate material is reacted with an alkali above its melting point to produce soluble silica and alumina precursor agents. Thereafter, the soluble salts are added to water and are hydrothermally treated for crystallization of the mixture to produce the zeolitic product (Lee et al., 2017, Khaleque et al., 2020). It has been documented that this approach can produce up to 60% yield of zeolite, however, the produced zeolite contains a high silica-to-alumina ratio (Lee et al., 2017). This is due to a higher amount of silica produced during the pre-treatment process and sodium aluminate may be required to reduce the ratio of the zeolite. Also, properties such as high crystallinity and surface area are among the advantages of this method (Samanta et al., 2022).

Ayele et al. (2016) investigated the synthesis of zeolite through the alkali-fusion-assisted hydrothermal method from kaolin clay. In the study, 3M of NaOH was used for the decomposition of silica and aluminum materials. The study concluded that hydrothermal treatment alone produced zeolite A with a crystallinity of 75% while the pre-fusion hydrothermal method produced the same zeolite with a higher crystallinity of 84%. This gives evidence to the positive effect of pre-fusion treatment of raw materials prior to hydrothermal treatment to produce a high crystalline zeolite structure.

Guozhi et al. (2019) prepared zeolite A through the fusion-assisted hydrothermal method employing fly ash as a precursor material. Prior to the fusion of the precursor materials, the materials were first subjected to calcination and acid leaching to remove the iron content of the raw materials. The obtained products were then fused with sodium aluminate and

sodium hydroxide at an optimum alkali fusion temperature of 850°C for 2 hours using 2.5 M of NaOH. The study noted that an increase in alkali fusion temperature beyond 850°C causes a decrease in the crystallinity of the zeolite while an increase in alkali concentration causes the transformation of zeolite into zeolite A.

Bai et al. (2018) investigated the alkali fusion hydrothermal synthesis of zeolite Na-X from oil shale ash. In this study, the effect of ash-to-NaOH ratio, temperature, solid-to-liquid ratio, and crystallization parameters such as temperature and time were investigated to outline the optimum conditions for alkali fusion-assisted hydrothermal synthesis. The study indicated that an optimum fusion temperature of 600°C completely converted the aluminosilicate materials of oil shale ash into soluble silicate and aluminate salts as it reacted with NaOH in an optimum ash-to-NaOH ratio of 1:1.2 grams. Moreover, the solid-to-liquid ratio evaluation proved that the amount of liquid added during the aging process can highly influence the crystallinity of the final zeolite. According to the study, the lowest solid-to-liquid ratio of 1:7 g/mL resulted in a highly reduced crystallinity of 7.89% which is due to a high volume of liquid which reduces the alkalinity of the mixture. On the contrary, the highest solid-to-liquid ratio of 1:3 g/mL also resulted in low crystallinity of 20.64% which was due to the low volume of water and high alkalinity of the solution which further dissolved the already formed crystals. However, an optimum solid-to-liquid ratio of 1:4 g/mL was obtained which resulted in 76.22% of crystallinity of the zeolite. Thereafter, the optimum crystallization parameters were 80 for 24 hours which resulted in high crystallinity of 91.32%.

2.9.3.2.2 Microwave-assisted hydrothermal method

Another novel synthesis method includes the microwave-assisted technique. The microwave technique releases microwaves in the frequency of 915 to 2450 MHz that directly interact with polar or ionic group molecules and cause these molecules to rapidly oscillate and heat up (Bukhari et al., 2015, Patuwan and Arshad, 2021). Mainly water molecules absorb this heat causing a rise in the temperature of the mixture which initiates the formation of crystal nuclei and recrystallisation of silica and aluminum. Electromagnetic radiation also influences the rapid and homogeneous mixing of the sol-gel and the faster rate of reaction along with the high yield of the zeolite (Samanta et al., 2022). The microwave-assisted synthesis produces zeolites which are highly crystalline at a short interval of time in comparison with the conventional hydrothermal synthesis technique. However, limitations such as low surface area and porosity are often encountered with this technique. This is due to the production of impurities and lack of control over the zeolite conversion rate (Ren et al., 2020)

A study by Tayraukham et al. (2020) investigated the synthesis of zeolite through conventional hydrothermal synthesis and microwave-assisted hydrothermal methods for

comparison. The findings of the study revealed that zeolite NaP was obtained after 24 hours of conventional hydrothermal treatment at a temperature of 150°C. In contrast, zeolite NaP was obtained after 1 hour of microwave irradiation at a similar temperature. This gives evidence of the power of the microwave irradiation method which reduces the duration of zeolite synthesis. Also, similar observations were made in a study by (Bunmai et al., 2020, Makgabutlane et al., 2020, Zhou et al., 2023). Le et al. (2023) hinted at the sustainability of the microwave-assisted hydrothermal method during the fabrication of zeolite 4A from kaolin clay. The study was able to synthesize zeolite 4A type within 6 minutes of microwave irradiation. Furthermore, the zeolite produced was of high quality which emphasizes the applicability of the microwave-assisted technique.

Abdellaoui et al. (2021) described microwave assisted synthesis as a green cost-effective method for restructuring strategies for the production of synthetic microporous materials. The study further emphasized that microwave synthesis reduces the time and energy needed to synthesize zeolite materials making it an ideal sustainable approach. Similarly, Le et al. (2023) and Zhou et al. (2023) documented that, the utilization of the microwave irradiation technique reduces energy consumption while also reducing heat loss which is required for pressure build-up and crystallization.

Ramírez Bocanegra et al. (2022) combined both hydrothermal treatment and microwave irradiation to synthesize FAU zeolite type using colloidal silica and aluminum hydroxides as precursor material. The study concluded that the use of microwave prior to hydrothermal treatment reduced the crystallization time from 8 to 1 hour along with the reduction of the energy cost. This study also emphasized that microwave treatment influenced pore formation on the zeolite while promoting the reduction of particle size. Another study by Bunmai et al. (2020) confirmed that employment of the microwave-assisted method exhibited positive effects on the nucleation, crystal growth, and formation of stable phases in a short time of irradiation of 1 hour.

2.9.3.2.3 Ultrasonication assisted hydrothermal method

To reduce the synthesis time and maintain a sustainable synthesis route for zeolite synthesis, research studies have developed a breakthrough using techniques such as ultrasound method-assisted hydrothermal method. The ultrasound technique utilizes powerful ultrasound waves in the range of 20 kHz-10 MHz to dissolve zeolite precursor materials and extract silica and alumina species prior to the hydrothermal treatment process (Patuwan and Arshad, 2021). This process causes acoustic cavitation which influences depolymerization-polymerization equilibria through implosive collapse of microbubbles in the reaction mixture which reduces the reaction time and improves product quality (Cao et al.,

2023). The ultrasound technology also assists in homogenization, nucleation, and crystal formation during the treatment process of the mixture (Khaleque et al., 2020). The use of sonochemistry has been widely recognized and emphasized as it offers accelerated crystallization, and reduced energy consumption while also producing a zeolitic material with a higher surface area and smaller particle sizes (Ju et al., 2020, Lin et al., 2022, Zhang et al., 2022).

To synthesize nanosized zeolite composite from bentonite clay using sonochemistry, Khatamian et al. (2019) deduced that as higher power of sonication increases, the nucleation speed also increases and causes the formation of more and more nanosized particles in the range of 40 nm. Also, the study discovered that ultrasonic treatment provides a homogeneous porous layer with high quality, high crystallinity, and uniform particle sizes. Ramírez Bocanegra et al. (2022) reported similar effects wherein the ultrasonic-treated materials in FAU zeolite synthesis had more crystalline matrices than those treated in the absence of ultrasound.

A study by Zhang et al. (2022) conducted the fabrication of zeolite NaP using waste coal fly ash via the ultrasonic-assisted hydrothermal technique. The study hinted that the employment of ultrasonication for the dissolution of precursor material reduced the crystallization time and temperature from 8 hours to 4 hours and 120 °C to 90 °C respectively. Similar findings were reported in (Adamczyk et al., 2021, Rozhkovskaya et al., 2021). Vaičiukynienė et al. (2020) compared the effect of ultrasonic treatment vs non-ultrasonic treatment synthesis of zeolite NaA. The study revealed that the solution where no ultrasound was employed exhibited amorphous irregularly ordered structures while the solution where ultrasound was used showed pronounced crystalline structures owing to the effect of ultrasound treatment at constant dissolution conditions.

A study by Ojumu et al. (2016) which aimed at substituting the high-temperature fusion treatment method employed ultrasonic treatment prior to hydrothermal treatment in zeolite A synthesis from waste coal fly ash. The study compared fusion treatment with ultrasonic treatment prior to hydrothermal treatment. In this study, it was observed that high-temperature fusion treatment for 90 minutes was successfully replaced with 10 minutes of ultrasound treatment. After ultrasound treatment, the study revealed that crystallization of a purer zeolite was archived in 2 hours with undesirable phases of hydroxy sodalite developing as the time increased at 90 °C. Therefore, this study emphasized that ultrasonic treatment has a positive effect on reducing crystallization treatment time.

2.10. Application of zeolites in fluoride removal in water

The utilization of natural and synthetic zeolitic materials for fluoride removal has been investigated throughout as a low-cost and sustainable approach in defluoridation studies (Zhao et al., 2023). According to Jia et al. (2022) and He et al. (2020), the alumina framework of the zeolite has a net negative charge which is repulsive towards anionic species such as fluoride. This lowers the efficiency of fluoride removal in water using zeolitic adsorbents. Because of this, natural zeolites are less favorable in defluoridation studies and studies tackle this issue through modification of zeolite with certain metal oxides to improve the zeolite adsorption efficiency (Yang et al., 2022a). Cations such as aluminum (Al), iron (Fe), lanthanum (La), and zirconium (Zr) have been employed in zeolite modification studies to enhance the fluoride adsorption efficiency and results indicate a recognized improvement of fluoride adsorption percentage of 80-99% by modified zeolitic material (Naskar, 2020, Chen et al., 2022, Yang et al., 2022b). Table 2.1 depicts the application of different modified zeolites in defluoridation studies and shows case their fluoride removal percentage along with their adsorption capacity throughout the years.

Table 2.1: Overview of zeolitic materials performance in defluoridation studies

Author	Zeolite type	F^- initial (mg/L)	Removal %	Adsorption Capacity (mg/g)
Sampedro-Duran et al. (2018)	Na Mod Zeolite	10	13	0.01
Panda and Kar (2018)	Zeolite A	25	70	-
Mukherjee et al. (2018)	Zeolite NaA	10	90	22.83
Nuñez et al. (2019)	Clinoptilolite zeolite	15	10	-
	Ca Mod Zeolite	15	45	-
Rahmani et al. (2019)	Al Mod Zeolite	10	-	1.14
	Fe Mod Zeolite	10	-	2.4
Ilayperuma and Attanayake (2019)	Zeolite	10	45	-
Mahvi et al. (2019)	Chitosan-Zeolite	100	95.2	47.6
Tian and Gan (2019)	Zeolite NaA	20	52.5	161
Naskar (2020)	Al Mod Zeolite NaA	50	99	36.13
Savari et al. (2020)	Zr Mod Zeolite	100	80	32.98
Tabi et al. (2021)	Al Mod zeolite	5	98.89	2.43
Yang et al. (2021)	Mn-Ti Mod zeolite	10	80	2.18
Aloulou et al. (2021)	CTAB Mod Zeolite	10	85	2.99
Gao et al. (2021)	Zr Mod Zeolite	5	94.89	0.36
Jia et al. (2022)	La-Fe Mod Zeolite	10	85	2.64
Yang et al. (2022b)	La Mod Zeolite	300	90	141
Chen et al. (2022)	AlOH Mod Zeolite	100	92	18.12
Yang et al. (2022a)	Fe-Zr Mod Zeolite	15	80	-
Ebsa (2023)	Zeolite Na-LSX	10	84.4	-

Cheng et al. (2018), conducted a study on the adsorption efficiency of titanium (Ti), magnesium (Mg), and aluminum (Al)-zeolite in fluoride adsorption studies from wastewater. The study observed a higher fluoride adsorption capacity of 1.64 mg/g in Ti^{4+} modified zeolite. However, Mg^{2+} and Al^{3+} modified zeolites exhibited low fluoride adsorption capacities of 0.80 mg/g and 0.88 mg/g respectively. The study explained that the higher adsorption capacity observed in Ti^{4+}-modified zeolite is due to more active sites found in the zeolite composite compared to Mg^{2+} and Al^{3+} modified zeolites. However, this could also be due to the high affinity of transition metals such as titanium towards halogen ions such as fluoride rather than magnesium and aluminum metals which are alkaline earth metals. Furthermore, the study concluded that the fluoride adsorption mechanism in modified zeolites is due to chemisorption. In contrast, the study documented a low adsorption capacity of fluoride of 0.48 mg/g in natural/ unmodified zeolite which indicates the low adsorption efficiency of unmodified zeolite structures.

Velazquez-Peña et al. (2017), iron-zirconium (FeZr) modified zeolite was investigated for its efficiency in fluoride adsorption studies. Initially, individual iron (Fe) incorporated zeolite and zirconium (Zr) incorporated zeolite were investigated in defluoridation studies. An adsorption capacity of 2.2 mg/g, 2.5 mg/g, and 1.9 mg/g was observed in zirconium (Zr) incorporated chabazite, mordenite, and clinoptilolite respectively. On the other hand, the adsorption capacities of 1.6 mg/g, 1.1 mg/g, and 0.8 mg/g were observed in iron (Fe) modified chabazite, clinoptilolite, and mordenite respectively. Furthermore, the higher adsorption capacities of 3.5 mg/g, 2.6 mg/g, and 1.8 mg/g were observed in FeZr-modified mordenite, chabazite, and clinoptilolite respectively. As a result, the study concluded that zirconium-modified zeolites have higher adsorption capacity due to the high affinity of zirconium to fluoride species. Hence, this study will utilize zirconium-modified zeolites for fluoride adsorption exploiting the intrinsic chemical affinity between zirconium and fluoride species and functionalized the adsorbent with silver metal oxides for simultaneous removal of pathogens. This affinity and adsorption efficiency of metals modified zeolite towards fluoride ions was also documented in a study by Zhou et al. (2014) and Gao et al. (2021). Additional advantages of metal-modified zeolites include high thermal and chemical stability and regeneration capability (Gao et al., 2021).

2.11. Application of zeolites in pathogens removal studies

Zeolites are among the notable water purification materials in a wide range of applications including pathogens removal in water. However, studies indicate that zeolite has minimal antimicrobial potency (Sutianingsih and Kurniawan, 2022). This is induced by the electronegative charge found in the alumina framework of the zeolite. Hence, this

electronegative charge repels the negative charges in the bacterial membrane causing no effect on the bacterial activity (Nikolov et al., 2023). Such a minimal effect of natural zeolite has been reported in several studies (Reeve and Fallowfield, 2018). Consequently, studies suggest that as the alumina framework of the zeolite is balanced by cations, monovalent cations such as copper, iron, zinc, and silver can be exchanged with these cations thereby enhancing the antimicrobial potency of the zeolite (Yao et al., 2019). The exchanged cations are then bonded with the zeolite matrices by electrostatic forces (Nikolov et al., 2023).

Mintcheva et al. (2021) investigated the potency of zinc oxide (ZnO) modified zeolite and copper-zinc oxide (Cu^{2+}/ZnO) loaded zeolite against *E. coli* and *S. aureus* pathogens. Using the agar well diffusion method the study conducted an antimicrobial test to calculate the minimum inhibition concentration (MIC) of the composite zeolite. The findings showed that ZnO-zeolite and $Cu2^{+}$/ZnO-zeolite effectively inhibited *E. Coli* bacteria with MIC values of 1 mg/mL and 0.2 mg/mL respectively. A similar trend was also observed against *S. aureus* bacteria in the study. In contrast, the study observed that unmodified synthetic zeolite had no antimicrobial activity toward both pathogens. Similar observations were made in a study by Vergara-Figueroa et al. (2019) and Kaali and Czél (2012).

Krishnani et al. (2012) also documented the potency of silver-exchanged zeolite against *V. cholerae*, *V. parahaemolyticus*, *V. harveyi,* and *E. coli* species. The study observed that the MIC of the composite against *E. coli* and *V. harveyi* was 0.04 and 0.05 mg/mL whilst for *V. parahaemolyticus* and *V. cholerae* and was 0.06. These results were observed after 48 hours of contact with the composite and show fast and effective potency of silver exchanged zeolite against pathogens. Similar potency of microbial inactivation was also reported and recommended in Dutta and Wang (2019) and Boschetto et al. (2012) studies.

Egger et al. (2009) incorporated silver ions in zeolite A and investigated its efficiency against multiple pathogens. The study determined the minimum inhibition concentration of the composite against various pathogens. The study recorded MIC values of 0.08, 0.04, 0.02, and 0.02 mg/ml against *enterococcus faecalis, E. coli*, *salmonella enterica,* and *staphylococcus aureus* respectively. The study reported that silver-exchanged zeolite exhibited excellent growth inhibition potency against a wide range of microorganisms. These results give evidence of metal oxide-modified zeolites' potency against pathogens. Several studies have reported the removal efficiency of pathogens of up to 90%. Table 2.2 shows the reported efficiency of various functionalized zeolites and their reported zones of inhibition.

Table 2.2: Overview studies of functionalized zeolite materials as antimicrobial agents

Author	Zeolite material	Volume (µL)	Concentration	Strains	MIC efficiency (%)	Zone of inhibition (mm)
Rodríguez et al. (2017)	Ag Mod Zeolite	-	-	*E. coli*	-	2.21
Sánchez et al. (2017)	Ag Mod Zeolite ZSM-5	-	-	*C. albicans*	-	3
				P. aeruginosa	-	5
				E. coli		10
Azizi et al. (2019)	ZnO-TiO2 Mod Zeolite 4A	20 µL	-	*L. monocytogenes*	-	9.51
				P. fluorescens	-	9.85
				E. Coli	-	10.73
				S. aureus	-	9.22
Cui et al. (2019)	Ag-Cu-Zn Mod Zeolite		-	*S. aureus*	-	7.68
				P. aeruginosa	-	8.77
				E. coli	-	9.75
				C. albicans	-	7.66
Vergara-Figueroa et al. (2019)	Cu2+ Mod Zeolite		1 mg/mL	*E. coli*	-	20.2
				S. aureus	-	23
Mortezaei et al. (2019)	Nano-Cu Mod Zeolite NaY	0,04mg	-	*P. aeruginosa*	-	22.5
				E. Coli	-	16.5
				S. aureus	-	28
				B. subtilis	-	24
Salar et al. (2020)	Ag-Chitosan Zeolite	-	-	*Streptococcus iniae*	-	16.25
Zendehdel et al. (2020)	Zn/Ag/Cu Exchanged Nano zeolite Y	10 µL	-	*E. coli*	-	18
				S. aureus	-	17.5
Rakesh and Antony (2021)	Cu Mod Zeolite 4A	-	-	*E. Coli*	-	16
				Bacillus subtilis	-	20
Amin et al. (2021)	Ag exchanged zeolite A		1.5 M	*V. parahaemolyticus*	60.2	
				V. Campbell	77.3	
Obijole et al. (2021)	Sod Zeolite	30 µL	-	*E. coli*	-	15
Muleja et al. (2022)	Co Mod Zeolite	20 µL	0.025 M	*E. coli*	90	36
Ibrahim et al. (2022)	Chitosan Np Zeolite Y	-	-	*S. mutans*	-	9.57
				E. faecalis	-	7.85
Wakweya and Jifar (2023)	Ag-ZnO Zeolite	10 µL	-	*S. aureus*	-	19.6
				E. coli	-	15.5

The reported mechanism of inactivation of pathogens through metal oxides incorporated in zeolites is through their release from the zeolite framework (Salim et al., 2017). The metal ions in the zeolite framework are then slowly released through electrostatic interaction with the bacterial membrane. According to Nikolov et al. (2023), some microbes have a membrane wall composed of anionic surface charges that interact with positively charged ions present in the zeolite framework. This interaction stimulates the reactive oxygen species and induces oxidation of the bacteria through oxidative stress (Ayinde et al., 2022). Consequently, this results in disruption of the cell membrane, and damage of the mitochondria and structural DNA. Hence, microbial production activity is ceased.

2.12. Conclusion

This review has provided an understanding on fluoride and pathogens as contaminants in drinking water at elevated levels causing diseases such as fluorosis, cholera, fever, and diarrhea. More than 200 million people have been reported suffering from endemic fluorosis while 1 million people succumb to death due to waterborne pathogen diseases. The literature revealed that cases of groundwater contamination have been documented in several countries such as Nigeria, Thailand, India, and South Africa with levels exceeding 10 mg/L for fluoride and 100 cfu/100 mL for pathogens. Factors such as rock weathering, mobility, and climate are the main drivers of groundwater contamination by fluoride and anthropogenic activities for pathogens in groundwater. Several methods such as ion exchange, coagulation, adsorption, disinfection, and UV irradiation are among the employed treatment strategies for fluoride and pathogens in water. Adsorbents functionalized with cations such as red mud doped iron, silver, loaded cellulose, iron-loaded polymer composite, and mechanochemically activated adsorbents are among the investigated adsorbents with a percentage fluoride removal of up to 90% and exhibited antimicrobial potency.

In addition, this section provided an overview of zeolite adsorbents as multifunctional adsorbents for fluoride and pathogens removal. Zeolite adsorbents are eco-friendly and less costly, with simplicity of use, molecular sieving capability, and regeneration potential which showcases their practicality and sustainability. Outlined synthesis routes of zeolites such as the traditional hydrothermal method coupled with ultrasound technologies offer advantages including high cation exchange capacity and higher surface area. Also, important parameters such as concentrations of dissolution agent, aging times, hydrothermal temperatures, and times can be adjusted to produce zeolite with unique properties. Scientists have investigated several adsorbents exchanged with cations for reinforced fluoride and pathogen removal hence this study aims to develop a multifunctional zeolite adsorbent for fluoride and pathogens removal in water.

References

Abdellaoui, Y., Abou Oualid, H., Hsini, A., El Ibrahimi, B., Laabd, M., El Ouardi, M., Giácoman-Vallejos, G. & Gamero-Melo, P. 2021. Synthesis of zirconium-modified merlinoite from fly ash for enhanced removal of phosphate in aqueous medium: Experimental studies supported by monte carlo/sa simulations. *Chemical Engineering Journal,* 404.

Abdullahi, T., Harun, Z. & Othman, M. H. D. 2017. A review on sustainable synthesis of zeolite from kaolinite resources via hydrothermal process. *Advanced Powder Technology,* 28**,** 1827-1840.

Adamczyk, Z., Cempa, M. & Białecka, B. 2021. The influence of ultrasound on fly ash zeolitisation process efficiency. *Mineral Processing and Extractive Metallurgy Review,* 43**,** 427-439.

Akkoca, D. B., Yılgın, M., Ural, M., Akçin, H. & Mergen, A. 2013. Hydrothermal and thermal treatment of natural clinoptilolite zeolite from bigadiç, turkey: An experimental study. *Geochemistry International,* 51**,** 495-504.

Aloulou, H., Ghorbel, A., Aloulou, W., Ben Amar, R. & Khemakhem, S. 2021. Removal of fluoride ions (f(-)) from aqueous solutions using modified turkish zeolite with quaternary ammonium. *Environmental Technology,* 42**,** 1353-1365.

Amin, Z., Waly, N. A. & Arshad, S. E. 2021. Biofilm inhibition and antimicrobial properties of silver-ion-exchanged zeolite a against vibrio spp marine pathogens. *Applied Sciences,* 11.

Arni, S., Sumari, S., Santoso, A. & Tamara, T. 2020. The effect of aging and crystallization time on the synthesis and characteristics of zeolite-y from malang-quartzite silica.

Ayele, L., Pérez-Pariente, J., Chebude, Y. & Díaz, I. 2016. Conventional versus alkali fusion synthesis of zeolite a from low grade kaolin. *Applied Clay Science,* 132-133**,** 485-490.

Ayinde, W. B., Gitari, M. W., Smith, J. A. & Samie, A. 2022. Sorption of fluoride and bacterial disinfection property of biosynthesized nanofibrous cellulose decorated ag-mgo-nanohydroxyapatite composite for household water treatment. *Polymers (Basel),* 14.

Ayoola, A. A., Hymore, F. K., Ojewumi, M. E. & Uwoghiren, O. J. 2018. Effects of sodium hydroxide concentration on zeolite y synthesized from elefun kaolinite clay in nigeria. *International Journal of Applied Engineering Research*, 1536-1536.

Azizi, L. M., Ehsani, A., Divband, B. & Alizadeh, S. M. 2019. Antimicrobial activity of titanium dioxide and zinc oxide nanoparticles supported in 4a zeolite and evaluation the morphological characteristic. *Scientific Reports,* 9**,** 17439.

Baek, W., Ha, S., Hong, S., Kim, S. & Kim, Y. 2018. Cation exchange of cesium and cation selectivity of natural zeolites chabazite, stilbite, and heulandite. *Microporous and Mesoporous Materials*.

Bahri, A., Drechsel, P., Raschid-Sally, L. & Redwood, M. 2009. *Wastewater irrigation and health: Assessing and mitigating risk in low-income countries*, Routledge.

Bai, S.-X., Zhou, L.-M., Chang, Z.-B., Zhang, C. & Chu, M. 2018. Synthesis of na-x zeolite from longkou oil shale ash by alkaline fusion hydrothermal method. *Carbon Resources Conversion,* 1**,** 245-250.

Bhatt, A., Arora, P. & Prajapati, S. K. 2020. Occurrence, fates and potential treatment approaches for removal of viruses from wastewater: A review with emphasis on sars-cov-2. *Journal of Environmental Chemical Engineering,* 8**,** 104429.

Bhowmik, A. D., Shaw, P., Mondal, P., Munshi, C., Chatterjee, S., Bhattacharya, S. & Chattopadhyay, A. 2019. Incidence of fluorosis and urinary fluoride concentration are not always positively correlated with drinking water fluoride level. *Current Science,* 116.

Boschetto, D. L., Lerin, L., Cansian, R., Pergher, S. B. C. & Di Luccio, M. 2012. Preparation and antimicrobial activity of polyethylene composite films with silver exchanged zeolite-y. *Chemical Engineering Journal,* 204-206**,** 210-216.

Bradford, S. A. & Harvey, R. W. 2016. Future research needs involving pathogens in groundwater. *Hydrogeology Journal,* 25**,** 931-938.

Bukhari, S. S., Behin, J., Kazemian, H. & Rohani, S. 2015. Conversion of coal fly ash to zeolite utilizing microwave and ultrasound energies a review. *Fuel*, 250-266.

Bunmai, K., Osakoo, N., Deekamwong, K., Kosri, C., Khemthong, P. & Wittayakun, J. 2020. Fast synthesis of zeolite nap by crystallizing the nay gel under microwave irradiation. *Materials Letters,* 272.

Campoverde, J. & Guaya, D. 2023. From waste to added-value product: Synthesis of highly crystalline lta zeolite from ore mining tailings. *Nanomaterials (Basel),* 13.

Cao, C., Xuan, W., Yan, S. & Wang, Q. 2023. Zeolites synthesized from industrial and agricultural solid waste and their applications: A review. *Journal of Environmental Chemical Engineering,* 11.

Cataldo, E., Salvi, L., Paoli, F., Fucile, M., Masciandaro, G., Manzi, D., Masini, C. M. & Mattii, G. B. 2021. Application of zeolites in agriculture and other potential uses: A review. *Agronomy,* 11.

Chakraborty, R., Asthana, A., Singh, A. K., Jain, B. & Susan, A. B. H. 2020. Adsorption of heavy metal ions by various low-cost adsorbents: A review. *International Journal of Environmental Analytical Chemistry,* 102**,** 342-379.

Chen, J., Yang, R., Zhang, Z. & Wu, D. 2022. Removal of fluoride from water using aluminum hydroxide-loaded zeolite synthesized from coal fly ash. *Journal of hazardous materials,* 421**,** 126817.

Cheng, L., Guan, Z., Si, L., Mang, C., Weng, X., Zhang, Q. & Ma, Z. 2018. Fluoride ion adsorption from wastewater using magnesium(ii), aluminum(iii) and titanium(iv) modified natural zeolite: Kinetics, thermodynamics, and mechanistic aspects of adsorption. *Journal of Water Reuse and Desalination,* 8**,** 479-489.

Ciobanu, R., Mihai, M. & Teodosiu, C. 2022. An overview of natural organic matter removal by coagulation in drinking water treatment. *Gheorghe Asachi Technical University of Iaşi,***,** 69-92.

Collins, F., Rozhkovskaya, A., Outram, J. G. & Millar, G. J. 2020. A critical review of waste resources, synthesis, and applications for zeolite lta. *Microporous and Mesoporous Materials,* 291.

Corma, A., Zones, S. & Cejka, J. 2010. Zeolites and catalysis synthesis, reactions and applications. *John Wiley & Sons*.

Crini, G. & Lichtfouse, E. 2018. Advantages and disadvantages of techniques used for wastewater treatment. *Environmental Chemistry Letters,* 17**,** 145-155.

Cui, J., Yeasmin, R., Shao, Y., Zhang, H., Zhang, H. & Zhu, J. 2019. Fabrication of ag+, cu2+, and zn2+ ternary ion-exchanged zeolite as an antimicrobial agent in powder coating. *Industrial & Engineering Chemistry Research,* 59**,** 751-762.

Dabbawala, A. A., Ismail, I., Vaithilingam, B. V., Polychronopoulou, K., Singaravel, G., Morin, S., Berthod, M. & Al Wahedi, Y. 2020. Synthesis of hierarchical porous zeolite-y for enhanced co2 capture. *Microporous and Mesoporous Materials,* 303.

Dandie, C. E., Ogunniyi, A. D., Ferro, S., Hall, B., Drigo, B., Chow, C. W. K., Venter, H., Myers, B., Deo, P., Donner, E. & Lombi, E. 2019. Disinfection options for irrigation water: Reducing the risk of fresh produce contamination with human pathogens. *Critical Reviews in Environmental Science and Technology,* 50**,** 2144-2174.

Dayarathne, H. N. P., Angove, M. J., Aryal, R., Abuel-Naga, H. & Mainali, B. 2021. Removal of natural organic matter from source water: Review on coagulants, dual coagulation, alternative coagulants, and mechanisms. *Journal of Water Process Engineering,* 40.

Delorme, M. M., Guimarães, J. T., Coutinho, N. M., Balthazar, C. F., Rocha, R. S., Silva, R., Margalho, L. P., Pimentel, T. C., Silva, M. C., Freitas, M. Q., Granato, D., Sant'ana, A. S., Duart, M. C. K. H. & Cruz, A. G. 2020. Ultraviolet radiation: An interesting technology to preserve quality and safety of milk and dairy foods. *Trends in Food Science & Technology,* 102**,** 146-154.

Dong, Y., Jiang, Z., Hu, Y., Jiang, Y., Tong, L., Yu, Y., Cheng, J., He, Y., Shi, J. & Wang, Y. 2023. Pathogen contamination of groundwater systems and health risks. *Critical Reviews in Environmental Science and Technology***,** 1-23.

Dutta, P. & Wang, B. 2019. Zeolite-supported silver as antimicrobial agents. *Coordination Chemistry Reviews,* 383**,** 1-29.

Ebsa, D. G. 2023. Defluoridation of drinking water by modified natural zeolite with cationic surfactant, in the case of ziway town, ethiopia. *Cleaner Engineering and Technology,* 12.

Edokpayi, J. N., Rogawski, E. T., Kahler, D. M., Hill, C. L., Reynolds, C., Nyathi, E., Smith, J. A., Odiyo, J. O., Samie, A., Bessong, P. & Dillingham, R. 2018. Challenges to

sustainable safe drinking water: A case study of water quality and use across seasons in rural communities in limpopo province, south africa. *Water (Basel),* 10.

Egger, S., Lehmann, R. P., Height, M. J., Loessner, M. J. & Schuppler, M. 2009. Antimicrobial properties of a novel silver-silica nanocomposite material. *Appl Environ Microbiol,* 75**,** 2973-6.

Elumalai, V., Rajmohan, N., Sithole, B., Li, P., Uthandi, S. & Van Tol, J. 2023. Geochemical evolution and the processes controlling groundwater chemistry using ionic ratios, geochemical modelling and chemometric analysis in umhlathuze catchment, kwazulu-natal, south africa. *Chemosphere,* 312**,** 137179.

Enitan-Folami, A. M., Mutileni, N., Odiyo, J. O., Swalaha, F. M. & Edokpayi, J. N. 2019. Hydrochemical, bacteriological assessment, and classification of groundwater quality in thulamela municipality, south africa: Potential health risk. *Human and Ecological Risk Assessment: An International Journal,* 26**,** 2044-2058.

Gao, Y., Li, M., Ru, Y. & Fu, J. 2021. Fluoride removal from water by using micron zirconia/zeolite molecular sieve: Characterization and mechanism. *Groundwater for Sustainable Development,* 13.

Gitari, W. M., Obijole, O. A. & Mudzielwana, R. 2023. Synthesis of porous hydroxysodalite from aluminosilicate rich clay soils application towards fluoride and pathogen removal.

Grzegorzek, M., Wartalska, K. & Kaźmierczak, B. 2023. Review of water treatment methods with a focus on energy consumption. *International Communications in Heat and Mass Transfer,* 143.

Guozhi, L., Zhang, T., Cheng, C., Zhang, W., Wang, L., Wang, Y. & Zhang, Z. 2019. Zeolite a preparation from high alumina fly ash of china using alkali fusion and hydrothermal synthesis method. *Materials Research Express,* 6.

Gupta, A. & Ayoob, S. 2016. *Fluoride in drinking water.* .

Gupta, A. R., Ranawat, B., Singh, A., Yadav, A. & Sharma, S. 2021. Zirconium-silver nano organo-bimetallic network for scavenging hazardous ions from water and its antibacterial potentiality: An environment-friendly approach. *Journal of Environmental Chemical Engineering,* 9.

Habibi-Yangjeh, A., Asadzadeh-Khaneghah, S., Feizpoor, S. & Rouhi, A. 2020. Review on heterogeneous photocatalytic disinfection of waterborne, airborne, and foodborne viruses: Can we win against pathogenic viruses? *Journal of colloid and interface science,* 580**,** 503-514.

Habiyakare, T., Schurer, J. M., Poole, B., Murcott, S., Migabo, B., Mardochee, B., Amuguni, J. H. & Morgan, J. P. 2021. Dental fluorosis among people and livestock living on gihaya island in lake kivu, rwanda. *One Health Outlook,* 3**,** 23.

He, J., Yang, Y., Wu, Z., Xie, C., Zhang, K., Kong, L. & Liu, J. 2020. Review of fluoride removal from water environment by adsorption. *Journal of Environmental Chemical Engineering,* 8.

Hong, S. & Um, W. 2021. Top-down synthesis of nap zeolite from natural zeolite for the higher removal efficiency of cs, sr, and ni. *Minerals,* 11.

Hossain, M. & Patra, P. K. 2020. Hydrogeochemical characterisation and health hazards of fluoride enriched groundwater in diverse aquifer types. *Environmental Pollution,* 258**,** 113646.

Ibrahim, A. I., Moodley, D., Maboza, E., Olivier, A. & Petrik, L. 2022. Zeolite-y loaded chitosan nanoparticles nanocomposite as endodontic intra-canal medicament: Synthesis, antimicrobial and cytotoxic activity: An in vitro study.

Ibsaine, F., Azizi, D., Dionne, J., Tran, L. H., Coudert, L., Pasquier, L.-C. & Blais, J.-F. 2023. Synthesis of zeolites using aluminosilicate residues from the lithium extraction.

Ilayperuma, T. D. & Attanayake, A. M. a. N. B. 2019. Removal of fluoride from water using zeolite.

Izah, S. C., Ngun, C. T. & Richard, G. 2022. Microbial quality of groundwater in the niger delta region of nigeria: Health implications and effective⇓ treatment technologies. *Current directions in water scarcity research.* Elsevier.

Jayashree, E., D., Pooja, G., Senthil Kumar, P. & Prasannamedha, G. 2020. A review on fluoride: Treatment strategies and scope for further research. *Desalination and Water Treatment,* 200**,** 167-186.

Jha, S. K., Singh, R. K., Damodaran, T., Mishra, V. K., Sharma, D. K. & Rai, D. 2013. Fluoride in groundwater: Toxicological exposure and remedies. *Journal of Toxicology and Environmental Health: Part B, Critical Reviews,* 16**,** 52-66.

Jia, C., Fan, Y., Jiang, R., Su, P., Liu, S., Zhang, X. & Wang, J. 2022. Preparation of la(iii), fe(iii) modified zeolite molecular sieves for the removal of fluorine from water. *Water,* 14.

Johnson, E. B. G. & Arshad, S. E. 2014. Hydrothermally synthesized zeolites based on kaolinite: A review. *Applied Clay Science,* 97-98**,** 215-221.

Ju, T., Jiang, J., Meng, Y., Yan, F., Xu, Y., Gao, Y. & Aihemaiti, A. 2020. An investigation of the effect of ultrasonic waves on the efficiency of silicon extraction from coal fly ash. *Ultrasonics sonochemistry,* 60**,** 104765.

Kaali, P. & Czél, G. 2012. Single, binary and ternary ion exchanged zeolite as an effective bioactive filler for biomedical polymer composites. *Materials Science Forum,* 729**,** 234-239.

Kabir, H., Gupta, A. K. & Tripathy, S. 2019. Fluoride and human health: Systematic appraisal of sources, exposures, metabolism, and toxicity. *Critical Reviews in Environmental Science and Technology,* 50**,** 1116-1193.

Khabo-Mmekoa, C. M., Genthe, B. & Momba, M. N. B. 2022. Enteric pathogens risk factors associated with household drinking water: A case study in ugu district kwa-zulu natal province, south africa. *International Journal of Environmental Research and Public Health,* 19.

Khairnar, M. R., Dodamani, A. S., Jadhav, H. C., Naik, R. G. & Deshmukh, M. A. 2015. Mitigation of fluorosis - a review. *Journal of Clinical and Diagnostic Research,* 9**,** ZE05-9.

Khaleque, A., Alam, M. M., Hoque, M., Mondal, S., Haider, J. B., Xu, B., Johir, M. a. H., Karmakar, A. K., Zhou, J. L., Ahmed, M. B. & Moni, M. A. 2020. Zeolite synthesis from low-cost materials and environmental applications: A review. *Environmental Advances,* 2.

Khan, M. S. & Ahmad, S. R. 2012. Microbiological contamination in groundwater of wah area. *Pakistan Journal of Science***,** 20-23.

Khatamian, M., Divband, B. & Shahi, R. 2019. Ultrasound assisted co-precipitation synthesis of fe3o4bentonite nanocomposite performance for nitrate, bod and cod water treatment. *Journal of Water Process Engineering*.

Kothari, V., Vij, S., Sharma, S. & Gupta, N. 2021. Correlation of various water quality parameters and water quality index of districts of uttarakhand. *Environmental and Sustainability Indicators,* 9.

Krishnani, K. K., Zhang, Y., Xiong, L., Yan, Y., Boopathy, R. & Mulchandani, A. 2012. Bactericidal and ammonia removal activity of silver ion-exchanged zeolite. *Bioresource Technology,* 117**,** 86-91.

Król, M. 2020. Natural vs. Synthetic zeolites. *Crystals,* 10.

Kumar, M. M. & Jena, H. 2022. Direct single-step synthesis of phase pure zeolite na–p1, hydroxy sodalite and analcime from coal fly ash and assessment of their cs+ and sr2+ removal efficiencies. *Microporous and Mesoporous Materials,* 333.

Kumar, N., Tiwari, K. R., Meenu, K., Sharma, A., Jain, A., Singh, S. & Tomar, R. 2019. Utilization of various analogy of synthetic nanoporous zeolites and composite of zeolites for decontamination/detoxification of cwa simulants—an updated review. *International Journal of Nonferrous Metallurgy,* 08**,** 35-71.

Kumar, R., Ali, S., Sandun Sandanayake, S., Islam, M. A., Ijumulana, J., Maity, J. P., Vithanage, M., Armienta, M. A., Sharma, P., Hamisi, R. & Kimambo, V. 2023. Fluoride as a global groundwater contaminan.

Lacson, C. F. Z., Lu, M.-C. & Huang, Y.-H. 2021. Fluoride-containing water: A global perspective and a pursuit to sustainable water defluoridation management -an overview. *Journal of Cleaner Production,* 280.

Latif, S., Alim, M. A. & Rahman, A. 2022. Disinfection methods for domestic rainwater harvesting systems: A scoping review. *Journal of Water Process Engineering,* 46.

Le, T. M., Nguyen, G. T., Dat, N. D. & Tran, N. T. 2023. An innovative approach based on microwave radiation for synthesis of zeolite 4a and porosity enhancement. *Results in Engineering,* 19.

Lee, W.-H., Lin, Y.-W. & Lin, K.-L. 2022. Parameter optimization, characterization, and crystallization mechanisms underlying the synthesis of zeolite a using liquid crystal

display waste glass and sandblasting waste as alternative raw materials. *Journal of Environmental Chemical Engineering,* 10.

Lee, Y.-R., Soe, J. T., Zhang, S., Ahn, J.-W., Park, M. B. & Ahn, W.-S. 2017. Synthesis of nanoporous materials via recycling coal fly ash and other solid wastes: A mini review. *Chemical Engineering Journal,* 317**,** 821-843.

Li, M., Li, X., Jiang, M., Liu, X., Chen, Z., Wang, S., James, T. D., Wang, L. & Xiao, H. 2020. Engineering a ratiometric fluorescent sensor membrane containing carbon dots for efficient fluoride detection and removal. *Chemical Engineering Journal,* 399.

Li, Y., Zhang, M., Mi, W., Ji, L., He, Q., Xie, S., Xiao, C. & Bi, Y. 2024. Spatial distribution of groundwater fluoride and arsenic and its related disease in typical drinking endemic regions. *Science of The Total Environment,* 906**,** 167716.

Lin, S., Jiang, X., Zhao, Y. & Yan, J. 2022. Zeolite greenly synthesized from fly ash and its resource utilization: A review. *Science of The Total Environment,* 851**,** 158182.

Ling, Y., Podgorski, J., Sadiq, M., Rasheed, H., Eqani, S. & Berg, M. 2022. Monitoring and prediction of high fluoride concentrations in groundwater in pakistan. *Science of The Total Environment,* 839**,** 156058.

Liu, J., Yang, S., Luo, M. J., Chen, T., Ma, X. J., Tao, N., Zhao, X. & Wang, D. H. 2019. Association between dietary patterns and fluorosis in guizhou, china. *Frontiers in Nutrition,* 6**,** 189.

Liu, J., Zhang, J., Zhang, H., Zhang, F., Zhu, M., Hu, N., Chen, X. & Kita, H. 2020. Synthesis of hierarchical zeolite t nanocrystals with the assistance of zeolite seed solution. *Journal of Solid State Chemistry,* 285.

Lugo, J. L., Lugo, E. R. & Puente, M. D. L. 2021. A systematic review of microorganisms as indicators of recreational water quality in natural and drinking water systems. *Journal of Water and Health,* 19**,** 20-28.

Lv, Y., Ye, C., Zhang, J. & Guo, C. 2020. Rapid and efficient synthesis of highly crystalline ssz-13 zeolite by applying high shear mixing in the aging process. *Microporous and Mesoporous Materials,* 293.

Mahagamage, M. G. Y. L., Pathirage, M. V. S. C. & Manage, P. M. 2020. Contamination status of salmonella spp., shigella spp. And campylobacter spp. In surface and groundwater of the kelani river basin, sri lanka. *Water,* 12.

Mahima Kumar, M., Irshad, K. A. & Jena, H. 2021. Removal of cs+ and sr2+ ions from simulated radioactive waste solutions using zeolite-a synthesized from kaolin and their structural stability at high pressures. *Microporous and Mesoporous Materials,* 312.

Mahvi, A. H., Mostafapour, F. K., Balarak, D. & Khatibi, A. D. 2019. Adsorption of fluoride from aqueous solutions by a chitosanzeolite composite. 546-552.

Makgabutlane, B., Nthunya, L. N., Nxumalo, E. N., Musyoka, N. M. & Mhlanga, S. D. 2020. Microwave irradiation-assisted synthesis of zeolites from coal fly ash: An optimization study for a sustainable and efficient production process. *ACS Omega,* 5**,** 25000-25008.

Mccaffrey, L. P. & Willis, J. P. 2001. Distribution of fluoride-rich groundwater in the eastern and mogwase regions of the northern and north-west provinces. *Pretoria Water Research Commission*.

Messing, G. L. 2021. Calcination and phase transformations. *In:* POMEROY, M. (ed.) *Encyclopedia of materials: Technical ceramics and glasses.* Oxford: Elsevier.

Mgbemere, H., Ekpe, I. & Lawal, G. 2017. Zeolite synthesis, characterization and application areas a review. *International Research Journal of Environmental Science*.

Mintcheva, N., Panayotova, M., Gicheva, G., Gemishev, O. & Tyuliev, G. 2021. Effect of exchangeable ions in natural and modified zeolites on ag content, ag nanoparticle formation and their antibacterial activity. *Materials (Basel),* 14.

Mitiku, A. A. 2020. A review on water pollution causes, effects and treatment methods. *International Journal of Pharmaceutical Sciences Review***,** 94-101.

Mohd, N., Liyana, S. Y., Yin, F. C. & Thiam, L. 2020. Controlled growth of faujasite zeolite with nax topology by manipulating solution aging and na2o/al2o3 ratios. *Colloids and Surfaces A: Physicochemical and Engineering Aspects,* 600.

Mortezaei, Z., Zendehdel, M. & Bodaghifard, M. A. 2019. Cu complex grafted on the porous materials: Synthesis, characterization and comparison of their antibacterial activity with nano-cu/nay zeolite. *Journal of the Iranian Chemical Society,* 17**,** 283-295.

Mukherjee, I. & Singh, U. K. 2018. Groundwater fluoride contamination, probable release, and containment mechanisms: A review on indian context. *Environmental Geochemistry and Health,* 40**,** 2259-2301.

Mukherjee, S., Barman, S. & Halder, G. 2018. Fluoride uptake by zeolite naa synthesized from rice husk: Isotherm, kinetics, thermodynamics and cost estimation. *Groundwater for Sustainable Development,* 7**,** 39-47.

Muleja, A., Tshangana, C., Gorimbo, J., Kamika, I. & Mamba, B. 2022. The inactivation of escherichia coli using cobalt-modified natural zeolite from a south african mine. *International Journal of Environmental Science and Technology,* 19**,** 9377-9392.

Munzhelele, E. P., Ayinde, W. B., Mudzielwana, R. & Gitari, W. M. 2021. Synthesis of fe doped poly p-phenylenediamine composite: Co-adsorption application on toxic metal ions (f(-) and as(3+)) and microbial disinfection in aqueous solution. *Toxics,* 9.

Mutileni, N., Mudau, M. & Edokpayi, J. N. 2023. Water quality, geochemistry and human health risk of groundwater in the vyeboom region, limpopo province, south africa. *Scientific Reports,* 13**,** 19071.

Nakhaei, P. A. & Mohammadi, A. 2021. Effects of synthesis parameters on organic template-free preparation of zeolite y. *Journal of Inorganic and Organometallic Polymers and Materials,* 31**,** 2501-2510.

Naskar, M. K. 2020. Preparation of colloidal hydrated alumina modified naa zeolite derived from rice husk ash for effective removal of fluoride ions from water medium. *Journal of Asian Ceramic Societies,* 8**,** 437-447.

Ncube, E. J. & Schutte, C. F. 2005. The occurrence of fluoride in south african groundwater a water quality and health problem. *Water Sa***,** 35-40.

Nehra, S., Dhillon, A. & Kumar, D. 2020. Freeze–dried synthesized bifunctional biopolymer nanocomposite for efficient fluoride removal and antibacterial activity. Journal of environmental sciences, 94,.Pdf>.

Nguyen, D. K., Dinh, V. P., Dang, N. T., Khan, D. T., Hung, N. T. & Thi Tran, N. H. 2023. Effects of aging and hydrothermal treatment on the crystallization of zsm-5 zeolite synthesis from bentonite. *Royal Society of Chemistry Advances,* 13**,** 20565-20574.

Nikolov, A., Dobreva, L., Danova, S., Miteva-Staleva, J., Krumova, E., Rashev, V. & Vilhelmova-Ilieva, N. 2023. Natural and modified zeolite clinoptilolite with antimicrobial properties a review.

Nuñez, I. L., Perez, M. V. & Dosamante, K. A. 2019. Clinoptilolite modified by calcium and hydroxyl ions for removal of fluoride from aqueous solution. *Journal of Physics Conference Series* 1.

Obijole, O., Mugera, G. W., Mudzielwana, R., Ndungu, P., Samie, A. & Babatunde, A. 2021. Hydrothermally treated aluminosilicate clay (htac) for remediation of fluoride and pathogens from water: Adsorbent characterization and adsorption modelling. *Water Resources and Industry,* 25.

Obijole, O. A., Gitari, M. W., Ndungu, P. G. & Samie, A. 2019. Mechanochemically activated aluminosilicate clay soils and their application for defluoridation and pathogen removal from groundwater. *International Journal of Environmental Research and Public Health,* 16.

Odiyo, J. O. & Makungo, R. 2012. Fluoride concentrations in groundwater and impact on human health in siloam village, limpopo province, south africa. *Water SA,* 38.

Odiyo, J. O. & Makungo, R. 2018. Chemical and microbial quality of groundwater in siloam village, implications to human health and sources of contamination. *International Journal of Environmental Research and Public Health,* 15.

Ojumu, T. V., Du Plessis, P. W. & Petrik, L. F. 2016. Synthesis of zeolite a from coal fly ash using ultrasonic treatment–a replacement for fusion step. *Ultrasonics sonochemistry,* 31**,** 342-349.

Onipe, T., Edokpayi, J. N. & Odiyo, J. O. 2020. A review on the potential sources and health implications of fluoride in groundwater of sub-saharan africa. *Journal of environmental science and health. Part A, Toxic/Hazardous Substances and Environmental Engineering* 55**,** 1078-1093.

Onipe, T., Edokpayi, J. N. & Odiyo, J. O. 2021. Geochemical characterization and assessment of fluoride sources in groundwater of siloam area, limpopo province, south africa. *Scientific Reports,* 11**,** 14000.

Panagiotopoulou, C., Kontori, E., Perraki, T. & Kakali, G. 2006. Dissolution of aluminosilicate minerals and by-products in alkaline media. *Journal of Materials Science,* 42**,** 2967-2973.

Panda, L. & Kar, B. B. 2018. Preparation of fly ash based zeolite for fluoride removal. *Asian Journal of Water, Environment and Pollution,* 15**,** 105-113.

Pandey, P. K., Kass, P. H., Soupir, M. L., Biswas, S. & Singh, V. P. 2014. Contamination of water resources by pathogenic bacteria. *Amb Express***,** 1-16.

Patuwan, S. Z. & Arshad, S. E. 2021. Important synthesis parameters affecting crystallization of zeolite t a review. *Materials*.

Pei, Y., Zhong, Y., Xie, Q. & Chen, N. 2022. Two-step hydrothermal synthesis and conversion mechanism of zeolite x from stellerite zeolite. *Royal Society of Chemistry Advances,* 12**,** 3313-3321.

Pillai, P., Dharaskar, S., Pandian, S. & Panchal, H. 2021. Overview of fluoride removal from water using separation techniques. *Environmental Technology & Innovation,* 21.

Price, L. A., Ridley, C. J., Bull, C. L., Wells, S. A. & Sartbaeva, A. 2021. Determining the structure of zeolite frameworks at high pressures. *CrystEngComm,* 23**,** 5615-5623.

Pullerits, K., Ahlinder, J., Holmer, L., Salomonsson, E., Öhrman, C., Jacobsson, K., Dryselius, R., Forsman, M., Paul, C. J. & Rådström, P. 2020. Impact of uv irradiation at full scale on bacterial communities in drinking water. *NPJ Clean Water,* 3**,** 11.

Qu, L., Gan, Y., Xu, B., Wu, B., Wu, W., Huang, T., Kong, M., Chao, J., Ding, C. & Cui, Y. 2023. Application of a novel zirconium coagulant in the coagulation-ultrafiltration process: Fluoride removal and membrane fouling alleviation. *Chemical Engineering Journal,* 478.

Rahmani, K., Rahmani, H., Moeinian, K., Sarafraz, M. & Rahmani, A. 2019. Water defluoridation using modify zeolite by al+ 3 ions and nanoscale zero-valent iron (nzvi) in a fixed bed column. *Iranian Jour*.

Rai, A. 2020. Fluoride contamination issues of groundwater in rajasthan: A review. *SGVU J. Centre for Climate Change & Water Research,* 7**,** 18-33.

Rakesh, K. E. & Antony, R. 2021. Controlled drug release and efficient cod removal using copper immobilized zeolite 4a nanocomposite. *Biocatalysis and Agricultural Biotechnology,* 33.

Ramírez Bocanegra, N., Suarez Vázquez, S. I., Sandoval Rangel, L., Garza Navarro, M. A., Rivera De La Rosa, J., Lucio Ortiz, C. J., Flores-Escamilla, G. A., Santos López, I. A., Carrillo Pedraza, E. S., Bravo Sánchez, M. & De Haro Del Río, D. A. 2022. Catalytic conversion of gvl to biofuels using cu and pt catalysts over microwave-synthesized fau zeolite. *Catalysis Today,* 392-393**,** 105-115.

Reeve, P. J. & Fallowfield, H. J. 2018. Natural and surfactant modified zeolites: A review of their applications for water remediation with a focus on surfactant desorption and toxicity towards microorganisms. *Journal of Environmental Management,* 205**,** 253-261.

Ren, X., Qu, R., Liu, S., Zhao, H., Wu, W., Song, H., Zheng, C., Wu, X. & Gao, X. 2020. Synthesis of zeolites from coal fly ash for removal of harmful gaseous pollutants: A review. *Aerosol and Air Quality Research,* 20**,** 1127-1144.

Rodríguez, B. G., López, C. R., Olguín, M. T., Valencia, A., Mercado, C. A., Peña, E. R. & Muñoz, A. E. 2017. Growth of ag particles from ag-zeolite by pulsed discharges in water and their antibacterial activity. *Microporous and Mesoporous Materials,* 244**,** 235-243.

Rozhkovskaya, A., Rajapakse, J. & Millar, G. J. 2021. Optimisation of zeolite lta synthesis from alum sludge and the influence of the sludge source. *Journal of Environmental Sciences (China),* 99**,** 130-142.

Ryu, G. U., Khalid, H. R., Lee, N., Wang, Z. & Lee, H. K. 2020. The effects of naoh concentration on the hydrothermal synthesis of a hydroxyapatite–zeolite composite using blast furnace slag. *Minerals,* 11.

Salahudeen, N. 2022. A review on zeolite: Application, synthesis and effect of synthesis parameters on product properties. *Chemistry Africa,* 5**,** 1889-1906.

Salar, H. F., Ramezanian, N. & Shokouh, S. Z. Synthesis of chitosan/zeolite/silver nanoparticles composites: Antibacterial activity against aquatic bacteria. Eco-friendly and Smart Polymer Systems 13, 2020. Springer, 306-309.

Salim, M. M., Ahmad, N. & Malek, N. N. 2017. Review of modified zeolites by surfactant and silver as antibacterial agents. 1-20.

Samanta, N. S., Das, P. P., Mondal, P., Changmai, M. & Purkait, M. K. 2022. Critical review on the synthesis and advancement of industrial and biomass waste-based zeolites and their applications in gas adsorption and biomedical studies. *Journal of the Indian Chemical Society,* 99.

Sampedro-Duran, J., Torres-Rodríguez, M., Gutiérrez-Arzaluz, M. & Mugica-Álvarez, V. 2018. Removal of fluoride in water with mexican natural zeolite. *The 2nd International Research Conference on Sustainable Energy, Engineering, Materials and Environment.*

Sánchez, M. J., Mauricio, J. E., Paredes, A. R., Gamero, P. & Cortés, D. 2017. Antimicrobial properties of zsm-5 type zeolite functionalized with silver. *Materials Letters,* 191**,** 65-68.

Savari, A., Hashemi, S., Arfaeinia, H., Dobaradaran, S., Foroutan, R., Mahvi, A. H., Fouladvand, M., Sorial, G. A., Farjadfard, S. & Ramavandi, B. 2020. Physicochemical characteristics and mechanism of fluoride removal using powdered zeolite-zirconium in modes of pulsed& continuous sonication and stirring. *Advanced Powder Technology,* 31**,** 3521-3532.

Sazali, N. & Harun, Z. 2022. One shot of the hydrothermal route for the synthesis of zeolite lta using kaolin. *Journal of Inorganic and Organometallic Polymers and Materials,* 32**,** 3508-3520.

Sazali, N., Harun, Z., Abdullahi, T., Kamarudin, N. H., Sazali, N., Jamalludin, M. R., Hubadillah, S. K. & Alias, S. S. 2022. The route of hydrothermal synthesis zeolite-a from the low-grade perak kaolin, malaysia. *Silicon*.

Singh, S., German, M., Chaudhari, S. & Sengupta, A. K. 2020. Fluoride removal from groundwater using zirconium impregnated anion exchange resin. *Journal of Environmental Management,* 263**,** 110415.

Solanki, Y. S., Agarwal, M., Gupta, A., Gupta, S. & Shukla, P. 2022. Fluoride occurrences, health problems, detection, and remediation methods for drinking water: A comprehensive review. *Science of The Total Environment,* 807**,** 150601.

Sutianingsih, Y. & Kurniawan, T. 2022. A review: Antibacterial activity of metal impregnated zeolite in water treatment process. *Jurnal Kartika Kimia,* 5**,** 24-34.

Suvaci, E. & Özel, E. 2021. Hydrothermal synthesis. *Encyclopedia of materials: Technical ceramics and glasses.*

Tabi, R. N., Agyemang, F. O., Mensah-Darkwa, K., Arthur, E. K., Gikunoo, E. & Momade, F. 2021. Zeolite synthesis and its application in water defluorination. *Materials Chemistry and Physics,* 261.

Tayraukham, P., Jantarit, N., Osakoo, N. & Wittayakun, J. 2020. Synthesis of pure phase nap2 zeolite from the gel of nay by conventional and microwave-assisted hydrothermal methods. *Crystals,* 10.

Tian, Z. & Gan, Y. 2019. In situsynthesis of structural hierarchy flowerlike zeolite and its application for fluoride removal in aqueous solution. *Journal of Nanomaterials,* 2019**,** 1-11.

Vaičiukynienė, D., Jakevičius, L., Kantautas, A., Vaitkevičius, V. & Vaičiukynas, V. 2020. The effect of ultrasound on na-a zeolite synthesis based on sodium aluminosilicate gels and solid materials.

Velazquez-Peña, G. C., Olguín-Gutiérrez, M. T., Solache-Ríos, M. J. & Fall, C. 2017. Significance of fezr-modified natural zeolite networks on fluoride removal. *Journal of Fluorine Chemistry,* 202**,** 41-53.

Vergara-Figueroa, J., Alejandro-Martín, S., Pesenti, H., Cerda, F., Fernández-Pérez, A. & Gacitúa, W. 2019. Obtaining nanoparticles of chilean natural zeolite and its ion exchange with copper salt.

Vithanage, M. & Bhattacharya, P. 2015. Fluoride in the environment: Sources, distribution and defluoridation. *Environmental Chemistry Letters,* 13**,** 131-147.

Waghmare, S. S. & Arfin, T. 2015. Fluoride removal from water by various techniques. *International journal of innovative science, engineering and technology***,** 560-571.

Wakweya, B. & Jifar, W. W. 2023. In vitro evaluation of antibacterial activity of synthetic zeolite supported agzno nanoparticle against a selected group of bacteria. *Journal of Experimental Pharmacology,* 15**,** 139-147.

Wang, C., Leng, S., Guo, H., Yu, J., Li, W., Cao, L. & Huang, J. 2019. Quantitative arrangement of si/al ratio of natural zeolite using acid treatment. *Applied Surface Science,* 498.

Wang, M., Zhu, J. & Mao, X. 2021. Removal of pathogens in onsite wastewater treatment systems: A review of design considerations and influencing factors. *Water,* 13.

Who 2019. Preventing disease through healthy environments inadequate or excess fluoride a major public health concern. *World Health Organisation*.

Xiao, Y., Liu, K., Hao, Q., Li, Y., Xiao, D. & Zhang, Y. 2022. Occurrence, controlling factors and health hazards of fluoride-enriched groundwater in the lower flood plain of yellow river, northern china. *Exposure and Health,* 14**,** 345-358.

Yadav, M., Singh, G. & Jadeja, R. N. 2021. Fluoride contamination in groundwater, impacts, and their potential remediation techniques. *Groundwater Geochemistry Pollution and Remediation Methods***,** 22-41.

Yan, J., Chen, J., Zhang, W. & Ma, F. 2020. Determining fluoride distribution and influencing factors in groundwater in songyuan, northeast china, using hydrochemical and isotopic methods. *Journal of Geochemical Exploration,* 217.

Yang, B., Jia, C., Sun, G., Quan, B., Zhang, C., Huo, Q. & Su, P. 2022a. Enhancing the adsorption function of f- by iron and zirconium doped zeolite: Characterization and parameter optimization. *Environmental Engineering Research,* 28**,** 220010-0.

Yang, B., Sun, G., Quan, B., Tang, J., Zhang, C., Jia, C., Tang, Y., Wang, X., Zhao, M., Wang, W. & Xiao, B. 2021. An experimental study of fluoride removal from wastewater by mn-ti modified zeolite. *Water,* 13.

Yang, R., Chen, J., Zhang, Z. & Wu, D. 2022b. Performance and mechanism of lanthanum-modified zeolite as a highly efficient adsorbent for fluoride removal from water. *Chemosphere,* 307**,** 136063.

Yao, G., Lei, J., Zhang, W., Yu, C., Sun, Z., Zheng, S. & Komarneni, S. 2019. Antimicrobial activity of x zeolite exchanged with cu(2+) and zn(2+) on escherichia coli and

staphylococcus aureus. *Environmental Science and Pollution Research,* 26**,** 2782-2793.

Yemmireddy, V., Adhikari, A. & Moreira, J. 2022. Effect of ultraviolet light treatment on microbiological safety and quality of fresh produce: An overview. *Frontiers in Nutrition,* 9**,** 871243.

Zendehdel, R., Goli, F. & Hajibabaei, M. 2020. Comparing the microbial inhibition of nanofibres with multi-metal ion exchanged nano-zeolite y in air sampling. *Journal of Applied Microbiology,* 128**,** 202-208.

Zhang, X., Liu, Q. & Yang, S. 2020. Investigations on hydrothermal synthesis parameters in preparation of zeolite w. *Digest Journal Of Nanomaterials And Biostructures***,** 769-779.

Zhang, Y., Zhang, Z., Han, H., Zhang, M., Wang, H., Song, H. & Chen, Y. 2022. Effective removal of organic dyes using the ultrasonic-assisted hydrothermal synthesis of nap zeolite doping cu or fe in fenton-like oxidation systems. *Separation and Purification Technology,* 299.

Zhao, M. M., Wang, Q., Krua, L. S. N., Yi, R. N., Zou, R. J., Li, X. Y. & Huang, P. 2023. Application progress of new adsorption materials for removing fluorine from water. *Water,* 15.

Zhou, H., Chen, W., Gao, Z. Y. & Chen, D. 2014. Removal of fluoride from aqueous media by zirconium modified zeolite. *Asian Journal of Chemistry,* 26**,** 8062-8068.

Zhou, Q., Jiang, X., Qiu, Q., Zhao, Y. & Long, L. 2023. Synthesis of high-quality nap1 zeolite from municipal solid waste incineration fly ash by microwave-assisted hydrothermal method and its adsorption capacity. *Science of The Total Environment,* 855**,** 158741.

Chapter 3: Ultrasonication assisted synthesis of zeolite from bentonite clay: optimization of synthesis conditions using response surface methodology

Abstract

The aim of this chapter was to optimize conditions for the synthesis of zeolite from bentonite clay using the response surface methodology approach. Calcined bentonite clay was subjected to alkali dissolution using ultrasonication followed by hydrothermal treatment to obtain the zeolite. To determine the optimum ultrasonication conditions, NaOH concentration was varied from 0.5 to 2.5 M while the duration of aging was varied from 10 to 120 minutes. The optimum dissolution conditions under ultrasonication determined by the RSM were found to be 2.5 M of NaOH and 120 minutes of aging time. To determine the optimum hydrothermal conditions, hydrothermal treatment was evaluated at treatment times ranging from 1.5 hours to 6 hours and temperatures ranging from 70°C to 140°C. The obtained hydrothermally treated materials were characterized using scanning electron microscopy (SEM), X-ray diffraction (XRD), and Fourier-transform infrared spectroscopy (FTIR). Results showed that the crystallinity of the obtained zeolite samples increased with the increase in hydrothermal temperature and time. Moreover, the XRD analysis revealed that lower temperature of 105 °C to 70 °C and time of 90 minutes resulted in pure zeolite NaP phases with higher hydrothermal temperature of 140 °C and time of 6 hours resulting in the formation of hydroxy sodalite mineral phases. Defluoridation experiments were conducted using all obtained samples to select the zeolite sample with higher fluoride removal efficiency for subsequent experiments. The sample prepared at a sonication duration of 2 hours and hydrothermal treatment conditions of 105°C for temperature and 90 minutes for treatment time demonstrated the greatest fluoride adsorption capacity at 0.19 mg/g, making it the preferred choice for subsequent use in fluoride removal applications.

Keywords: Bentonite clay, Zeolite, Hydrothermal, Sonication, Optimization, RSM

3.1. Introduction

Zeolites are distinguished as crystalline aluminosilicate minerals which are characterized by their unique properties such as uniform pore size, high cation exchange capacity (CEC), molecular sieving, high surface area, and thermal stability (Salahudeen, 2022). According to (Sazali and Harun, 2022), zeolites exhibit high mechanical strength and are non-toxic making them preferable adsorbents in water purification and wastewater treatment processes. Due to their unique properties, these materials have been extensively utilized in several industries for catalysis, gas separation, nuclear waste management, water softening, and purification (Khaleque et al., 2020). In water purification studies, reports indicate their excellent adsorption capacity towards heavy metals, ammonium ions, hydrocarbons, and anions such as fluorides (Adamczyk et al., 2021, Obijole et al., 2021).

Research articles have reported mainly two types of zeolites namely, synthetic and natural zeolites (Król, 2020). Natural zeolites include clay minerals such as mordenite, clinoptilolite, kaolin, analcime, and chabazite. Conversely, synthetic zeolites include zeolite FAU, ZSM-5, LTA, SSZ, and P which are distinguished mainly by their framework and silica to alumina ratio (Shahmansouri et al., 2019). Among the two, synthetic zeolites are widely preferred due to their unique range of properties including higher surface area, small crystal size, purity, and higher CEC which can align with the user's applications. These types of zeolites can be fabricated from waste materials including coal fly ash and rice husks and natural materials including clays, silica sand, and volcanic ash (Lin et al., 2022). Synthetic zeolites from waste and natural sources contribute to waste management and sustainable practices. Conversely, methods such as hydrothermal synthesis, alkali fusion, and sonochemistry are among the utilized methods in the fabrication of synthetic zeolite (Khaleque et al., 2020).

One of the most prevalent zeolite synthesis methods is the hydrothermal synthesis technique. The traditional hydrothermal technique is regarded as the cornerstone of the production of microporous and crystalline materials hence its widespread application in several industries (Salahudeen, 2022). This process involves the formation of zeolites from silica and alumina precursors in an aqueous environment at elevated temperatures and pressure (Sazali and Harun, 2022). During this process, nucleation and crystal growth within the solution occur thereby resulting in the recrystallization of zeolitic materials. The downside of this approach is the long duration of hydrothermal treatment which could take hours to several days and high energy cost (Behin et al., 2016, Dewes et al., 2022). According to Behin et al. (2016) and Khaleque et al. (2020), lack of nucleation control resulting in larger crystal size, slow rate of mixing, use of higher temperatures of up to 200°C and less surface

area are among the difficult challenges faced in traditional hydrothermal synthesis method. Moreover, ongoing research has adopted advanced techniques such as microwave and ultrasonication-assisted hydrothermal methods for better zeolite structural characteristics.

As an alternative method, the use of ultrasound technique for better control of the zeolite properties and significant reduction of zeolite synthesis time and energy consumption has captured researcher's interest worldwide (Chen et al., 2020). Ultrasound utilizes sound waves at high frequencies generally above 20 kHz to influence chemical reactions in aqueous solutions. These waves generate microscopic bubbles that violently implode at short intervals creating shock waves, high pressures, and heat (Dewes et al., 2022). This mechanism influences the mobility of mass from one another and thereby facilitates mixing and nucleation processes in zeolite synthesis (Adamczyk et al., 2021). The facilitation of nucleation greatly favors the crystallization of zeolitic materials as nuclei required for crystal growth are made available at a shorter sonication time which therefore reduces the traditional hydrothermal time of nucleation and crystallization. In addition, the sound waves generated are distributed uniformly which results in homogeneous mixing of the solution along with the creation of smaller nuclei thereby reducing the crystal size instead of the few nuclei in the traditional hydrothermal synthesis which results in larger crystal size (Askari et al., 2012). Reduction of crystal size paves the way to an increased surface area of the zeolite product.

The response surface methodology (RSM) plays a significant role in optimizing zeolite synthesis parameters such as crystallization time, temperature, pH, silica-to-alumina ratios, and concentrations of reactants (Lee et al., 2022). The RSM makes use of mathematical equations and models to generate experimental designs, analyzing interrelationships between multiple parameters and deduce the optimal conditions for obtaining the zeolite with the desired properties (Ibsaine et al., 2023). The RSM develops minimal experimental designs for the prediction of multiple parameters on the characteristics of the zeolite through predictive modeling. This technique enhances fine-tuning of the structural properties of zeolite including pore size distribution, crystal size, and surface area.

Overall, this chapter seeks to utilize, the ultrasonication assisted hydrothermal method coupled with the use of the response surface methodology for the optimization of synthesis parameters of the zeolite from raw bentonite clay. The ultrasonication was used for reduction of hydrothermal treatment time while enhancing the nucleation induction and RSM assisted in deducing the optimal synthesis conditions for the zeolite with minimal experimental runs. This represents an innovative and sustainable approach towards the development of an advanced and systematic method of zeolite with enhanced properties in a short duration

compared to the traditional hydrothermal synthesis technique. Physicochemical characterization was also conducted along with preliminary defluoridation experiments to deduce the performance of the synthesized zeolite as an adsorbent.

3.2 Methodology

3.2.1 Materials

Bentonite clay used in this study was bought from the Cape Bentonite Mine, Western Cape. All chemicals including sodium fluoride and sodium hydroxide were supplied by Merck, South Africa and were of analytical grade. Field fluoride rich groundwater was collected from Siloam Village, Limpopo.

3.2.2 Material Preparation

Raw bentonite clay was washed with Milli Q water (18.2 MΩ/cm) in a mass to liquid ratio of 1:100. This was done three times before overnight drying in an oven at 105°C. Thereafter, the dry bentonite was milled into fine powder by a vibratory disc mill RS20 with particle range size of 200 to 63 µm at 700 rpm for 3 minutes. The milled bentonite clay was stored in sample bags for further experimental processes, analysis and to ovoid moisture.

3.2.3 Experimental Method

3.2.3.1 Synthesis of zeolite from bentonite clay

The synthesis of zeolite materials from bentonite clay was carried out under ultrasound assisted hydrothermal treatment following procedure described by Ojumu et al. (2016) with modification. Briefly, three steps were carried out to synthesize zeolite from bentonite clay namely, calcination of bentonite clay, dissolution of calcined clay and lastly hydrothermal treatment of sonicated gel.

3.2.3.1.1 Optimization of calcination temperature

To determine the optimum calcination temperature and time, 10 g of raw bentonite clay were transferred into a crucible and then calcined in a Scientific Slab Furnace 930 at varying times of 10, 30 and 60 minutes and temperatures of 400°C, 600°C and 800°C as depicted in Table 3.1. The obtained samples were then characterized using X-ray Fluorescence for chemical composition and to determine the optimum calcination conditions.

Table 3.1: Variation of calcination temperature and time for dihydroxylation of bentonite clay

Name	Time (Minutes)	Temperature (˚C)
Raw	0	0
D1	60	400
D2	60	600
D3	60	800
D4	10	800
D5	30	800

3.2.3.1.2 Ultrasonication assisted dissolution of silica and aluminum from calcined clay

To identify the ideal conditions for the dissolution of alumina and silica from the calcined bentonite clay, the NaOH concentration and reaction time were varied using RSM. Table 3.2 depicts how the dissolution conditions were varied. Briefly, 100 mL of known concentration of NaOH was pipetted into a 250 mL plastic bottle and 10 grams of calcined bentonite clay were dispersed into the alkaline solution. Thereafter, mixtures were subjected to ultra-sonication (UP400s Heilscher, Germany) at an amplitude of 100% for varying durations indicated in Table 3.2. The obtained mixtures were then centrifuged using the Hermle Z-366 (USA) centrifuge access liquids were stored and the remaining solids were dried in the oven overnight at 90°C. The dried solids were characterized using XRF to determine the optimum dissolution conditions by examining the remaining silica and alumina composition in the solid samples.

Table 3.2: Dissolution conditions for Si and Al from the calcined bentonite clay

Sample Name	Aging Time (Minutes)	Concentration of NaOH (Molar)
C111	120	1.5
C112	65	1.5
C113	10	2.5
C114	10	1.5
C115	65	0.5
C116	10	0.5
C117	120	2.5
C118	120	0.5
C119	65	2.5

3.2.3.1.3 Optimization of Hydrothermal Treatment Conditions

For the hydrothermal treatment, the optimum temperature and time were evaluated using RSM. The solution obtained at optimum dissolution conditions was subjected to recrystallization at varying hydrothermal conditions depicted in Table 3.3. Briefly, 20 mL of the aged mixture was transferred into a 45 mL capacity autoclave reactor. The autoclave reactor was then placed into a 220V~50Hz EcoTherm oven at varying temperatures and times as indicated in Table 3.3. Thereafter, the obtained recrystallized zeolite mixture was diluted with 2 L deionized water and then centrifuged until neutral pH was reached followed by drying overnight in an oven at 90°C. The dried samples were kept safe for further analysis. The crystallinity percentage of the obtained samples was also calculated using equation 3.1 along with defluoridation studies to determine the optimum hydrothermal conditions of the zeolite.

$$Percentage\ crystalinity\ (\%) = \frac{Area\ of\ crystalline\ peaks}{Area\ of\ all\ peaks\ (Crystalline + Amorphous} \times 100 \qquad (3.1)$$

Table 3.3: Varied conditions for hydrothermal treatment

Name	Time (Hours)	Temperature (˚C)
VN1	3.75	105
VN2	6	140
VN3	3.75	70
VN4	1.5	70
VN5	3.75	140
VN6	6	70
VN7	1.5	140
VN8	1.5	105
VN9	6	105

3.2.4 Physicochemical characterization

The synthesized samples were analyzed using various analytical instruments under specific operating conditions. Elemental composition was determined using the S1TITAN 600 X-ray Fluorescence (XRF) analyzer, at operating voltage of 40 kV and a current of 100 mA. Mineral phases and crystallinity were identified using the PANalytical X'Pert Pro powder diffractometer (XRD) operating at 40 kV, 40 mA and copper fo radiation. Functional groups were characterized using the Platinum ATR Fourier Transform Infrared (FTIR) spectrometer, utilizing a spectral range of 4500-400 cm^{1}. Morphological and elemental analysis was performed using the TESCAN Scanning Electron Microscope-Energy Dispersive Spectroscopy (SEM-EDS), at an accelerating voltage of 15 kV. Particle size distribution analysis was conducted using the Shimadzu SALD-2300 laser diffraction analyzer, employing a laser wavelength of 633 nm. Pore size and surface area analysis were carried out using the TriStar II 3020 Brunauer Emmett Teller (BET) analyzer, operated under nitrogen gas at -196°C..

3.2.5 Fluoride experiments

Preliminary fluoride adsorption experiments were conducted using filed groundwater collected from a borehole located in Siloam village, Limpopo. The field groundwater had fluoride concentration of 6.2 mg/L and pH of 8. A mass of 0.5 g of the zeolite sample was added in 100 mL of fluoride rich field groundwater in a 250 mL capacity polyethylene bottle

and agitated for 60 minutes at 250 rpm using the SSL2 reciprocating shaker. Thereafter, the solution was filtered using a 0.45 µm membrane filter and the filtrate was characterized for fluoride concentration using the ORION Ion Selective Electrode (ISE, 9609BNWP) meter. Prior to fluoride analysis, TISAB (III) was added to the filtrate in a ratio of 1:10 mL to increase the ionic strength of the solution. The fluoride percentage removal was calculated using equation 3.2 where Ci is the initial fluoride concentration and Cf is the final fluoride concentration in the filtrate.

$$Percentage\ fluoride\ removal\ (\%) = \frac{C_i - C_f}{C_i} \times 100 \quad (3.2)$$

3.3. Results and discussion

3.3.1 Optimization of calcination conditions for the raw bentonite clay

Table 3.4 depicts the variation of Al and Si percentage compositions at various temperatures and times. It was observed that the percentage of silica and alumina increases with the increase in temperature and time. The physicochemical process responsible for this increase could be due to the decomposition of hydroxyl bonds or water molecules in high temperatures leading to the release and formation of silica and alumina oxides (Wang, 2016, Cheng et al., 2019). This in turn increases their composition as observed in the calcinated samples. Sample number D3 which was calcinated at 800°C for 1 hour was selected as the optimum calcination conditions for the raw bentonite clay since there was no longer a noticeable difference in the percentage of silica and aluminum.

In addition, both increases in calcination temperature and time resulted in a decrease in the silica-to-aluminum ratio from 5.43 to 4.80. This is due to the increase in the aluminum composition during the dihydroxylation process. As the temperature and time increased more and more aluminum oxides were formed whilst minimal silica was formed after 600°C and thereby favored the decrease in the ratio. According to Abdullahi et al. (2017), silica-to-alumina molar ratios below 5 often produce hydroxy sodalite zeolites which coincide with the obtained XRD results. Similar observations were made in a study by Menshaz et al. (2017).

Table 3.4: Calcination conditions of bentonite clay and the composition of silica and aluminium,

Name	Time (Minutes)	Temperature (˚C)	Silica (%)	Alumina (%)	SiO_2/Al_2O_3 ratio
Raw	0	0	49.03	9.03	5.43
D1	60	400	61.75	11.53	5.36
D2	60	600	63.89	13.00	4.91
D3	60	800	63.91	13.41	4.77
D4	10	800	61.85	12.85	4.81
D5	30	800	62.91	13.11	4.80

3.3.2 Dissolution of calcined bentonite clay

3.3.2.1 Optimization of dissolution condition

The silica and aluminum percentage compositions in the treated residues which were dissolved at various sonication times using different NaOH concentrations are presented in Table 3.5. Also, three-dimensional surface graph plots constructed to showcase the changes in the residue's compositions obtained after each dissolution experiment and the interrelationship between the response factors are shown in Figure 3.1. During higher concentrations of NaOH observation shows that more silica and aluminum were leached out of the clay. This was determined by the lower silica and aluminum oxide percentage composition remaining on the analyzed residues as observed in sample C117. Equations 3.3 and 3.4 summarize the dissolution reaction between Al and Si in the clay mineral with sodium hydroxide forming sodium silicate and sodium aluminate (Lee et al., 2017).

$$SiO_{2(s)} + 2NaOH_{(aq)} \rightarrow Na_2SiO_{3(aq)} + H_2O_{(aq)} \quad (3.3)$$

$$Al_2O_{3(s)} + NaOH_{(aq)} \rightarrow NaAlO_{2(aq)} + H_2O_{(aq)} \quad (3.4)$$

In this reaction, the hydroxyl ions (-OH) from sodium hydroxide attack the silica and aluminum in the clay breaking the bonds between silica and oxygen (Si-O) to form sodium silicate which is soluble or aluminum and oxygen (Al-O) to form soluble sodium aluminate. As the sodium hydroxide concentration increases, more hydroxyl ions become available causing an increase in the rate of breaking the Al-O and Si-O bonds of calcined material and

thereby increasing the dissolution process (Hamidi et al., 2016). Similar observations were made in a study by Zhang et al. (2020).

Furthermore, at a longer aging time, more silica and aluminum were leached out which was observed by a lower percentage composition of silica and aluminum in the residues as observed in sample C117. This could be due to more opportunity for hydroxyl ions(-OH) from NaOH molecule to interact with the surfaces of the calcined clay prolonging the breaking of Al-O and Si-O bonds hence the dissolution process increases (Pan et al., 2021). In addition, the 3D plots showed that aging time and NaOH concentration have a directly proportional effect on the dissolution of silica and aluminum as the dissolution process increases with the increase of both NaOH concentration and aging time which is in agreement with Hajimohammadi and van Deventer (2016) and Król et al. (2019). Therefore, the optimum dissolution conditions were a 2.5 M concentration of NaOH and an aging time of 2 hours observed in sample C117 which had the least silica and aluminum percentage composition of 26.93% and 4.64% respectively.

Table 3.5: Percentage composition of silica and alumina oxides in residues at varying dissolution conditions

Name	**Aging Time (Minutes)**	**Concentration of NaOH (Molar)**	**SiO_2 (%)**	**Al_2O_3 (%)**
C111	120	1.5	40.94	8.1
C112	65	1.5	51.85	10.83
C113	10	2.5	39.42	7.51
C114	10	1.5	47.52	9.14
C115	65	0.5	56.68	11.89
C116	10	0.5	57.64	11.93
C117	120	2.5	26.93	4.64
C118	120	0.5	56.28	11.68
C119	65	2.5	36.24	6.55

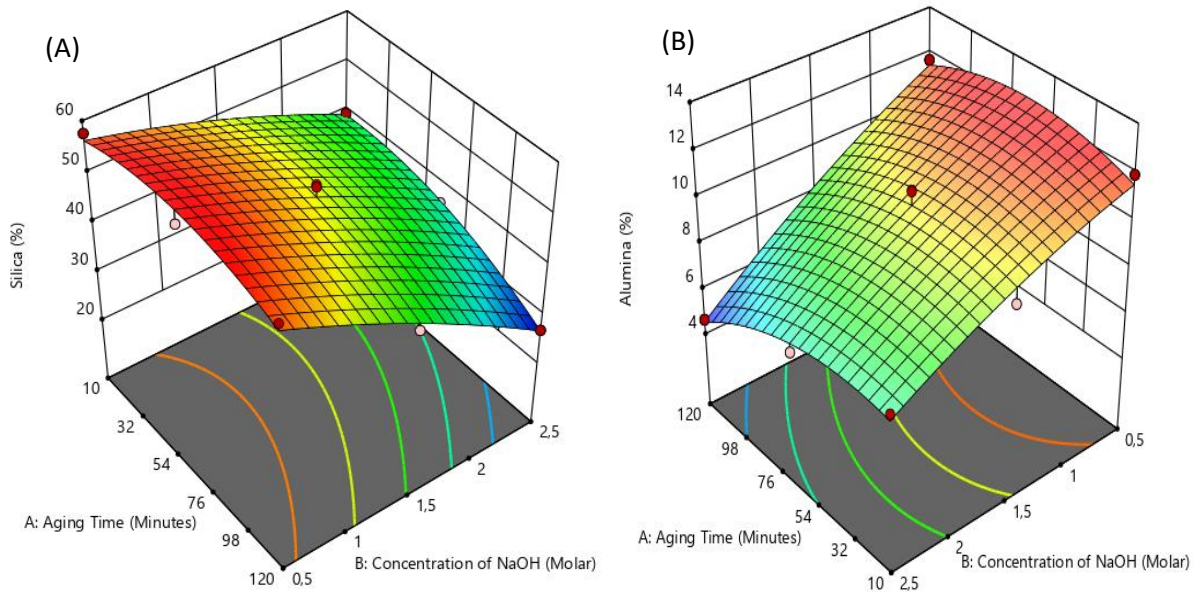

Figure 3.1: Three-dimensional surface plots of residual silica (A) and aluminum (B) percentage compositions at varying dissolution conditions.

3.3.2.2 Actual vs Predicted values

The actual values of silica and alumina composition were compared against the predicted values presented in Figure 3.2. This was to provide the regression coefficient of the model data. The actual vs predicted dissolution of silica and alumina plot in Figure 3.2 demonstrated that the prediction line passes through the middle of the experimental data range for both silica and alumina. This implies that the model's predictions and actual values are within the range. Moreover, the regression coefficient of the model function for silica and alumina data was 0.9734 and 0.9622, respectively. Therefore, the obtained regression values indicate that the model could predict 97.34% and 96.22% of the experimental data. This indicates that there is a correlation between the variables and hence, optimization of dissolution conditions was accurately predicted.

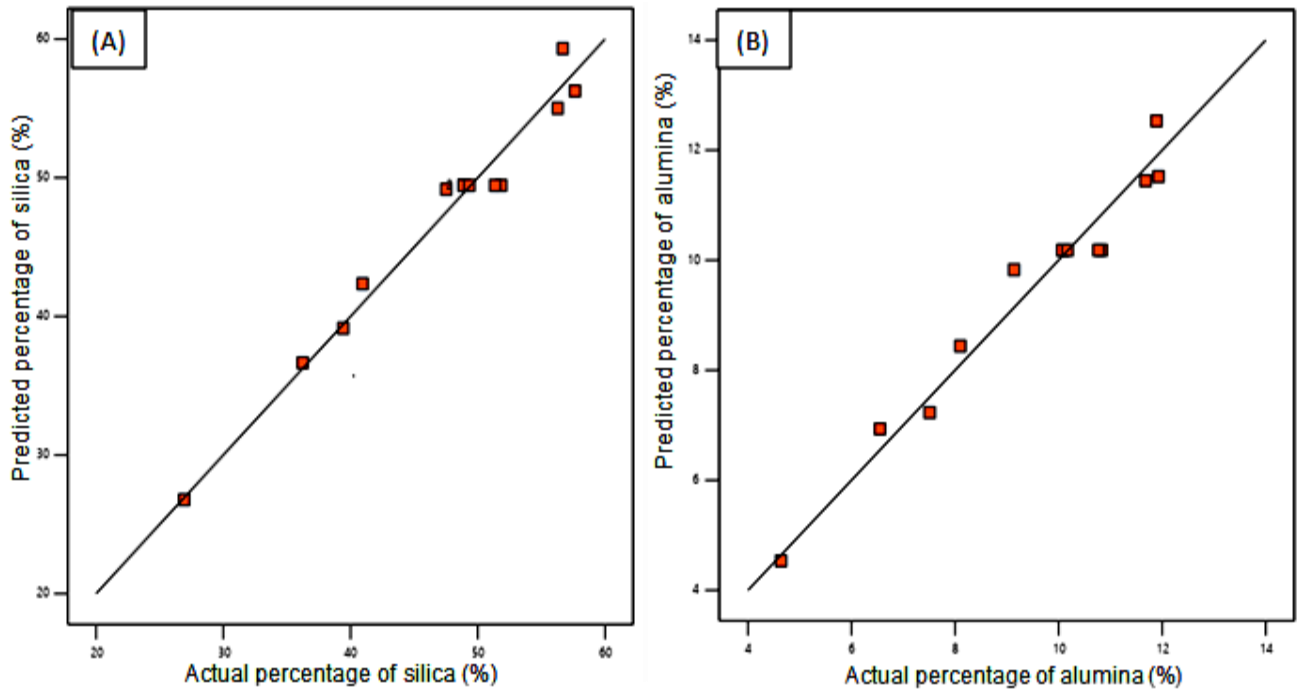

Figure 3.2: Actual vs predicted values plots of dissolution of silica (A) and alumina (B) from calcined bentonite clay.

3.2.3 Analysis of Variance Results

The Analysis of Variance (ANOVA) was employed to determine the goodness of fit of the model towards the dissolution of silica and aluminum from calcined bentonite clay's experimental data and presented in Table 3.6. The ANOVA indicated that the quadratic model is the effective and rational method for the analysis of the experimental data. This is indicated by the model's significant p-value of 0.0001 as observed in Table 3.6. Studies indicate that a p-value lower than 0.05 significance level shows that the model is significant and insignificant if it is above 0.05 significance level (Mourabet et al., 2017). The model also exhibited a lack of fit p-value of 0.1708 which is insignificant. Also, the aging time and NaOH concentration factor had a significant influence on the silica and aluminum composition from the residues. This is justified by increased leaching of silica and aluminum as aging time and NaOH concentration increases. Therefore, the quadratic model is best fitted and adequate in the analysis of the optimum dissolution conditions.

Table 3.6: ANOVA statistics of dissolution of silica and alumina from calcined clay

Source	Sum of Squares	df	Mean Square	F-value	p-value	
Model	935.51	5	187.10	51.24	< 0.0001	Significant
A-Aging Time (Min)	69.56	1	69.56	19.05	0.0033	
B-Concentration (Molar)	770.89	1	770.89	211.13	< 0.0001	
AB	30.97	1	30.97	8.48	0.0226	
A^2	37.58	1	37.58	10.29	0.0149	
B^2	5.88	1	5.88	1.61	0.2451	
Residual	25.56	7	3.65			
Lack of Fit	17.36	3	5.79	2.82	0.1708	Not significant

3.3 Hydrothermal treatment

3.3.1 Optimization of hydrothermal treatment conditions

Hydrothermal conditions such as time and temperature were varied, and the crystallinity of the hydrothermally treated samples characterized using XRD analysis and fluoride adsorption capacity results of the treated samples are shown in Table 3.7. Three-dimensional plots were constructed to showcase the effect and interrelationship of varying the hydrothermal temperature and time toward the crystallinity of the recrystallized mixtures as presented in Figure 3.4. It was observed that at the lowest hydrothermal conditions of 1.5 hours at a temperature of 70 °C, the obtained material exhibited a profound crystallinity of 69.78% as observed in sample VN4 which aligns with the results of Dewes et al. (2022). The surface plot showed that the crystallinity of the produced samples increases with an increase in both hydrothermal temperature and time (Figure 3.4). This is due to the increase in temperature which increases the reaction rates, formation of crystal nuclei, and faster crystal growth hence the crystallinity of the obtained samples increases as observed in samples VN4, 8 to 7, or VN6, 9 to 2 (Zhang et al., 2013).

Also, increased hydrothermal time increases the duration of the formation and crystal growth. According to (Lee et al., 2022), hydrothermal time is proportional to the crystallinity

of the obtained zeolite. Hence, an increase in hydrothermal time increases the crystallinity of the zeolitic product as observed between samples VN7,5 to 2 or VN4, 3 to 6. The obtained recrystallized samples were subjected to defluoridation studies to evaluate the adsorption capacity of each hydrothermally treated sample and documented in Table 3.7. Observations show that there was minimal relationship between the crystallinity of the hydrothermally treated samples and their adsorption capacity. However, a maximum adsorption capacity of 0.19 mg/g was observed in sample VN8. Therefore, sample VN8 synthesized at a hydrothermal time of 90 minutes and temperature of 105 °C was selected as the optimum hydrothermal treatment conditions.

Table 3.7: Percentage of crystallinity and defluoridation efficiency of synthesized zeolite materials at different conditions

Name	Time (Hours)	Temperature (°C)	Crystallinity (%)	F- Adsorption Capacity (mg/g)
VN1	3.75	105	75.16	0.14
VN2	6	140	83.03	0.18
VN3	3.75	70	71.09	0.15
VN4	1.5	70	69.78	0.17
VN5	3.75	140	77.13	0.16
VN6	6	70	73.52	0.16
VN7	1.5	140	75.7	0.18
VN8	1.5	105	70.49	0.19
VN9	6	105	78.75	0.16

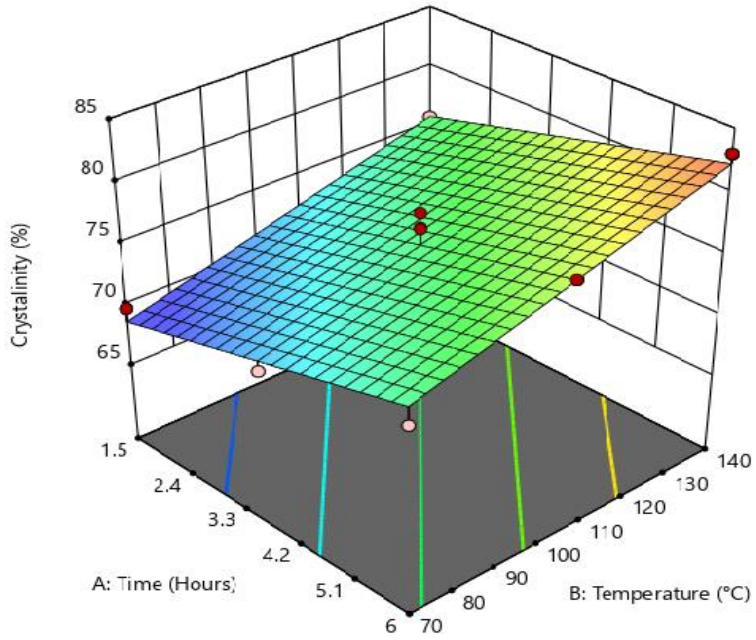

Figure 3.3: 3D plot of the crystallinity of the synthesized zeolite at different crystallization conditions

3.3.2 Actual vs Predicted Values

Comparison of the predicted values by the model and the actual values of the experimental data were plotted against each other in Figure 3.5. This was to deduce how the model predicts over the experimental data range. It was observed that the line of the model's regression passes through the middle of the experimental data range. Also, the obtained regression coefficient of 0.8616 indicates that the actual and the predicted values are in good agreement. This further justifies the accuracy of the RSM model and it is effective and rational for the optimization of crystallization conditions for zeolite.

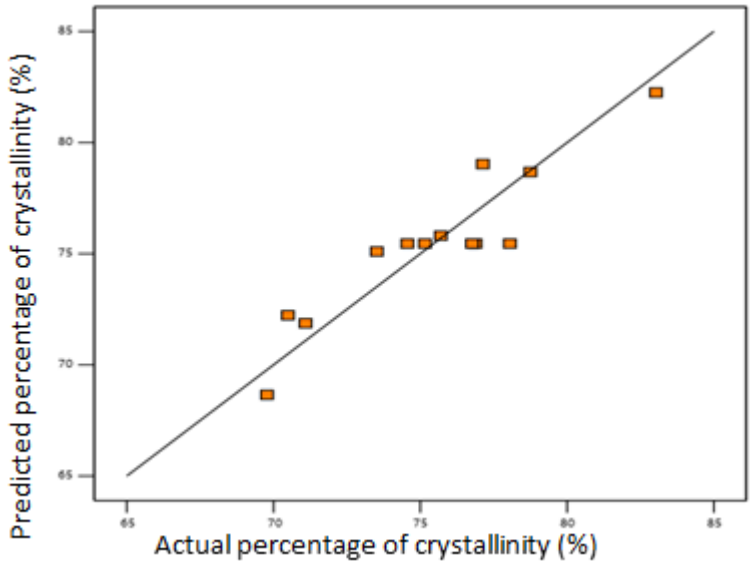

Figure 3.4: Predicted vs actual percentage values for crystallinity of hydrothermally treated samples.

3.3.3 ANOVA results

Table 3.8 summarizes the statistical analysis of the hydrothermal treatment conditions using ANOVA. The experimental data was analyzed using the linear model function of RSM. The results indicate that the model showed a significant p-value of 0.0001 which is lower than the 0.05 significance level. Also, a lack of fit p-value of 0.4470 was obtained which indicates that the lack of fit error was insignificant for the model. Therefore, the linear model function's analysis of the optimal crystallization conditions is adequately fit for the analysis of the experimental data.

Table 3.8: ANOVA statistics of hydrothermal treatment conditions

Source	Sum of Squares	df	Mean Square	F-value	p-value	
Model	138.96	2	69.48	31.13	< 0.0001	significant
A-Time	63.77	1	63.77	28.57	0.0003	
B-Temperature	75.19	1	75.19	33.69	0.0002	
Residual	22.32	10	2.23			
Lack of Fit	14.38	6	2.40	1.21	0.4470	not significant

3.4 Physicochemical characterization

3.4.1 X-ray Diffraction Analysis

Figure 3.3 depicts the XRD band of the calcined clay including the hydrothermally treated samples at various hydrothermal times and temperatures. It was observed that the spectra of the calcined clay exhibited three mineral phases namely quarts (Q) phases at 24°, 30°, 58°, and 81° 2θ, muscovite (M) phases at 10° and 23° two theta, and albite high phases at 25° and 32° 2θ. The presence of quarts mineral phases was also observed in all hydrothermally treated samples which indicates that both calcined and hydrothermally treated materials maintained their aluminosilicate nature. This also aligns with the presence of Al-O and Si-O functional groups in FTIR analysis results in Figure 3.6.

After hydrothermal treatment, the muscovite peak at 10° 2θ was substituted with the zeolite SSZ-73 (S) phase peak as observed in all hydrothermal treated samples. Also, the development of new phases attributed to zeolite NaP (Z) phases at 14°, 20°, and 38° two theta were observed as shown in samples VN1, 3, 4, 6, 7, and 8. Similar observations were made in a study by Shaban et al. (2017). However, these peaks were observed at lower hydrothermal treatment conditions of 105°C at 3.75 hours of treatment time and below. This could be due to the incomplete crystallization process, resulting in reduced crystallinity and peak intensity. The peak intensity of the zeolite NaP phases increased from the hydrothermal temperature of 70 °C to 105 °C and 1.5 hours to 3.75 hours of treatment time. The optimal sample VN8 synthesized at 105 °C and 1.5 hours of treatment time reported in the RSM section exhibited strong peaks of zeolite NaP phases.

At higher treatment conditions of 140°C and 6 hours of treatment time, new phases of hydroxy sodalite (H) developed at 16°, 28°,37°, 40°, 48° and 50° 2θ in sample VN2 and 5. Similar observations were made in a study by Obijole et al. (2019). The development of sodalite phases is a common occurrence during the zeolite synthesis process. According to Kucuk et al. (2023), this is due to the Ostwald rule of stages where the transition of less stable zeolite into a more stable sodalite phase occurs. This effect was also documented in a study by Shahmansouri et al. (2019). Therefore, the dominant mineral phases in the hydrothermal treated samples are zeolite NaP and hydroxy sodalite. Similar results were reported in (Bunmai et al., 2020, Tayraukham et al., 2020, Zhang et al., 2022).

In addition, samples that had hydroxy sodalite phases namely VN2 and 5 synthesized at higher hydrothermal treatment conditions of 6 hours for treatment time and 140 °C for hydrothermal temperature exhibited higher crystallinity of 83.03% and 77.13% respectively as shown in Table 3.7. In contrast, samples that had zeolite NaP treated at lower

hydrothermal conditions of 70 °C and 1.5 hours of treatment time exhibited lower crystallinity of 69.78%, 70.79%, and 71.09% due to reduced temperature and time resulting in partial crystallization of the synthesized material as observed in samples VN4, 8, and 3 respectively. Higher crystallinity of sodalite phases at higher treatment times was also documented in a study by Rozhkovskaya et al. (2021) and Campoverde and Guaya (2023).

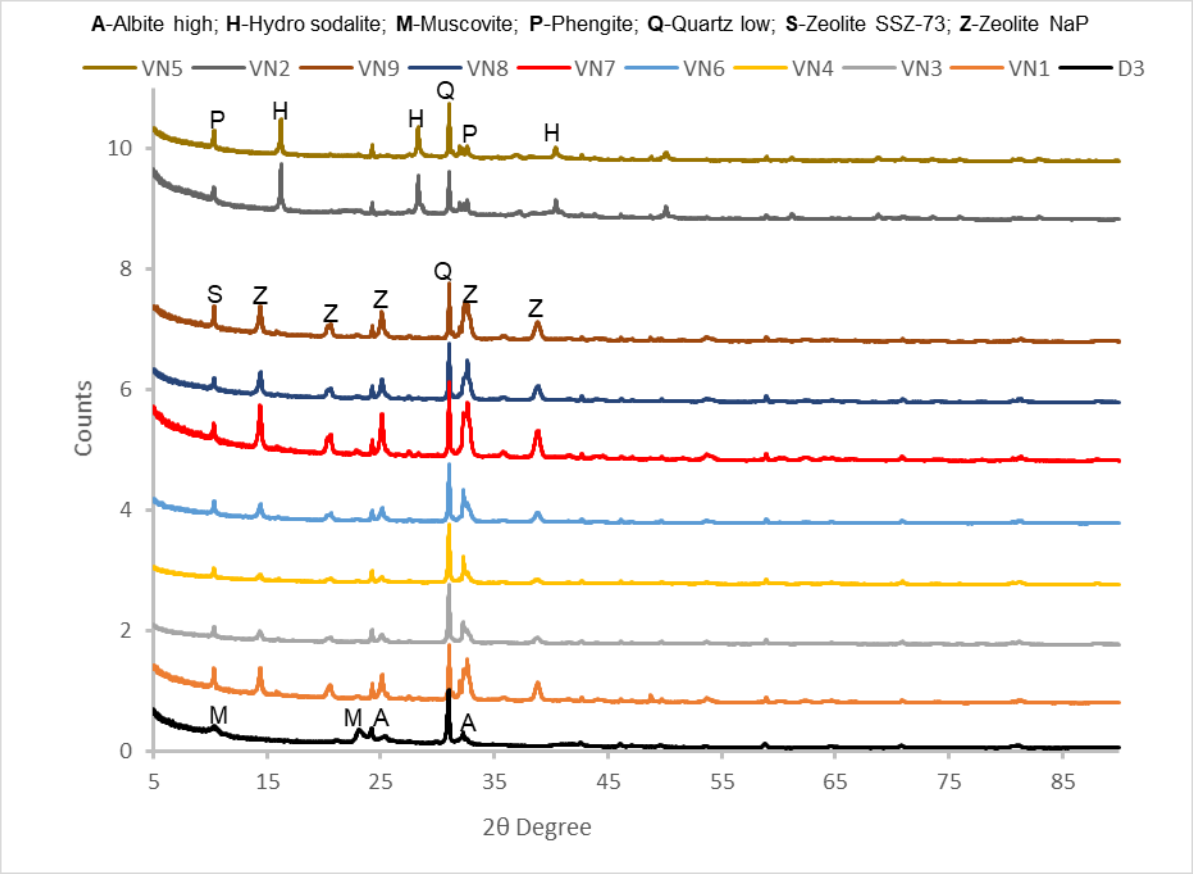

Figure 3.5: XRD spectra of calcined bentonite clay (D3) and hydrothermally treated samples at varying conditions

3.4.2 X-ray fluorescence analysis

The main elemental percentage values of the calcined bentonite clay (D3) and the hydrothermally treated samples are reported in Table 3.9. Observations show that as the hydrothermal temperature increases, the percentage of silica composition decreases while the aluminum composition increases. Sample VN4 treated at lower hydrothermal conditions of 70 °C at 1.5 hours of treatment time had a silica and aluminum composition of 42.44% and 10.38%, respectively while sample VN5 treated at higher hydrothermal treatment conditions at 140 °C at 3.75 hours of treatment time had a silica and aluminum composition of 33.95% and 15.05%, respectively. At lower hydrothermal temperatures and time, the crystallization rate is relatively slow hence more opportunity for soluble silica to be incorporated during crystallization thereby increasing the silica composition of the zeolite and

vice versa at higher hydrothermal temperatures and time. Consequently, the Si/Al ratio decreases as the silica composition decreases as observed in samples VN4 and 5 which had a Si/Al ratio of 4.09 and 2.26, respectively. Similar results were documented in articles by Behin et al. (2016) and Padilla et al. (2022)

In addition, samples with lower Si/Al ratio namely sample VN 2 and 5 synthesized at higher hydrothermal conditions of 140 °C and 6 hours of treatment time had higher crystallinity and composed of hydroxy sodalite phases as reported in XRD analysis. Samples with higher Si/Al ratio namely VN4 synthesized at lower hydrothermal conditions of 140 °C at 1.5 hours of hydrothermal time exhibited lower crystallinity and were composed of zeolite NaP phases. Therefore, the crystallinity of the synthesized material is inversely related to the Si/Al ratio. However, this study recommends further study on the interrelationship of crystallinity and silica to alumina ratio of the synthesized zeolite.

Table 3.9: Chemical composition of calcined bentonite clay (D3) and hydrothermally treated zeolite samples and their Si/Al ratios

Name	Time (Hours)	Temp (°C)	SiO_2 (%)	Al_2O_3 (%)	Si/Al Ratio	MgO (%)	K_2O (%)	CaO (%)	Fe_2O_3 (%)
D3	-	-	63.91	13.41	4.77	3.46	0.79	0.86	3.38
VN1	3.75	105	32.15	12.58	2.56	1.05	0.54	1.26	2.64
VN2	6	140	25.52	9.9	2.58	1.74	0.46	1.00	2.91
VN3	3.75	70	39.56	10.92	3.62	1.05	0.48	1.14	2.25
VN4	1.5	70	42.44	10.38	4.09	1.02	0.56	1.11	2.50
VN5	3.75	140	33.95	15.05	2.26	1.52	0.65	1.03	2.91
VN6	6	70	31.93	11.06	2.89	0.86	0.46	1.16	2.29
VN7	1.5	140	29.74	11.92	2.49	0.78	0.46	1.19	2.53
VN8	1.5	105	32.33	11.43	2.83	0.89	0.46	1.21	2.38
VN9	6	105	31.03	12.62	2.46	0.83	0.49	1.34	2.45

3.4.3 Fourier Transform Infrared Analysis

Figure 3.6 depicts the FTIR spectra of the calcined and hydrothermally treated samples. A spectral band corresponding to the bridge bonds of Al-O-Si internal bending vibration was

observed at =605 cm^{-1}. It was observed that the =605 cm^{-1} band was absent in the calcined clay in comparison to the hydrothermally treated samples which is due to the dihydroxylation/calcination treatment carried out on the calcined clay. The =605 cm^{-1} band was observed in hydrothermally treated samples. However, during hydrothermal treatment, this band decreases in intensity with an increase in both hydrothermal temperature and time. In addition, a shift in the =605 cm^{-1} band to the =669 cm^{-1} peak position was observed at a higher aging time of 6 hours and temperature of 140 in sample VN2.

The band depicting Al-O symmetric bending of aromatic functional groups at =818 cm^{-1} narrow band position was observed. This band was observed in both calcined clay and hydrothermally treated samples. However, in calcined clay, the =818 cm^{-1} band had low intensity in comparison to hydrothermally treated samples. In hydrothermally treated samples, the =818 cm^{-1} band exhibited a more profound intensity at lower hydrothermal treatment conditions as observed in samples VN4 and VN3. However, this band disappears as both hydrothermal temperature and time increases. Which could be due to the transformation of precursor species into the desired crystalline phase, leading to the elimination of intermediate phases.

Furthermore, a strong band attributed to the asymmetric stretching of Si-O functional groups was observed at the =1034 cm^{-1} band position. This band exhibited a lower intensity in calcined clay samples compared to the hydrothermally treated counterparts. The reduction in the intensity of the =1034 cm^{-1} band is associated with the convention of aluminosilicate species into their respective oxides during dihydroxylation treatment. A shift of the =1034 cm^{-1} band to the =964 cm^{-1} band position was observed in all hydrothermally treated samples along with an increase in the band intensity. The shift in the Si-O band showcases recrystallization and the formation of a new zeolite framework. In addition, the =964 cm^{-1} band narrows and increases in intensity as hydrothermal temperature and time increases. According to Pangan et al. (2021), the observed bands from =400 to 1500 cm^{-1} exhibited a comparative series of Si oxides which corresponds to aluminosilicate materials.

New bands associated with the Na-O stretching vibration were observed in the =1415 cm^{-1} and 1481 cm^{-1} band positions. These new peaks were observed only at higher hydrothermal conditions of 140 °C and 6 hours of treatment time as shown in samples VN2 and VN5. The XRD analysis showed that samples VN2 and VN5 are composed of hydroxy sodalite phases which indicates that the Na-O bands are attributed to sodalite phases which agrees with the (Obijole et al., 2021) study. In addition, bands associated with the -OH functional groups at =1640 cm^{-1} and 3470 cm^{-1} absorbance bands were observed. According to Pei et al. (2022), these bands correspond to the absorbed water molecules on the zeolite. The calcined clay

exhibited no band associated with the -OH fictional group due to the removal of hydroxyl groups during calcination treatment. However, all hydrothermal treated samples showed the presence of the -OH functional groups which decrease in intensity with an increase in hydrothermal treatment conditions.

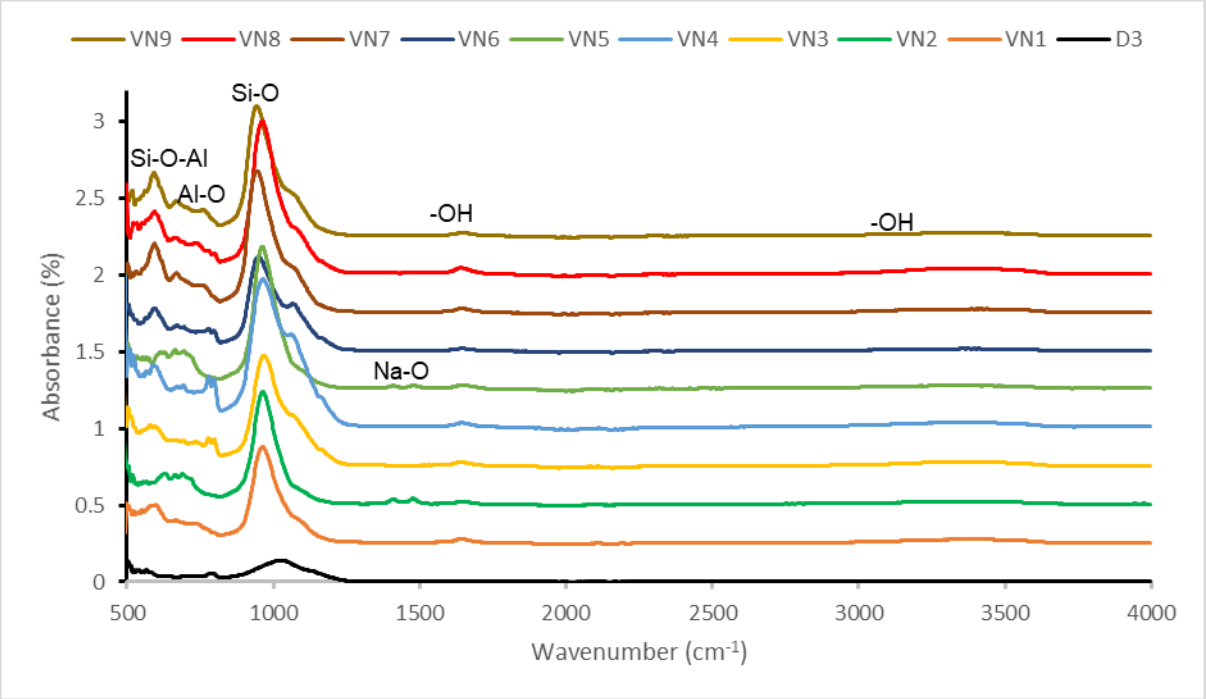

Figure 3.6: FTIR spectra of calcined bentonite clay (D3) and hydrothermally treated samples at varying conditions.

3.4.4 Scanning Electron Microscopy Analysis

Figure 3.7 depicts the morphological properties of the calcined clay and the hydrothermally treated samples at various hydrothermal temperatures and times. The morphology of the calcined clay (D3) exhibited large granules of irregular microstructures compared to all the hydrothermally treated samples. These large microstructure granules are due to the deterioration of the structure of the clay due to thermal treatment. Similar results were reported by Ahmed (2013). In addition, very small-sized cubic habit particles were observed attached throughout the surface of the calcined clay. These particles could be associated with the nucleation and formation of crystals during calcination at high temperatures. Shaban et al. (2017) also reported cubic habit particles attached to zeolite synthesized from bentonite clay.

Morphological changes were also observed in hydrothermally treated samples. At higher hydrothermal temperatures of 140 °C and a crystallization time of 6 hours uniform, large spherical crystals with some irregular granules were observed in samples VN 2 and 5. These large crystals are attributed to the hydroxy sodalite phases reported in XRD analysis. Also,

the observed large crystal morphologies had higher crystallinity as reported in Table 3.7. This could be due to the agglomeration of crystals at higher temperatures and time into large crystals (Shahmansouri et al., 2019). The micrographs of hydrothermally treated samples at lower conditions of 70 °C for 1.5 hours of treatment time exhibited small-sized uniform sphere-like particles as observed in samples VN 4 and 8. These small spherical crystals correspond to the zeolite NaP phases identified in the XRD analysis section. Also, the treated samples had lower crystallinity as reported in Table 3.7. According to Kucuk et al. (2023), lower hydrothermal conditions influence the dissolution and formation of multiple nuclei that crystallize and form small-sized crystals. Similar spherical morphology attributed to zeolite NaP was reported by (Huo et al., 2012, Behin et al., 2016, Tayraukham et al., 2020, Zhang et al., 2022).

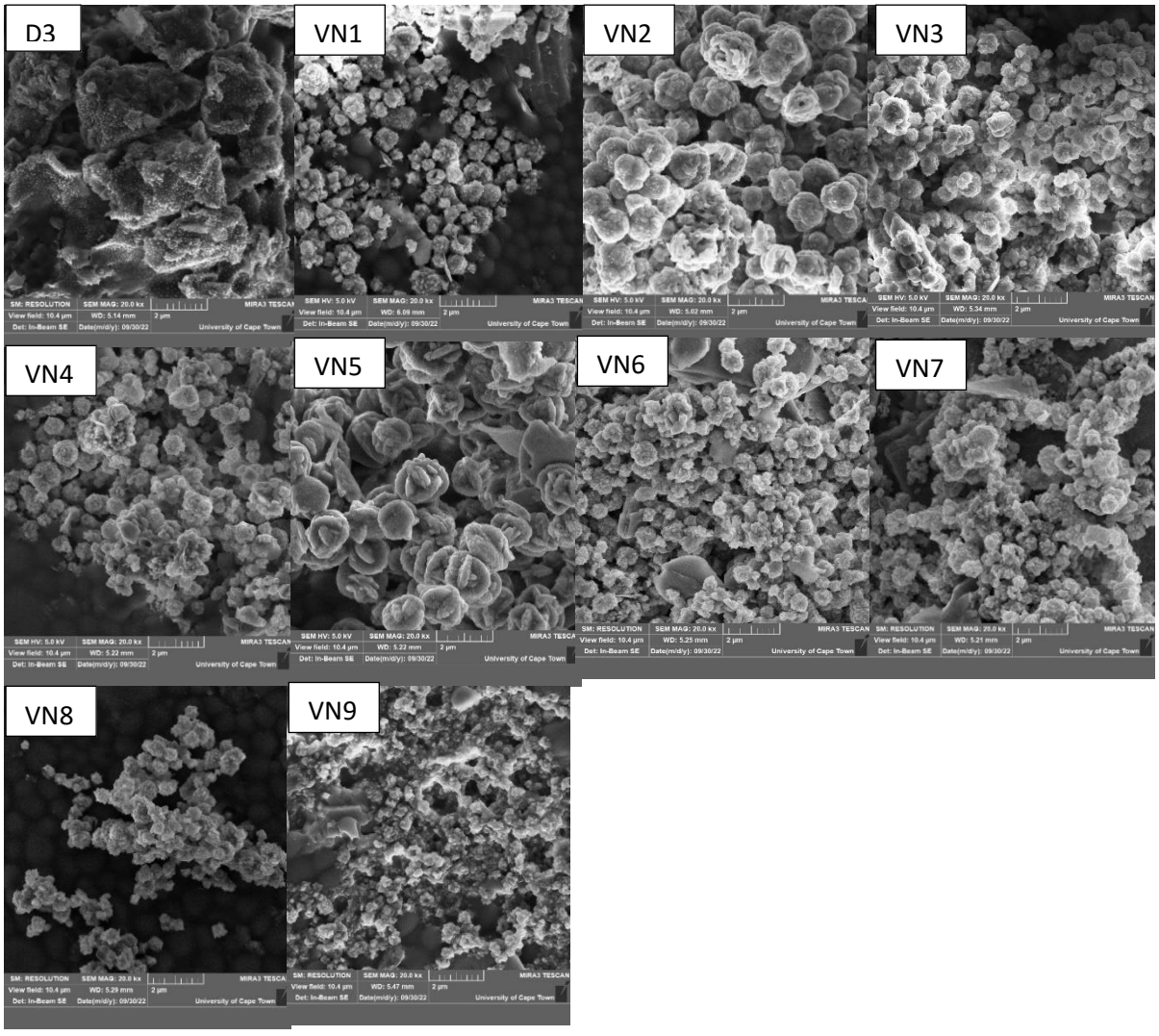

Figure 3.7: SEM micrographs of calcined bentonite clay (D3 and hydrothermally treated samples (VN1-VN9).

3.5 Conclusion

The overall aim of this chapter was to synthesize zeolite from bentonite clay using ultrasonication-assisted hydrothermal technique with the assistance of RSM for optimization of synthesis conditions. The response surface methodology successfully predicted the optimum zeolite synthesis conditions from bentonite clay. The optimum conditions were 1 hour at 800°C for calcination and NaOH molar concentration of 2.5 for dissolution of Al and Si in 2 hours of sonication time. The study revealed that during hydrothermal treatment, samples treated at higher hydrothermal treatment conditions of 140 °C at 6 hours of treatment time had higher silica composition and lower aluminum composition consequently higher Si/Al ratio from XRF analysis, composed of hydroxy sodalite phases with higher crystallinity in XRD analysis and uniform large crystals were reported in SEM analysis. In contrast, samples treated at lower hydrothermal treatment conditions of 70 °C at 1.5 hours of treatment time had lower silica composition and higher aluminum composition consequently lower Si/Al ratio from XRF analysis, composed of zeolite NaP phases with low crystallinity in XRD analysis and uniform multiple small sized crystals were reported in SEM analysis. Preliminary fluoride adsorption studies of hydrothermally treated samples revealed that sample VN8 which is composed of zeolite Nap phases synthesized at optimal conditions of 105 °C at 1.5 hours of treatment time exhibited a maximum adsorption capacity of 0.19 mg/g.

References

Abdullahi, T., Harun, Z. & Othman, M. H. D. 2017. A review on sustainable synthesis of zeolite from kaolinite resources via hydrothermal process. *Advanced Powder Technology,* 28**,** 1827-1840.

Adamczyk, Z., Cempa, M. & Białecka, B. 2021. The influence of ultrasound on fly ash zeolitisation process efficiency. *Mineral Processing and Extractive Metallurgy Review,* 43**,** 427-439.

Ahmed, N. M. 2013. Comparative study on the role of kaolin, calcined kaolin and chemically treated kaolin in alkyd-based paints for protection of steel. *Pigment & Resin Technology,* 42**,** 3-14.

Askari, S., Miar Alipour, S., Halladj, R. & Davood Abadi Farahani, M. H. 2012. Effects of ultrasound on the synthesis of zeolites: A review. *Journal of Porous Materials,* 20**,** 285-302.

Behin, J., Kazemian, H. & Rohani, S. 2016. Sonochemical synthesis of zeolite nap from clinoptilolite. Ultrasonics sonochemistry. 400-408.

Bunmai, K., Osakoo, N., Deekamwong, K., Kosri, C., Khemthong, P. & Wittayakun, J. 2020. Fast synthesis of zeolite nap by crystallizing the nay gel under microwave irradiation. *Materials Letters,* 272.

Campoverde, J. & Guaya, D. 2023. From waste to added-value product: Synthesis of highly crystalline lta zeolite from ore mining tailings. *Nanomaterials (Basel),* 13.

Chen, C.-T., Iyoki, K., Yonezawa, Y., Okubo, T. & Wakihara, T. 2020. Understanding the nucleation and crystal growth of zeolites: A case study on the crystallization of zsm-5 from a hydrogel system under ultrasonication. *The Journal of Physical Chemistry C,* 124**,** 11516-11524.

Cheng, H., Zhou, Y. & Liu, Q. 2019. Kaolinite nanomaterials: Preparation, properties and functional applications. *Nanomaterials from clay minerals.*

Dewes, R. M., Mendoza, H. R., Pereira, M. V. L., Lutz, C. & Gerven, T. V. 2022. Experimental and numerical investigation of the effect of ultrasound on the growth kinetics of zeolite a. *Ultrasonics sonochemistry,* 82**,** 105909.

Hajimohammadi, A. & Van Deventer, J. S. J. 2016. Dissolution behaviour of source materials for synthesis of geopolymer binders: A kinetic approach. *International Journal of Mineral Processing,* 153**,** 80-86.

Hamidi, R. M., Man, Z. & Azizli, K. A. 2016. Concentration of naoh and the effect on the properties of fly ash based geopolymer. *Procedia Engineering,* 148**,** 189-193.

Huo, Z., Xu, X., Lü, Z., Song, J., He, M., Li, Z., Wang, Q. & Yan, L. 2012. Synthesis of zeolite nap with controllable morphologies. *Microporous and Mesoporous Materials,* 158**,** 137-140.

Ibsaine, F., Azizi, D., Dionne, J., Tran, L. H., Coudert, L., Pasquier, L.-C. & Blais, J.-F. 2023. Synthesis of zeolites using aluminosilicate residues from the lithium extraction.

Khaleque, A., Alam, M. M., Hoque, M., Mondal, S., Haider, J. B., Xu, B., Johir, M. a. H., Karmakar, A. K., Zhou, J. L., Ahmed, M. B. & Moni, M. A. 2020. Zeolite synthesis from low-cost materials and environmental applications: A review. *Environmental Advances,* 2.

Król, M. 2020. Natural vs. Synthetic zeolites. *Crystals,* 10.

Król, M., Rożek, P., Chlebda, D. & Mozgawa, W. 2019. Atr/ft-ir studies of zeolite formation during alkali-activation of metakaolin. *Solid State Sciences,* 94**,** 114-119.

Kucuk, M. E., Makarava, I., Kinnarinen, T. & Hakkinen, A. 2023. Simultaneous adsorption of cu(ii), zn(ii), cd(ii) and pb(ii) from synthetic wastewater using nap and lta zeolites prepared from biomass fly ash. *Heliyon,* 9**,** e20253.

Lee, W.-H., Lin, Y.-W. & Lin, K.-L. 2022. Parameter optimization, characterization, and crystallization mechanisms underlying the synthesis of zeolite a using liquid crystal display waste glass and sandblasting waste as alternative raw materials. *Journal of Environmental Chemical Engineering,* 10.

Lee, Y.-R., Soe, J. T., Zhang, S., Ahn, J.-W., Park, M. B. & Ahn, W.-S. 2017. Synthesis of nanoporous materials via recycling coal fly ash and other solid wastes: A mini review. *Chemical Engineering Journal,* 317**,** 821-843.

Lin, S., Jiang, X., Zhao, Y. & Yan, J. 2022. Zeolite greenly synthesized from fly ash and its resource utilization: A review. *Science of The Total Environment,* 851**,** 158182.

Menshaz, A. M., Johari, M. a. M. & Ahmad, Z. A. 2017. Characterization of metakaolin treated at different calcination temperatures.

Mourabet, M., El Rhilassi, A., El Boujaady, H., Bennani-Ziatni, M. & Taitai, A. 2017. Use of response surface methodology for optimization of fluoride adsorption in an aqueous solution by brushite. *Arabian Journal of Chemistry,* 10**,** S3292-S3302.

Obijole, O., Mugera, G. W., Mudzielwana, R., Ndungu, P., Samie, A. & Babatunde, A. 2021. Hydrothermally treated aluminosilicate clay (htac) for remediation of fluoride and pathogens from water: Adsorbent characterization and adsorption modelling. *Water Resources and Industry,* 25.

Obijole, O. A., Gitari, M. W., Ndungu, P. G. & Samie, A. 2019. Mechanochemically activated aluminosilicate clay soils and their application for defluoridation and pathogen removal from groundwater. *International Journal of Environmental Research and Public Health,* 16.

Ojumu, T. V., Du Plessis, P. W. & Petrik, L. F. 2016. Synthesis of zeolite a from coal fly ash using ultrasonic treatment–a replacement for fusion step. *Ultrasonics sonochemistry,* 31**,** 342-349.

Padilla, I., Romero, M., López-Andrés, S. & López-Delgado, A. 2022. Sustainable management of salt slag. *Sustainability,* 14.

Pan, J., Hassas, B. V., Rezaee, M., Zhou, C. & Pisupati, S. V. 2021. Recovery of rare earth elements from coal fly ash through sequential chemical roasting, water leaching, and acid leaching processes. *Journal of Cleaner Production,* 284.

Pangan, N., Gallardo, S., Gaspillo, P. A., Kurniawan, W., Hinode, H. & Promentilla, M. 2021. Hydrothermal synthesis and characterization of zeolite a from corn (zea mays) stover ash. *Materials (Basel),* 14.

Pei, Y., Zhong, Y., Xie, Q. & Chen, N. 2022. Two-step hydrothermal synthesis and conversion mechanism of zeolite x from stellerite zeolite. *Royal Society of Chemistry Advances,* 12**,** 3313-3321.

Rozhkovskaya, A., Rajapakse, J. & Millar, G. J. 2021. Optimisation of zeolite lta synthesis from alum sludge and the influence of the sludge source. *Journal of Environmental Sciences (China),* 99**,** 130-142.

Salahudeen, N. 2022. A review on zeolite: Application, synthesis and effect of synthesis parameters on product properties. *Chemistry Africa,* 5**,** 1889-1906.

Sazali, N. & Harun, Z. 2022. One shot of the hydrothermal route for the synthesis of zeolite lta using kaolin. *Journal of Inorganic and Organometallic Polymers and Materials,* 32**,** 3508-3520.

Shaban, M., Abukhadra, M. R., Shahien, M. G. & Ibrahim, S. S. 2017. Novel bentonite/zeolite-nap composite efficiently removes methylene blue and congo red dyes. *Environmental Chemistry Letters,* 16**,** 275-280.

Shahmansouri, A. A., Akbarzadeh Bengar, H. & Jahani, E. 2019. Predicting compressive strength and electrical resistivity of eco-friendly concrete containing natural zeolite via gep algorithm. *Construction and Building Materials,* 229.

Tayraukham, P., Jantarit, N., Osakoo, N. & Wittayakun, J. 2020. Synthesis of pure phase nap2 zeolite from the gel of nay by conventional and microwave-assisted hydrothermal methods. *Crystals,* 10.

Wang, G. C. 2016. Ferrous metal production and ferrous slags. *The utilization of slag in civil infrastructure construction.*

Zhang, X., Tang, D., Zhang, M. & Yang, R. 2013. Synthesis of nax zeolite: Influence of crystallization time, temperature and batch molar ratio sio2/al2o3 on the particulate properties of zeolite crystals. *Powder Technology,* 235**,** 322-328.

Zhang, Y., Zhang, Z., Han, H., Zhang, M., Wang, H., Song, H. & Chen, Y. 2022. Effective removal of organic dyes using the ultrasonic-assisted hydrothermal synthesis of nap zeolite doping cu or fe in fenton-like oxidation systems. *Separation and Purification Technology,* 299.

Zhang, Y., Zhou, L., Chen, L., Guo, Y., Guo, F., Wu, J. & Dai, B. 2020. Synthesis of zeolite na-p1 from coal fly ash produced by gasification and its application as adsorbent for removal of cr(vi) from water. *Frontiers of Chemical Science and Engineering,* 15**,** 518-527.

Chapter 4: Evaluating the fluoride removal efficiency of zeolite NaP and its antimicrobial potency.

Abstract

This chapter aims to investigate the ideal conditions for fluoride removal using zeolite NaP adsorbent and evaluate its antimicrobial potency. Batch experiments were carried out to evaluate the effectiveness of zeolite NaP in the removal of fluoride from groundwater under several operating conditions. In addition, antimicrobial potency of the adsorbent was evaluated using the agar well diffusion essay against the gram-positive *S. aureus* and gram-negative *E. coli* strains. Under optimal adsorption conditions, a maximum adsorption capacity of 0.16 mg/g was achieved, with a contact time of 60 minutes, an initial concentration of 6.2 mg/L, an initial pH of 2, and an adsorbent dosage of 0.5 g/100 mL. The experimental adsorption data fitted to the *pseudo*-second order kinetic model indicating that fluoride adsorption took place through chemisorption process. Furthermore, the adsorption isotherm data fitted well to the Langmuir isotherm model which indicate that fluoride adsorption occurred in a monolayer surface with limited number of active sites. Anti-microbial studies revealed that zeolite NaP does not have potency against gram-negative *E. coli* and gram-positive *S. aureus* strains. In conclusion zeolite NaP exhibited minimal defluoridation efficiency while no antimicrobial potency was observed. Hence, this chapter recommend introduction of cations on the zeolite frameworks for improved fluoride ions adsorption, antimicrobial potency and reusability and regeneration of the zeolite material.

Keywords: Groundwater, Fluoride, Pathogens, Ultrasonication, Zeolite, Adsorption

4.1 Introduction

In the rural peripheries of developing nations, groundwater serves as the primary and crucial source of drinking water, primarily due to the scarcity of government-provided piped water. However, lack of water quality monitoring technological resources in these regions leads to health problems that are often detected after prolonged exposure to various contaminants. Contaminants such as fluoride and pathogens are often reported in groundwater sources at levels exceeding the World Health Organization (WHO) drinking water guidelines for human consumption (WHO, 2011, Mei et al., 2020). According to the World Health Organization, drinking water containing more than 1.5 mg/L of fluoride leads diseases such as fluorosis while drinking water containing more than 0 cfu/100 mL is linked to nausea, fever, cholera and diarrhea diseases (WHO, 2019, Gao et al., 2021).

Studies have reported exceedingly high levels of fluoride and pathogen of up to 10 mg/L and 10 cfu/100 mL in groundwaters worldwide, respectively (Mahagamage et al., 2020, Odiyo et al., 2020, Yadav et al., 2021, Ling et al., 2022). These results were reported in countries such as USA, Brazil, India, Ghana, Kenya, Botswana, Mozambique, Sri Lanka and South Africa (Aloulou et al., 2021). Likewise, cases of fluorosis and microbial infections have also been reported in the aforementioned countries due to drinking of contaminated groundwater sources (Malebatja and Mokgatle, 2022, Dong et al., 2023). Odiyo and Makungo (2012) investigated the prevalence of fluorosis in a primary school of Siloam, Limpopo South Africa and reported 50% cases of positive dental fluorosis among children between the age of 11 and 14. Furthermore, a study by Nguyen et al. (2021) investigated microbial infections cases in Limpopo, South Africa from 224 children of age 5 and below who drink water from groundwater and reported 85 positive cases of *giardia* infections. Groundwater quality analysis studies reveal co-occurrence of fluoride and pathogens in groundwater which potentially increases the health risks associated with these contaminants (Alqahtany, 2021, Bhandari et al., 2021, Ali et al., 2022). Hence, flexible and sustainable water treatment strategies are required in developing nations wherein clean water is scarce.

Several studies have developed multifunctional adsorbents targeting metals and pathogenic contaminants' removal in water simultaneously. These adsorbents includes silver-zeolite (Krishnani et al., 2012), activated clay soils (Obijole et al., 2019), biopolymer nanocomposite (Nehra et al., 2020), MgO nanostructures (Sivaselvam et al., 2020), iron-doped poly p-Phenylenediamine Composite (Munzhelele et al., 2021), Ag–MgO–Nanohydroxyapatite composite (Ayinde et al., 2022) and hydroxyapatite-bone particle-doped ceramic water filters (Omoniyi et al., 2022). Among other investigated adsorbents, zeolite materials have gained attention recently as a multifunctional adsorbent. These adsorbents are mostly preferred due

to their molecular sieve properties, higher surface area and porosity, and higher Cation Exchange Capacity (CEC) (Abdullahi et al., 2017, Zendehdel et al., 2020).

In the previous chapter, zeolite NaP was synthesized from bentonite using the ultrasonic-assisted hydrothermal approach. This chapter aims to apply the synthesized zeolite NaP to fluoride and pathogen removal in water as a multifunctional adsorbent. This chapter focuses on the application of the zeolite NaP adsorbent for fluoride removal and evaluates the effect of contact time, initial pH, temperature, and initial concentration. Also, antimicrobial studies will be conducted along with the reuse/ regeneration studies of the zeolite NaP material.

4.2. Methodology

4.2.1 Materials

Bentonite clay was supplied by the Cape Bentonite mine, in South Africa. Reagents such as sodium hydroxide (NaOH), sodium fluoride (NaF), TISAB (III) solution, and hydrochloric acid (HCl) were supplied by Sigma Aldrich, South Africa. Analytical grade reagents were used without purification prior to their use.

4.2.2 Material Preparation

Bentonite clay was prepared by washing using the Milli Q ultrapure water in three consecutive cycles. The obtained clay was dried at 70 °C for 12 hours using the EcoTherm 220V~50Hz oven. The dried clay was milled using the RS200 vibratory disc mill for 5 minutes at 700 rpm and stored for safekeeping and further experiments.

4.2.3 Zeolite synthesis

The procedures used for zeolite synthesis were described in the previous chapter along with the optimization of the synthesis parameters. Briefly, 10 g of the milled bentonite clay were calcined at 800 °C for 1 hour using the 930 Scientific Slab Furnace. Thereafter, the calcined clay was mixed with 2.5 M of NaOH solution of 100 mL by adding 10 g of the calcined clay. The mixture was then subjected to sonication for dissolution and extraction of silica and aluminum required for zeolite crystallization. This was done by aging the mixture for 2 hours in the UP400s Heilscher probe ultra-sonicator at an amplitude of 100%. A 20 mL of the sonicated gel was transferred into a 45 mL capacity autoclave reactor and then hydrothermally treated at 105 °C for 90 minutes in the oven for recrystallization. The crystallized mixture was then centrifuged using the Hermle Z-366 centrifuge and cleansed with deionized water until neutral pH. The mixture was then dried overnight at 70 °C and zeolite product was obtained.

4.2.4 Physiochemical characterization of the materials

All solid samples generated were characterized for their surface area using the TriStar II 3020 Brunauer Emmett Teller (BET) and morphology using the TESCAN Scanning Electron Microscopy- Energy Dispersive Spectroscopy (SEM-EDS) technique. The crystallinity of the materials was determined using the PANalytical X'Pert Pro powder diffractometer (XRD). The functional groups, elemental composition, and particle size distribution were determined using the platinum ATR Fourier Transform Infrared (FTIR), S1 TITAN 600 X-ray Fluorescence (XRF), and the Shimadzu SALD-2300 laser diffraction particle size analyzer, respectively.

4.2.5 Fluoride Removal Experiments

Field groundwater obtained from Siloam Village, Limpopo Province, South Africa was used to investigate the efficiency of synthesized zeolite towards fluoride removal. The field groundwater had pH of 8 ±0.5 and fluoride concentration of 6,2 mg/L. The batch fluoride removal experimentations were conducted by investigating the effect of initial pH, contact time, temperature, and initial fluoride concentration for optimization of fluoride adsorption. The contact time and adsorption kinetics were carried out by dissolving 0.5 g of zeolite in 100 mL of groundwater and then agitating at varying contact times of 1 to 180 minutes using shacking speed of 250 rpm. The effect of initial pH was conducted at 2, 4, 6, 8, and 10 by mixing 0.5 g of zeolite adsorbent in 100 mL of groundwater and agitated at 250 rpm for 60 min. The effect of initial concentration and adsorption isotherms was conducted at 5, 10, 15, 20, 30, 40, and 50 mg/L by adding 0.5 g of zeolite NaP and then agitated at 250 rpm for 60 min. After agitation, the mixtures were filtered using a 0.45 µm filter membrane, and the filtrate was characterized for residual fluoride concentration using the ORION Ion Selective Electrode (ISE, 9609BNWP) fluoride meter. Prior to fluoride analysis, Total Ionic Strength Adjustment Buffer III (TISABIII) was added following a volume ratio of 1:10 mL to increase the ionic strength of the solutions. Equation 4.1 was used to calculate the fluoride percentage removal in water with C_f (mg/L) indicating the final concentration of fluoride in the filtrate and C_i (mg/L) indicating the fluoride concentration prior to the fluoride adsorption experiment.

$$Percentage\ fluoride\ removal\ (\%) = \frac{C_i - C_f}{C_i} \times 100 \quad (4.1)$$

4.2.6 Regeneration studies

The zeolite enriched with fluoride, following defluoridation experiments, was regenerated to assess the reusability of the zeolite. This regeneration process involved introducing 0.5 g of fluoride-rich zeolite into 100 mL of 0.01 M hydrochloric acid. The mixture was then agitated for 30 minutes using the SSL2 Stuart reciprocating shaker at a speed of 250 rpm. Afterward,

the mixture underwent sieving with a 0.45 µm membrane filter, resulting in the acquisition of fluoride-free zeolite. The obtained zeolite was then dried at 110 °C for 6 hours. Subsequently, the regenerated zeolite was employed once more for fluoride adsorption. Regeneration of fluoride-rich zeolite adsorbent was repeated up to five times.

4.2.7 Antimicrobial studies

Antimicrobial assessments were carried out through the well-agar diffusion method. The effectiveness of the zeolite NaP material against microbes was determined by observing the minimum inhibition zone against gram-positive *S. aureus* and gram-negative *E. coli* indicator strains. Mueller Hinton agar with turbidity of 0.5 McFarland was used for microbial culture growth as described in Obijole et al. (2019). Thereafter, the grown culture strains were inoculated upon the prepared Mueller Hinton agar by adding 50 µl of the strain followed by digging of a well upon the agar with a sterile micro-pipette. A volume of 50 µm containing 10 mg/ml of the synthesized zeolite was pipetted upon the well followed by incubation of the agar at 37°C for 24 hours. A ruler was used to measure the inhibition zone and observed results were reported.

4.3. Results and discussion

4.3.1 Characterization

4.3.1.1 Chemical analysis

The chemical percentage compositions of the calcined clay and the zeolite NaP are reported in Table 4.1. The elemental composition analysis exhibited that major chemical oxides were SiO_2 and Al_2O_3 with percentage composition of 63.91% and 13.71% for calcined clay and 32.33% and 11.43% for the zeolite, respectively. This confirms that zeolite NaP is an aluminosilicate material. This lower silica and aluminum oxide percentage composition in the zeolite NaP could be due to the dissolution of the calcined clay materials in alkaline conditions with the influence of ultrasound (Behin et al., 2016). Also, the zeolite NaP material had lower percentage compositions of metals such as MgO, K_2O, and MnO in comparison to the calcined bentonite clay material. These results along with the reduction in the chemical composition of the synthesized zeolite were also been reported in other studies (Behin et al., 2016, Zhang et al., 2021).

Table 4.1: Principal and minor elemental compositions of calcined bentonite clay and synthesized zeolite

Name	Chemical composition							
	SiO_2	Al_2O_3	Fe_2O_3	MgO	K_2O	TiO_2	CaO	MnO
Calcined bentonite clay	63.91	13.71	3.38	3.46	0.79	0.38	0.86	0.05
Synthesized zeolite NaP	32.33	11.43	2.38	0.89	0.46	0.46	1.21	0.03

4.3.1.2 Fourier Transform Infrared (FTIR) analysis

Figure 4.1 illustrates the infrared spectra of calcined bentonite and synthesized zeolite NaP. The FTIR spectra unveiled bands at =650 cm^{-1}, 790 $cm^{-1,}$ and 1034 cm^{-1} bands which are attributed to the bending vibrations of Si-O-Al, symmetrical stretching of Al-O, and asymmetrical stretching of Si-O respectively. These functional groups were observed in both calcined clay and synthesized zeolite NaP. However, the intensity of these bands in calcined clay was very low which could be due to the decomposition of the clay during the calcination process. Also, the Si-O functional band number of the synthesized zeolite displayed a shift in position to the wavelength of =980 cm^{-1} which resembles the structural change/alteration made from the calcined clay (Shaban et al., 2017). Moreover, the synthesized zeolite exhibited a strong band at 980 cm^{-1} which could be attributed to the recrystallisation of the material during the zeolitization process. The presence of Al-O, Si-O-Al, and Si-O functional groups indicates the aluminosilicate nature of the zeolite which aligns with the XRF and XRD results (Kouznetsova et al., 2020). Furthermore, hydroxyl functional groups were observed at =1650 cm^{-1} and 3400-3650 cm^{-1} wavelengths. The presence of these groups was due to the hydrous nature of the zeolite (Mosai et al., 2019). According to Obijole et al. (2019) and Gao et al. (2021), the -OH groups interact with anionic species which consequently enables the adsorption of F^- ions. However, the calcined bentonite clay resembled no bands of the hydroxyl group which emphasizes that the bentonite clay underwent a dihydroxylation process.

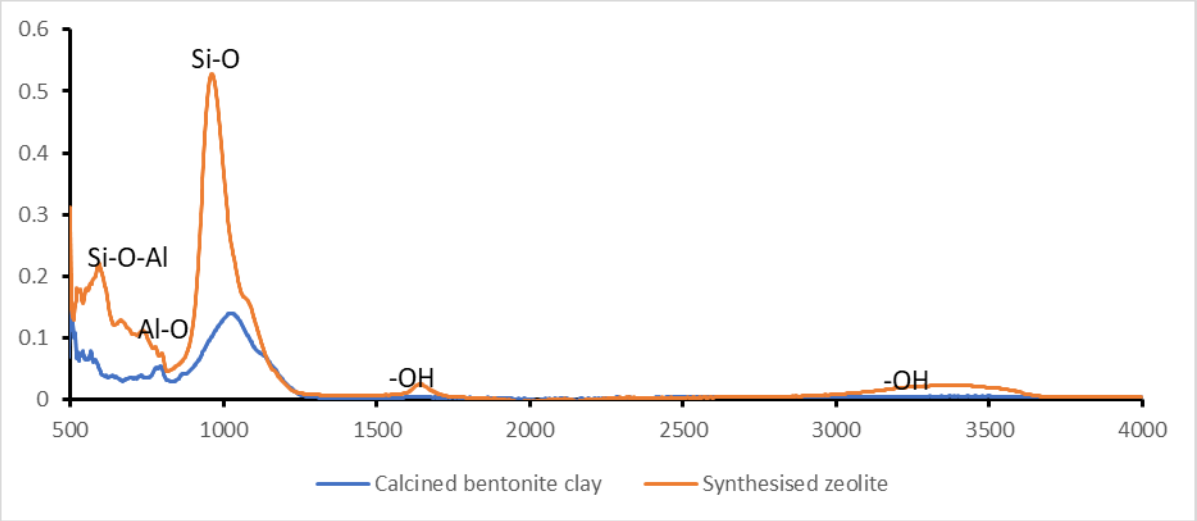

Figure 4.1: FTIR spectra for calcined bentonite clay and synthesized zeolite NaP

4.3.1.3 X-ray Diffraction (XRD) Analysis

The XRD spectra of calcined bentonite clay and synthesized zeolite NaP are presented in Figure 4.2. The calcined bentonite clay showed major peaks at 24.26, 31.02, 58.91, and 83,12 2θ which correspond to quartz mineral. A few peaks of muscovite were observed at 10.28 and 23.03 2θ while a single peak of albite high phase was observed at 32.41 2θ. The presence of these minerals also corresponds with the Si-O functional groups reported in FTIR analysis. The zeolite material showed high intensity peaks attributed to zeolite NaP at 14.40, 20.19, 25.28, 32.25, and 39.05 2θ. Similar results were reported by Musyoka et al. (2012), Shaban et al. (2017), Bunmai et al. (2020) and Hong and Um (2021). Also, single peaks of zeolite SSZ-73 at 10.45 2θ theta and quartz at 31.02 2θ theta were observed.

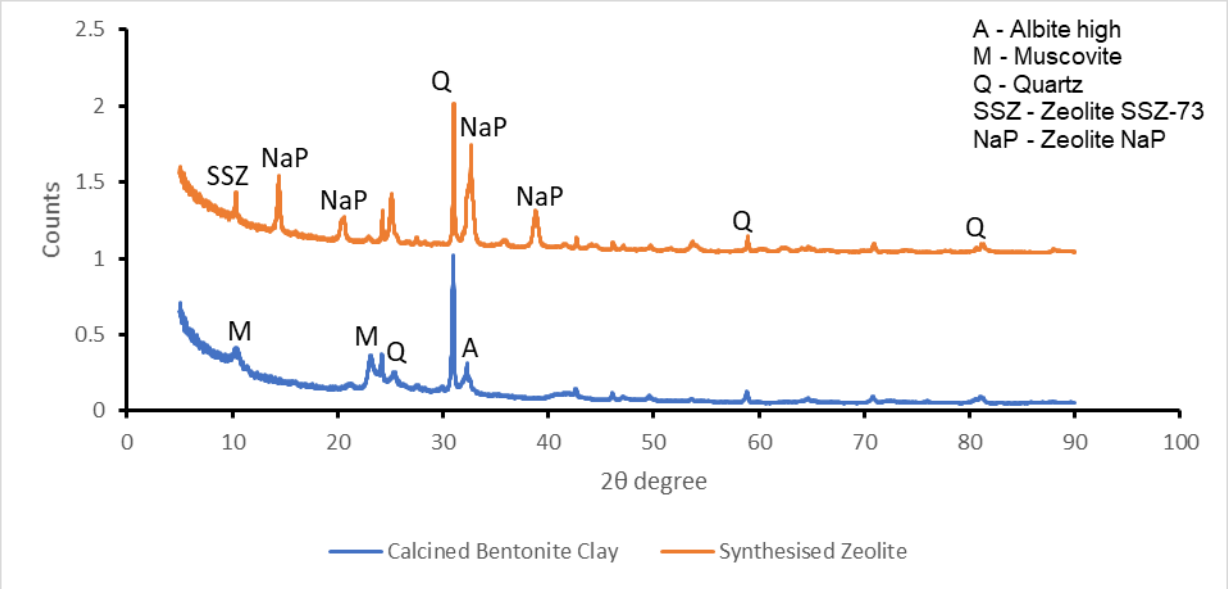

Figure 4.2: XRD spectra of the calcined bentonite clay and the synthesized zeolite NaP

4.3.1.4 Scanning Electron Microscopy (SEM) analysis

Figure 4.3 presents the morphological structure of the calcined bentonite clay and synthesized zeolite NaP along with their EDS micrographs. The surface morphology of the calcined bentonite consisted of irregular granules. However, the synthesized zeolite exhibited uniform small-sized crystals along with some very few irregular granules. According to Dewes et al. (2022), the presence of multiple uniform small sized crystals on the synthesized zeolite could be because of sonication which influence the nucleation and crystal growth during the initial stages of zeolite synthesis. The observed crystals of the zeolite were mellow spherical shaped crystals which agrees with the documented results from Huo et al. (2012), Lin et al. (2013) and Bunmai et al. (2020). The formation of zeolitic material is further emphasized by the EDS spectrum which indicate the presence of Na, Si, O and Al elements which were also reported in Dasgupta et al. (2021).

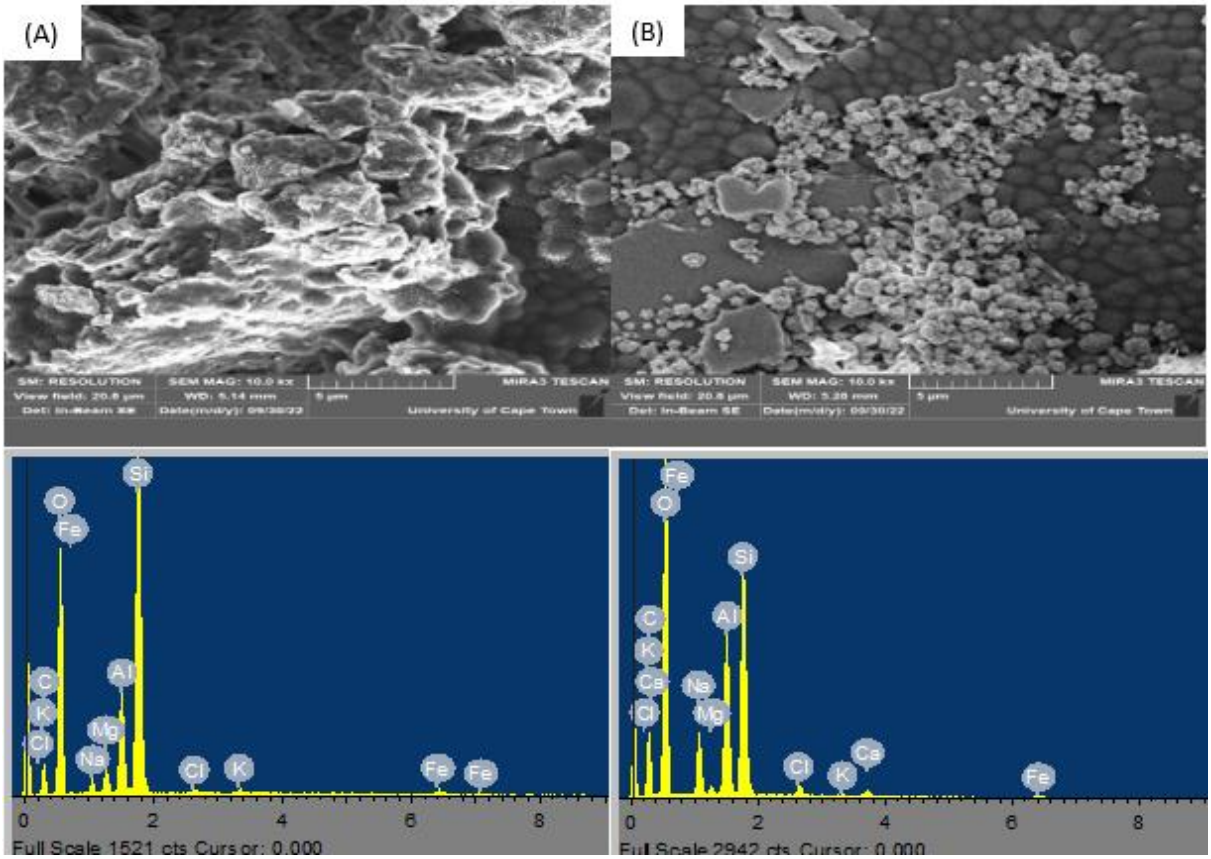

Figure 4.3: Morphological images and spectra of calcined bentonite clay (A) and synthesized zeolite NaP (B) and their corresponding EDS

4.3.1.5 Particle size distribution and BET results

The particle size distribution curves were reported in Figure 4.4. The observed particle size distribution curves displayed a broad curve for the calcined bentonite clay and a narrow distribution curve of the synthesised zeolite with some minor peaks at the range of 0 to 10 µm. According to (Dewes et al., 2022), this could be influenced by ultrasonication of the clay during zeolite synthesis which influences the reduction of particle sizes. This was also verified by the decrease in mean particle size from 79 to 22 µm as observed in Table 4.2. Decrease of particle distribution due to sonication treatment was also documented in (Ojumu et al., 2016, Chen et al., 2020).

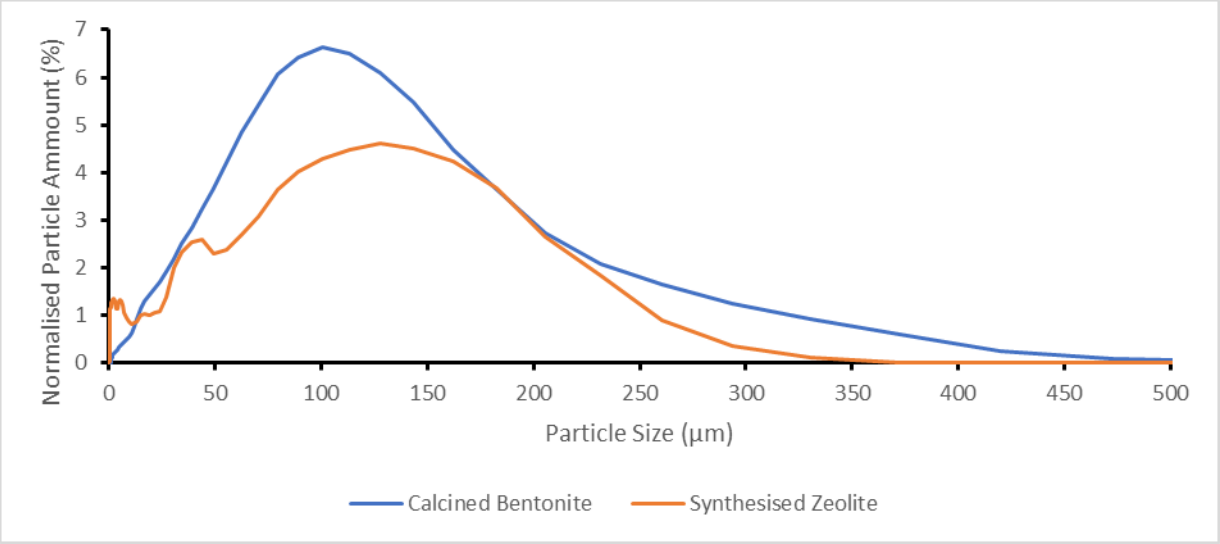

Figure 4.4 : Particle distribution curves for the calcined bentonite clay and synthesised zeolite NaP.

Table 4.2: Particle distribution size parameters of the calcined bentonite clay and synthesised Zeolite NaP.

Samples	Particle size at 90%	Mean Average
Calcined Bentonite clay	180µm	64µm
Synthesized Zeolite NaP	160µm	22µm

4.3.1.6 BET analysis

Figure 4.5 depicts the BET adsorption-desorption isotherms at 60°C ambient temperature for the synthesized optimal zeolite. The results show a very short negligible steep increase in A type IV (H4) isotherm was observed at high pressures from the adsorption-desorption curve indicating a mesoporous structure. Moreover, the pore size, pore volume and surface area of the fabricated zeolite was 46.65 nm, 0.11 cm^3/g and 102.18 m^2/g as reported in Table 4.3, respectively. In addition, the adsorbent exhibited a pore diameter in the ranges of 2 and 50 nm indicating that the synthesized zeolite NaP is mainly composed of mesoporous structures (Kumar and Jena, 2022). A large amount of surface area showcases multiple active sites that could accommodate adsorption of ions whilst a substantial pore volume provides the quantity of pores in the zeolite sample that can adsorb molecules there by influencing the adsorption capacity of the zeolite (Wu et al., 2020).

Table 4.3: The BET pore size, pore volume and surface area of the synthesised optimal zeolite

Sample	BET surface area (m^2/g)	Pore volume (cm^3/g)	Pore size (nm)
Optimal Zeolite (VN8)	102.18	0.11	46.65

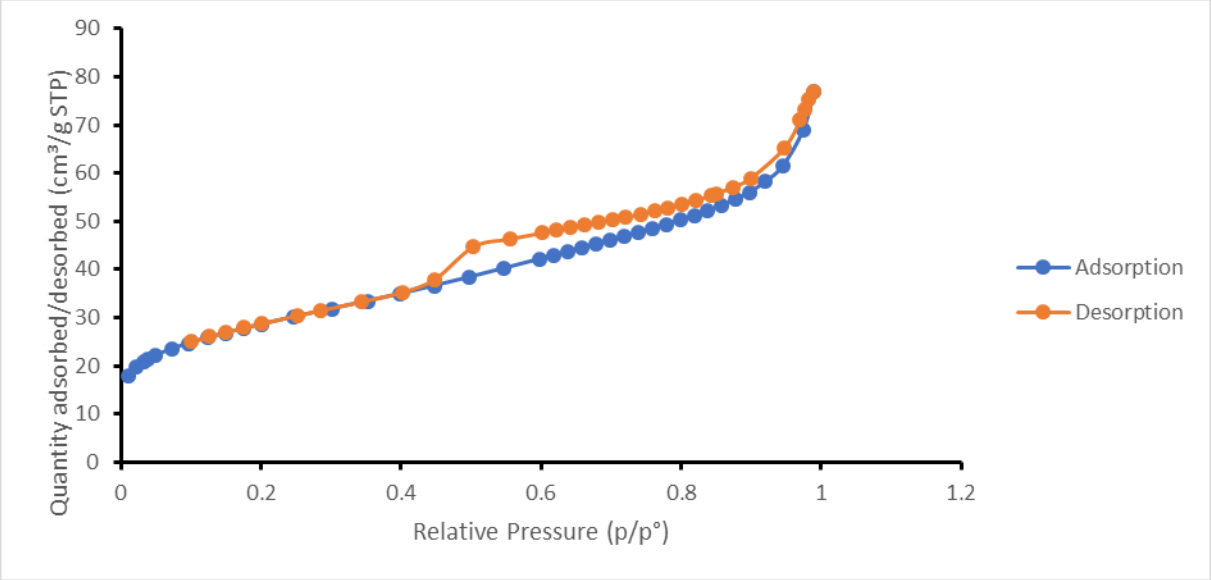

Figure 4.5: BET adsorption/desorption curve of the zeolite NaP.

4.3.2 Batch fluoride adsorption results

4.3.2.1 Effect of pH

The effect of initial pH was conducted for fluoride up take by the synthesised zeolite and the solution pH was adjusted from 2 to 10 using 0.1 M of HCl and 0.1 M of NaOH. The results of percentage fluoride removal against pH are presented in Figure 4.6. The results indicated a decreasing trend in fluoride (F^-) removal percentage as the initial pH in the fluoride solution increases. This could be a factor of the abundance of -OH ions in the solution as the pH increases. According to Jia et al. (2022), since -OH ions have similar charges with fluoride ions, competition of fluoride adsorption sites occur. Consequently, more hydroxyl ions (-OH) will be available resulting in their increase adsorption than fluoride ions hence fluoride removal percentage decreases at higher pH. In addition, Dong and Wang (2016) and Uddin et al. (2019) suggested that deprotonation occurs at higher pH creating a negatively charged surface in the adsorbent which lead to electrostatic repulsion of anions such as fluoride and decreases fluoride adsorption even further and vice versa at lower pH as indicated in equation 4.2 and 4.3. A maximum fluoride uptake of ≈ 27% was observed at pH of 2.

Positively charged surface at lower pH

$$Zeolite^{+} + F^{-} \rightarrow Zeolite.F \quad \text{(Attraction)} \qquad (4.2)$$

Negatively charged surface at higher pH

$$Zeolite^{-} + F^{-} \rightarrow Zeolite^{-} + F^{-} \quad \text{(Repulsion)} \qquad (4.3)$$

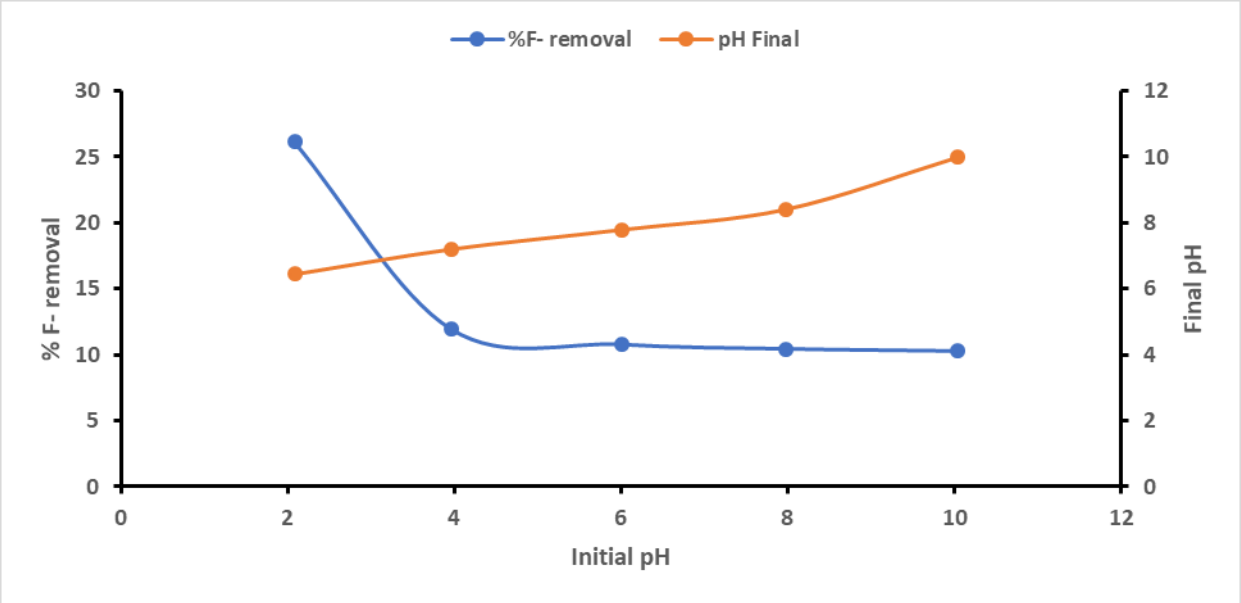

Figure 4.6 : Effect of pH vs fluoride adsorption percentage (0.5 g/100 mL adsorption dosage, 60 mins contact time at 250 rpm and initial F^- concentration of 6.2 mg/L)

4.3.2.2 Effect of contact time

The effect of contact time towards fluoride uptake by the synthesized zeolite was investigated. Figure 4.7 depicts the percentage fluoride uptake results between 1 to 180 minutes. The fluoride adsorption increased as contact time increased within the first 60 minutes with about 27% of defluoridation efficiency. After 60 minutes, no additional adsorption was observed, suggesting that equilibrium had been reached. This indicates that the adsorption sites were saturated. Therefore, the optimal conditions for subsequent experiments for contact time were 60 minutes.

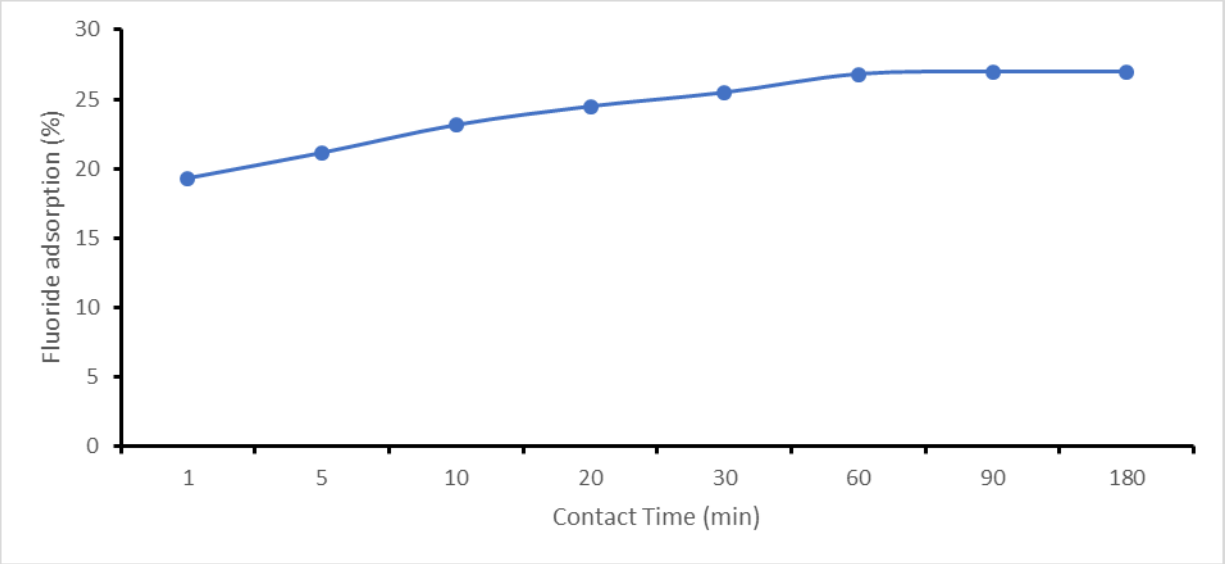

Figure 4.7: Effect of contact time vs fluoride adsorption percentage (0.5 g/100 mL adsorption dosage, agitation speed of 250 rpm, initial pH of 2, and initial F^- concentration of 6.2 mg/L)

4.3.2.3 Adsorption kinetics

The data obtained from the effect of contact time was fitted to adsorption kinetic models to provide insights into the fluoride removal mechanism. This was determined using the *pseudo*-second order (PSO) and the *pseudo* first order (PFO) kinetic models. The *pseudo* first-order kinetics assumes that adsorption occurs through physisorption wherein molecules are attracted to the sorbent's surface by forces such as weak van der Waals, London dispersion, or electrostatic interaction (Hu et al., 2021, Márquez et al., 2021). In PFO, one molecule from the solution is adsorbed by one active site in the adsorbent. On contrary, the pseudo-second order assumes that adsorption occurs through chemisorption wherein molecules are exchanged from the solution to the adsorbent (Jasper et al., 2020). In PSO, one molecule in the solution is adsorbed by two active sites in the adsorbent. The *pseudo*-first order and pseudo-second order are expressed through their nonlinear equation 4. 4 and 4.5 respectively.

$$q_t = q_e\left(1 - e^{-K_{ad}t}\right) \quad (4.4)$$

$$q_t = \frac{q_e^2 K_{2ads}\, t}{1 + K_2 q_e^2 t} \quad (4.5)$$

Where q_e and q_t represent the amount of fluoride ions adsorbed at equilibrium (mg/g) and at a time t (min). K_{ad} (min^{-1}) is the PFO kinetic rate of constant and K_{2ads} ($g.mg^{-1}/min$) is the PSO kinetic rate of constant.

Figure 4.8 and Table 4.4 represent the nonlinear plots of PFO and PSO and the calculated parameters of the kinetic models respectively. From Table 4.4, the correlation coefficient value of the PFO was lower whereas the PSO correlation coefficient value was higher. Therefore, the data fitted to the PSO kinetics. The PSO presumes that adsorption occurs through chemisorption. In chemisorption, adsorption of fluoride molecules occurs on the surface of the sorbent and reacts with atoms of the active sites (Márquez et al., 2021). The two share electrons causing the formation of complexes of chemical bonds which are irreversible.

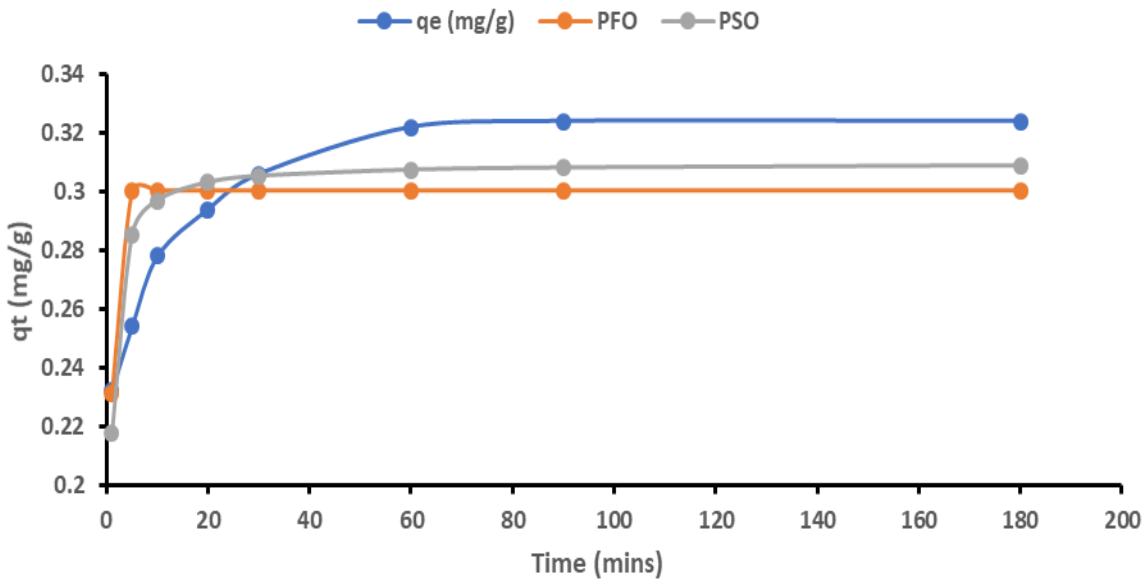

Figure 4.8: Nonlinear plots for the *pseudo*-second order (PSO) and *pseudo* first order (PFO) kinetic models.

Table 4.4: Parameters for the *pseudo*-second-order (PSO) and *pseudo*-first order (PFO) kinetic models

Experimental	***Pseudo* First Order (PFO)**			***Pseudo* Second Order (PSO)**		
Qe (mg/g)	K_{ads} (min^{-1})	Q_e (mg/g)	R^2	K_{2ads} ($g.mg^{-1}/min$)	Q_e (mg/g)	R^2
0.68	1.47	0.30	0.49	7.67	0.31	0.72

4.3.2.4 Initial fluoride concentration and isotherms models

Figure 4.9 depicts the adsorption capacity against equilibrium concentration at varying temperatures. This was done to analyse the impact of adsorbate concentration on fluoride removal at different temperatures. A discernible trend of increasing adsorption capacity was

observed as the initial fluoride concentration increased. This could be associated with the concentration gradient in the solution wherein the concentration gradient in the fluoride solution and the surface of the adsorbent is high promoting diffusion of fluoride ions from an area of higher concentration to an area of lower concentration (Banat et al., 2000, Velazquez-Jimenez et al., 2015, Parashar et al., 2019). As a result, the rate at which fluoride molecules adhere to the particle surface of the adsorbent increases. Furthermore, the adsorption capacity diminishes with the temperature increase from 25°C to 35°C, but it rises from 35°C to 45°C.

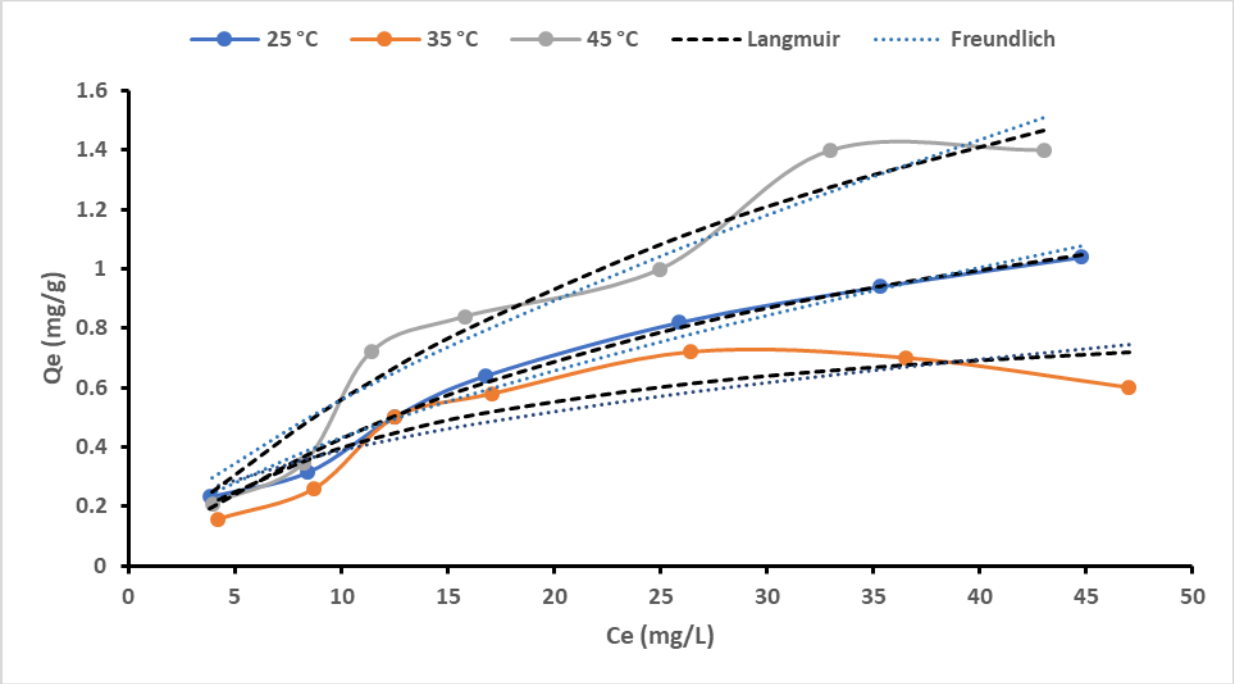

Figure 4.9: Initial concentration vs adsorption capacity at different temperatures, Langmuir and Freundlich plots for fluoride removal by the synthesized zeolite (0.5 g/100 mL adsorption dosage, 270 mins contact time at 250 rpm, initial pH of 6 and initial F^- concentration of 6.2 mg/L)

To determine the interrelationship between the adsorbate and the adsorbent, the Langmuir and the Freundlich isotherm models were employed. Langmuir isotherm models presume that an adsorbate is adsorbed in a monolayer surface of the adsorbent and only one molecule can be adsorbed in an active adsorption site (Uddin et al., 2019). Also, Freundlich assumes that an adsorbate is adsorbed in a surface with multiple active sites that can adsorb multiple molecules simultaneously (Jasper et al., 2020). These models are given by nonlinear equations 4.6 and 4.7 respectively.

$$q_e = \frac{Q_{max} K_L C_e}{1 + K_L C_e} \quad (4.6)$$

$$q_e = K_F C_e^{\frac{1}{n}} \quad (4.7)$$

Where qe represents the equilibrium adsorption capacity (mg/g), Ce represents the concentration equilibrium of the adsorbate, K_f represents the empirical Freundlich constant (mg/g) whilst K_L represents the Langmuir constant (L/mg), Q_{max} value showcases the maximum sorption capacity of an adsorption site which is saturated, and 1/n represents the adsorption intensity. When the 1/n values are 0<1/n<1, fluoride adsorption occurs. However, when 1/n=1 then adsorption cannot be reversed and is unfavourable if 1/n>1. The K_f and n values are determined using the slope and intercepts.

Figure 4.9 incorporates nonlinear adsorption isotherm plots, and the corresponding constant values are detailed in Table 5. Based on Table 4.5 showing the tabulated models' parameters, the regression coefficient value of the Langmuir isotherm (R^2=0.95) model was high compared to the Freundlich isotherm model (R^2=0.93). Hence, the Langmuir isotherm model provided a better description of the data, indicating the occurrence of fluoride adsorption on a surface with a limited number of active sites. According to Tran et al. (2017), high values of Q_{max} and K_L indicate a good adsorbent, hence synthesized zeolite is a good adsorbent. Also, a range of 0 to 1 of K_L value was observed hinting that fluoride adsorption was favourable.

Table 4.5: Parameters for the Freundlich and Langmuir isotherm models

Temperature (°C)	**Langmuir**			**Freundlich**		
	Q_{max} (mg/g)	K_L (L/mg)	R^2	K_F (mg/g)/(mg/L)^n	1/n	R^2
25 ºC	1.81	0.03	0.98	0.11	0.61	0.98
35 ºC	0.92	0.08	0.95	0.15	0.42	0.92
45 ºC	2.89	0.02	0.95	0.11	0.68	0.93

4.3.2.5 Thermodynamic studies

To further determine the randomness, spontaneity, and type of reaction of fluoride uptake mechanism by synthesized zeolite NaP adsorbent, thermodynamics studies were evaluated. The standard entropy change (ΔS^0), standard enthalpy (ΔH^0), and Gibbs free energy change (ΔG^0) of thermodynamics were calculated using equation 4.8-10. The parameters of thermodynamics were obtained from the $\ln K_L$ vs 1/T plot presented in Figure 4.10.

$$\Delta G^{\circ} = -RT\,InK_L = \Delta H^{\circ} - T\Delta S^{\circ} \quad (4.8)$$

$$K_L = \frac{(C_0 - C_e)}{C_e \times m} = \frac{q_e}{C_e} \quad (4.9)$$

$$In\,K_L = \frac{\Delta S^{\circ}}{R} - \frac{\Delta H^{\circ}}{RT} \quad (4.10)$$

Where distribution constant = K_L, ideal gas constant = R (J/mol. K), absolute temperature = T (kelvin), concentration at equilibrium = C_e (mg/L), adsorbent mass = m and adsorption capacity = qe (mg/g)

Table 4.6 represents the calculated thermodynamics parameters for fluoride adsorption via the zeolite NaP. Results show that the values of the ΔG^0 were positive. This implies that the defluorination process was non-spontaneous requiring an external energy input and as temperature increases, the ΔG^0 values increase. The ΔH^0 value was negative which represents an exothermic reaction that favors physisorption and chemisorption processes. The values of ΔS^0 were negative as well which indicates that the adsorption process decreased in randomness of fluoride ions at the liquid/solid interface. Similar observations were made in a study by Hellal et al. (2023) and Amanzadeh et al. (2024).

Table 4.6: Thermodynamics parameters for fluoride ions adsorption by the zeolite NaP adsorbent

Adsorbent	**Temperature (K)**	**ΔG° (KJ/mol)**	**ΔH° (J/mol)**	**ΔS° (J/mol)**
Zeolite NaP	298	8.69	-14.96	-76.16
	308	6.47		
	318	10.34		

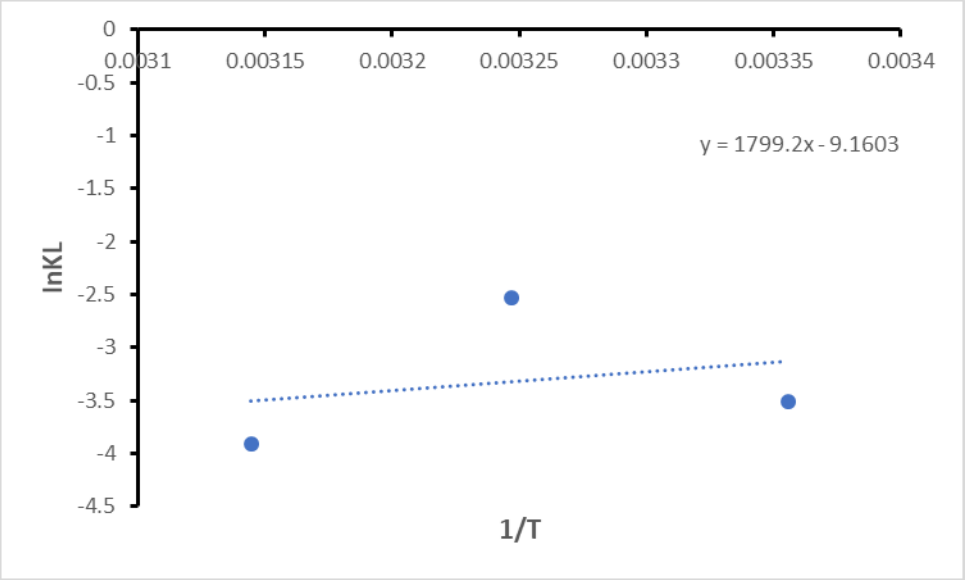

Figure 4.10: Thermodynamics plot of lnK_L as a function of 1/T

4.3.3 Regeneration experiment of the zeolite

The reusability potential of the zeolite was conducted in five sequential fluoride adsorption and desorption cycles. A concentration of 0.01 M of hydrochloric acid was used as a regenerant. The obtained results are presented in graphical plots in Figure 4.11. In the initial regeneration cycle, the zeolite adsorbent exhibited a maximum percentage fluoride removal of 23.57% while in the last cycle, a minimal fluoride removal percentage of 9.75% was observed. This phenomenon might be attributed to the irreversible reaction reported in the kinetics analysis section, wherein a reaction occurs between the surface of the sorbent and the fluoride ions. This irreversible reaction restricts the re-adsorption of fluoride molecules by the adsorbent's surface during regeneration cycles, as the reaction cannot be reversed and there is limited number of adsorption sites as explained in adsorption models' section. Hence, the incorporation of cations on the zeolite surface could improve the regeneration capability of the zeolite.

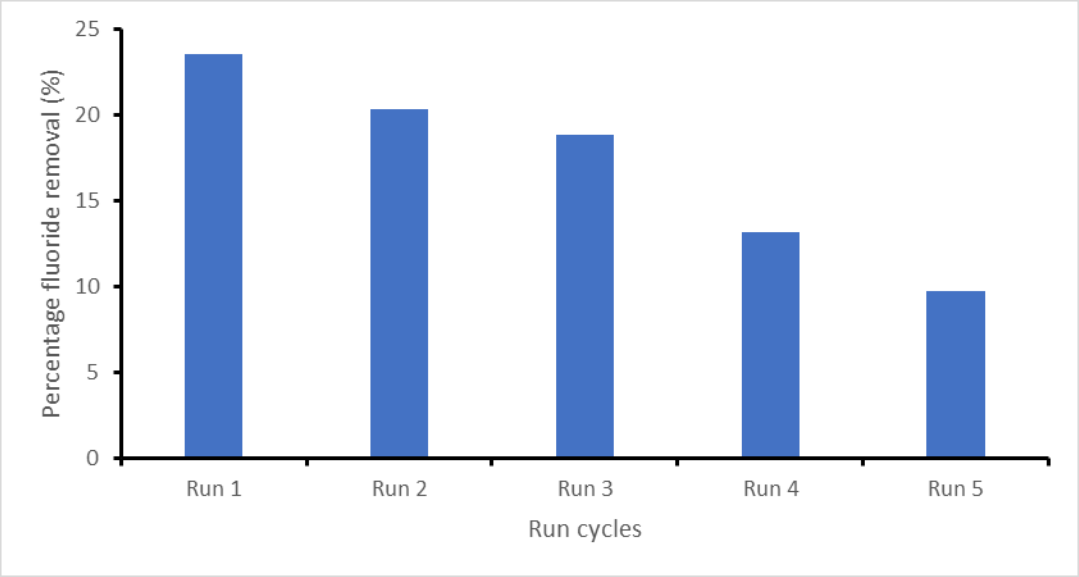

Figure 4.11: Percentage fluoride removal in sequential regeneration cycles of the zeolite using 0.01 M of HCl as a regenerant (≈ Fluoride concentration=4.92, agitation time=60 minutes, agitation speed=250 rpm and pH=2.22)

4.3.4 Antimicrobial potency

The antimicrobial potency of the synthesized zeolite against the gram-negative *E. coli* and gram-positive *S. aureus* strains is presented in Figure 4.12. The synthesized zeolite showed no zone of inhibition towards both *E. coli* and *S. aureus* strains which indicates that the adsorbent exhibits minimal antimicrobial potency. This could be due to the structural content of the synthesized zeolite which lacks antimicrobial agents. Similar observations were made in a study by Yao et al. (2019), Daou et al. (2020), and Abed et al. (2020).

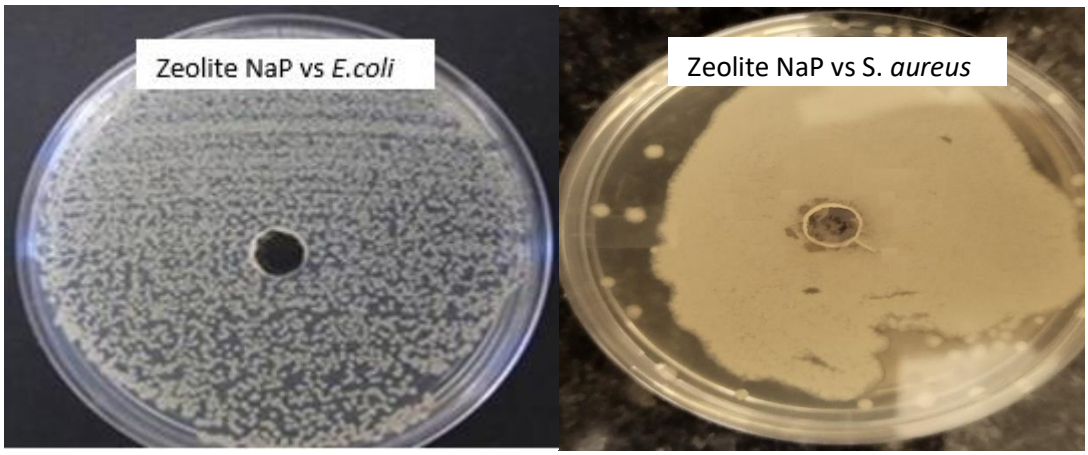

Figure 4.12: The minimum zone of inhibition for synthesised zeolite against *E. coli* and *S. aureus* strain

4.4 Conclusion and Recommendation

This study successfully characterized the synthesized zeolite NaP and elucidated its application in pathogens and fluoride removal in water. The XRD and SEM analysis results showed that the synthesised zeolite NaP is mainly composed of zeolite NaP phases with small uniform spherical crystals. In defluoridation studies, the zeolite adsorbent exhibited a maximum fluoride adsorption capacity of 0.32 mg/g at optimal conditions of 0.5g/100 mL for dosage,6 mg/L for initial fluoride, and pH of 2 at an agitation time of 60 minutes and speed of 250 rpm. The kinetic models indicated that fluoride adsorption by the zeolite NaP adsorbent occurred through chemisorption, as the *pseudo*-second-order model exhibited a superior fit to the adsorption data. Moreover, the Langmuir isotherm model exhibited a superior fit to the experimental data, indicating that the adsorption took place on a monolayer adsorbent surface. In antimicrobial studies, the synthesized zeolite exhibited zero antimicrobial potency against the *E. coli* and *S. aureus* strains. Regeneration experiments of the zeolite NaP adsorbent using 100 mL of 0.001 molar of hydrochloric acid as a regenerant showed that the adsorbent showed minimal regeneration efficiency. Hence, this study recommends the incorporation of cations onto the surfaces of the adsorbent to improve its pathogens and fluoride removal from water and improve the regeneration efficiency of the zeolite.

References

Abdullahi, T., Harun, Z. & Othman, M. H. D. 2017. A review on sustainable synthesis of zeolite from kaolinite resources via hydrothermal process. *Advanced Powder Technology,* 28**,** 1827-1840.

Abed, S., Bakhsheshi-Rad, H. R., Yaghoubi, H., Ning, L., Sadeghianmaryan, A. & Chen, X. 2020. Antibacterial activities of zeolite/silver-graphene oxide nanocomposite in bone implants. *Materials Technology,* 36**,** 660-669.

Ali, K. Y., Saleh, B. M. & Adam, K. M. 2022. Assessment of water quality from shallow hand-dug wells in dutse town, north west nigeria. *Arid Zone Journal of Basic and Applied Research,* 1**,** 47-61.

Aloulou, H., Ghorbel, A., Aloulou, W., Ben Amar, R. & Khemakhem, S. 2021. Removal of fluoride ions (f(-)) from aqueous solutions using modified turkish zeolite with quaternary ammonium. *Environmental Technology,* 42**,** 1353-1365.

Alqahtany, F. 2021. Chemical and bacteriological assessment of groundwater in tathleeth region of asir. *Egyptian Journal of Chemistry,* 0**,** 0-0.

Amanzadeh, O., Ahmadpour, J., Shabanian, S. R. & Nikzad, M. 2024. Experimental, isotherm, kinetic and thermodynamic studies of the novel modified zeolite zsm-5 adsorbent for use in clean fuel processing. *Chemical Engineering Research and Design*.

Ayinde, W. B., Gitari, M. W., Smith, J. A. & Samie, A. 2022. Sorption of fluoride and bacterial disinfection property of biosynthesized nanofibrous cellulose decorated ag-mgo-nanohydroxyapatite composite for household water treatment. *Polymers (Basel),* 14.

Banat, F. A., Al-Bashir, B., Al-Asheh, S. & Hayajneh, O. 2000. Adsorption of phenol by bentonite. Environmental pollution. 391-398.

Behin, J., Kazemian, H. & Rohani, S. 2016. Sonochemical synthesis of zeolite nap from clinoptilolite. Ultrasonics sonochemistry. 400-408.

Bhandari, P., Banjara, M. R., Singh, A., Kandel, S., Rawal, D. S. & Pant, B. R. 2021. Water quality status of groundwater and municipal water supply (tap water) from bagmati river basin in kathmandu valley, nepal. *Journal of Water, Sanitation and Hygiene for Development,* 11**,** 102-111.

Bunmai, K., Osakoo, N., Deekamwong, K., Kosri, C., Khemthong, P. & Wittayakun, J. 2020. Fast synthesis of zeolite nap by crystallizing the nay gel under microwave irradiation. *Materials Letters,* 272.

Chen, C.-T., Iyoki, K., Yonezawa, Y., Okubo, T. & Wakihara, T. 2020. Understanding the nucleation and crystal growth of zeolites: A case study on the crystallization of zsm-5 from a hydrogel system under ultrasonication. *The Journal of Physical Chemistry C,* 124**,** 11516-11524.

Daou, T. J., Dos Santos, T., Nouali, H., Josien, L., Michelin, L., Pieuchot, L. & Dutournie, P. 2020. Synthesis of fau-type zeolite membranes with antimicrobial activity. *Molecules,* 25.

Dasgupta, S., Klunk, M. A., Das, M., Xavier, S. J. S., Chemale, F., Wander, P. R. & Moraes, C. a. M. 2021. Hydrothermal synthesis of zeolite

y

from green materials. *The Canadian Journal of Chemical Engineering,* 99.

Dewes, R. M., Mendoza, H. R., Pereira, M. V. L., Lutz, C. & Gerven, T. V. 2022. Experimental and numerical investigation of the effect of ultrasound on the growth kinetics of zeolite a. *Ultrasonics sonochemistry,* 82**,** 105909.

Dong, S. & Wang, Y. 2016. Characterization and adsorption properties of a lanthanum-loaded magnetic cationic hydrogel composite for fluoride removal. *Water Res,* 88**,** 852-860.

Dong, Y., Jiang, Z., Hu, Y., Jiang, Y., Tong, L., Yu, Y., Cheng, J., He, Y., Shi, J. & Wang, Y. 2023. Pathogen contamination of groundwater systems and health risks. *Critical Reviews in Environmental Science and Technology***,** 1-23.

Gao, Y., Li, M., Ru, Y. & Fu, J. 2021. Fluoride removal from water by using micron zirconia/zeolite molecular sieve: Characterization and mechanism. *Groundwater for Sustainable Development,* 13.

Hellal, M. S., Rashad, A. M., Kadimpati, K. K., Attia, S. K. & Fawzy, M. E. 2023. Adsorption characteristics of nickel (ii) from aqueous solutions by zeolite scony mobile-5 (zsm-5) incorporated in sodium alginate beads. *Scientific Reports,* 13**,** 19601.

Hong, S. & Um, W. 2021. Top-down synthesis of nap zeolite from natural zeolite for the higher removal efficiency of cs, sr, and ni. *Minerals,* 11.

Hu, Y. Y., Pan, C., Zheng, X., Hu, F., Xu, L., Xu, G., Jian, Y. & Peng, X. 2021. Prediction and optimization of adsorption properties for cs(+)on nisio@nialfe ldhs hollow spheres from aqueous solution: Kinetics, isotherms, and bbd model. *Journal of hazardous materials,* 401**,** 123374.

Huo, Z., Xu, X., Lü, Z., Song, J., He, M., Li, Z., Wang, Q. & Yan, L. 2012. Synthesis of zeolite nap with controllable morphologies. *Microporous and Mesoporous Materials,* 158**,** 137-140.

Jasper, E. E., Ajibola, V. O. & Onwuka, J. C. 2020. Nonlinear regression analysis of the sorption of crystal violet and methylene blue from aqueous solutions onto an agro-waste derived activated carbon. *Applied Water Science,* 10.

Jia, C., Fan, Y., Jiang, R., Su, P., Liu, S., Zhang, X. & Wang, J. 2022. Preparation of la(iii), fe(iii) modified zeolite molecular sieves for the removal of fluorine from water. *Water,* 14.

Kouznetsova, T., Ivanets, A., Prozorovich, V., Hosseini-Bandegharaei, A., Tran, H. N., Srivastava, V. & Sillanpaa, M. 2020. Sorption and mechanism studies of cu(2+), sr(2+) and pb(2+) ions on mesoporous aluminosilicates/zeolite composite sorbents. *Water Sci Technol,* 82**,** 984-997.

Krishnani, K. K., Zhang, Y., Xiong, L., Yan, Y., Boopathy, R. & Mulchandani, A. 2012. Bactericidal and ammonia removal activity of silver ion-exchanged zeolite. *Bioresource Technology,* 117**,** 86-91.

Kumar, M. M. & Jena, H. 2022. Direct single-step synthesis of phase pure zeolite na–p1, hydroxy sodalite and analcime from coal fly ash and assessment of their cs+ and sr2+ removal efficiencies. *Microporous and Mesoporous Materials,* 333.

Lin, W. G., Wan, M. M., Zhou, Y., Gu, H. C., Zhou, S. L. & Zhu, J. H. 2013. Novel selective catalyst derived from uniform clustered nay zeolite microspheres. *Journal of Materials Chemistry A,* 1.

Ling, Y., Podgorski, J., Sadiq, M., Rasheed, H., Eqani, S. & Berg, M. 2022. Monitoring and prediction of high fluoride concentrations in groundwater in pakistan. *Science of The Total Environment,* 839**,** 156058.

Mahagamage, M. G. Y. L., Pathirage, M. V. S. C. & Manage, P. M. 2020. Contamination status of salmonella spp., shigella spp. And campylobacter spp. In surface and groundwater of the kelani river basin, sri lanka. *Water,* 12.

Malebatja, M. F. & Mokgatle, M. M. 2022. Diarrhoea among children aged 5 years and microbial drinking water quality compliance: Trends analysis study in south africa (2008–2018). *International Journal of Environmental Research and Public Health,* 20**,** 598.

Márquez, C. O., García, V. J., Guaypatin, J. R., Fernández-Martínez, F. & Ríos, A. C. 2021. Cationic and anionic dye adsorption on a natural clayey composite. *Applied Sciences,* 11.

Mei, L., Qiao, H., Ke, F., Peng, C., Hou, R., Wan, X. & Cai, H. 2020. One-step synthesis of zirconium dioxide-biochar derived from camellia oleifera seed shell with enhanced removal capacity for fluoride from water. *Applied Surface Science,* 509.

Mosai, A. K., Chimuka, L., Cukrowska, E. M., Kotzé, I. A. & Tutu, H. 2019. The recovery of rare earth elements (rees) from aqueous solutions using natural zeolite and bentonite. *Water, Air, & Soil Pollution,* 230.

Munzhelele, E. P., Ayinde, W. B., Mudzielwana, R. & Gitari, W. M. 2021. Synthesis of fe doped poly p-phenylenediamine composite: Co-adsorption application on toxic metal ions (f(-) and as(3+)) and microbial disinfection in aqueous solution. *Toxics,* 9.

Musyoka, N. M., Petrik, L. F., Gitari, W. M., Balfour, G. & Hums, E. 2012. Optimization of hydrothermal synthesis of pure phase zeolite na-p1 from south african coal fly ashes. *Journal of environmental science and health. Part A, Toxic/Hazardous Substances and Environmental Engineering* 47**,** 337-50.

Nehra, S., Dhillon, A. & Kumar, D. 2020. Freeze–dried synthesized bifunctional biopolymer nanocomposite for efficient fluoride removal and antibacterial activity. Journal of environmental sciences, 94,.Pdf>.

Nguyen, K. H., Operario, D. J., Nyathi, M. E., Hill, C. L., Smith, J. A., Guerrant, R. L., Samie, A., Dillingham, R. A., Bessong, P. O. & Rogawski Mcquade, E. T. 2021. Seasonality of drinking water sources and the impact of drinking water source on enteric infections among children in limpopo, south africa. *International Journal of Hygiene and Environmental Health,* 231**,** 113640.

Obijole, O. A., Gitari, M. W., Ndungu, P. G. & Samie, A. 2019. Mechanochemically activated aluminosilicate clay soils and their application for defluoridation and pathogen removal from groundwater. *International Journal of Environmental Research and Public Health,* 16.

Odiyo, J. O. & Makungo, R. 2012. Fluoride concentrations in groundwater and impact on human health in siloam village, limpopo province, south africa. *Water SA,* 38.

Odiyo, J. O., Mathoni, M. M. & Makungo, R. 2020. Health risks and potential sources of contamination of groundwater used by public schools in vhuronga 1, limpopo province, south africa. *International Journal of Environmental Research and Public Health,* 17.

Ojumu, T. V., Du Plessis, P. W. & Petrik, L. F. 2016. Synthesis of zeolite a from coal fly ash using ultrasonic treatment–a replacement for fusion step. *Ultrasonics sonochemistry,* 31**,** 342-349.

Omoniyi, O. A., Salifu, A. A., Obayemi, J. D., Oyewole, O. K., Nigay, P. M., Akin-Ojo, O. & Soboyejo, W. O. 2022. Hydroxyapatite and bone particle-doped ceramic water filters for the removal of fluoride and bacteria.

Parashar, K., Pillay, K., Das, R. & Maity, A. 2019. Fluoride toxicity and recent advances in water defluoridation with specific emphasis on nanotechnology. *Emerging nanostructured materials for energy and environmental science.*

Shaban, M., Abukhadra, M. R., Shahien, M. G. & Ibrahim, S. S. 2017. Novel bentonite/zeolite-nap composite efficiently removes methylene blue and congo red dyes. *Environmental Chemistry Letters,* 16**,** 275-280.

Sivaselvam, S., Premasudha, P., Viswanathan, C. & Ponpandian, N. 2020. Enhanced removal of emerging pharmaceutical contaminant ciprofloxacin and pathogen inactivation using morphologically tuned mgo nan.

Tran, H. N., You, S. J., Hosseini-Bandegharaei, A. & Chao, H. P. 2017. Mistakes and inconsistencies regarding adsorption of contaminants from aqueous solutions: A critical review. *Water Res,* 120**,** 88-116.

Uddin, M. K., Ahmed, S. S. & Naushad, M. 2019. A mini update on fluoride adsorption from aqueous medium using clay materials. *Desalination and Water Treatment,* 145**,** 232-248.

Velazquez-Jimenez, L. H., Vences-Alvarez, E., Flores-Arciniega, J. L., Flores-Zuniga, H. & Rangel-Mendez, J. R. 2015. Water defluoridation with special emphasis on adsorbents-containing metal oxides and/or hydroxides: A review. *Separation and Purification Technology,* 150**,** 292-307.

Who 2011. Guidelines for drinking-water quality. *WHO chronicle,* 4**,** 104-108.

Who 2019. Preventing disease through healthy environments inadequate or excess fluoride a major public health concern. *World Health Organisation*.

Wu, C., Klemes, M. J., Trang, B., Dichtel, W. R. & Helbling, D. E. 2020. Exploring the factors that influence the adsorption of anionic pfas on conventional and emerging adsorbents in aquatic matrices. *Water Res,* 182**,** 115950.

Yadav, M., Singh, G. & Jadeja, R. N. 2021. Fluoride contamination in groundwater, impacts, and their potential remediation techniques. *Groundwater Geochemistry Pollution and Remediation Methods***,** 22-41.

Yao, G., Lei, J., Zhang, W., Yu, C., Sun, Z., Zheng, S. & Komarneni, S. 2019. Antimicrobial activity of x zeolite exchanged with cu(2+) and zn(2+) on escherichia coli and staphylococcus aureus. *Environmental Science and Pollution Research,* 26**,** 2782-2793.

Zendehdel, R., Goli, F. & Hajibabaei, M. 2020. Comparing the microbial inhibition of nanofibres with multi-metal ion exchanged nano-zeolite y in air sampling. *Journal of Applied Microbiology,* 128**,** 202-208.

Zhang, K., Van Dyk, L., He, D., Deng, J., Liu, S. & Zhao, H. 2021. Synthesis of zeolite from fly ash and its adsorption of phosphorus in wastewater. *Green Processing and Synthesis,* 10**,** 349-360.

Chapter 5: Synthesis of zirconium (Zr^{4+}) and silver (Ag^{+}) modified zeolite for application in fluoride and pathogen removal

Abstract

This chapter aims to enhance the fluoride adsorption efficiency and antimicrobial potency of synthesized zeolite NaP through the incorporation of Zr^{4+} and Ag^{+} metal oxides. The Zr^{4+}/Ag^{+} modified zeolite was synthesized via ultrasound-assisted hydrothermal treatment at optimum conditions of 0.5 and 0.3 M for $ZrCl_4$ and $AgNO_3$ respectively, 2.5 M concentration of NaOH at 2 hours of sonication for dissolution and hydrothermal conditions of 105 °C for 90 minutes of hydrothermal time. The obtained material was characterized using X-ray Diffraction (XRD), X-ray Fluorescence (XRF), Fourier Transform Infrared (FTIR), Particle Distribution Analyzer, and Scanning Electron Microscopy Energy Dispersive Spectroscopy (SEM-EDS). The defluoridation and antimicrobial potency of the modified zeolite were evaluated through batch fluoride adsorption and well-assay diffusion experiments, respectively. A maximum fluoride removal percentage of 50% was achieved under optimal conditions, which included a pH of 6 ± 0.5, a contact time of 270 minutes, an aqueous solution with an initial fluoride concentration of 6.2 mg/L, and an adsorbent dosage of 0.5 g/100 mL, with agitation at a speed of 250 rpm. The adsorption data fitted better to the *pseudo*-second-order kinetic model which indicates that the adsorption of fluoride occurred through the chemisorption mechanism. The adsorption isotherm data showed a better fit to the Langmuir isotherm model which indicates that the adsorption occurred on a monolayered surface of the Zr^{4+}/Ag^{+} modified zeolite. Furthermore, the antimicrobial potency results showed a minimum zone of inhibition of 15 mm and 12 mm against the gram-negative *E. coli* and gram-positive *S. aureus* strains in the antimicrobial test. This study proved that the Zr^{4+}/Ag^{+} modified zeolite has potency towards fluoride and pathogen removal from groundwater.

Keywords: Groundwater, Fluoride, Pathogens, Adsorption, Zirconium, Silver

5.1. Introduction

Groundwater is regarded as a reliable water source in water-scarce areas mainly in arid to semi-arid regions. On occasion, groundwater is a carrier of toxic contaminants such as fluoride and pathogens depending on the factors surrounding the environment (Naskar, 2020). When exposed to the human system, these contaminants cause diseases such as fluorosis, cholera, fever, and diarrhea (Gao et al., 2021). Unfortunately, studies have reported the presence of high levels of fluoride and pathogenic contaminants in various spheres of the groundwater with levels surpassing the mandated levels of 1.5 mg/L and 0 cfu/mL of the World Health Organization's water guidelines (WHO, 2011, Mei et al., 2020).

According to Revelo-Mejia et al. (2021) and Yetis et al. (2021), over 100 million people are affected by fluorosis and pathogenic diseases worldwide. Countries including China, India, Mexico, Kenya, Malawi, Ethiopia, and South Africa have reported cases of fluorosis, cholera, and diarrheal disease as a consequence of drinking contaminated water (Liu et al., 2019, Menya et al., 2019, Addison et al., 2021, Yetis et al., 2021). In South Africa, cases of fluorosis have been documented in several provinces including North West, Western Cape, KwaZulu-Natal, and Limpopo (Edokpayi et al., 2018, Odiyo and Makungo, 2018, Khabo-Mmekoa et al., 2022).

Several water treatment strategies are placed to remove these toxic contaminants in water. These strategies include the precipitation method which utilizes a chemical agent and forms insoluble precipitates, the ion exchange method which utilizes an ion exchange resin for selectively removing fluoride ions in water through the exchange of ions and the membrane method which uses a semipermeable membrane that selectively allows ions depending on their size to pass through (He et al., 2020, Naskar, 2020). However, studies indicated that these methods offer a low fluoride removal efficiency of 40-60%, generate concentrated sludge, and use expensive and complex systems for the removal of these toxicants (Savari et al., 2020, Gao et al., 2021, Gitari et al., 2023).

The adsorption mechanism however, uses simple adsorption systems, has higher fluoride removal efficiency, and uses naturally abundant and eco-friendly materials such as clays, coal fly ash, chitosan, and zeolites are less costly compared to the above-mentioned defluoridation techniques (He et al., 2020, Naskar, 2020). Among the adsorbents, zeolite materials are widely recommended and preferred due to their molecular sieving properties, porosity, higher cation exchange capacity, thermal stability, and higher surface area. Zeolitic minerals are aluminosilicate in nature composed of alumina and silica tetrahedra which are balanced by one oxygen molecule. These materials can be found naturally or synthesized in the laboratory to suit their applications making them versatile adsorbents.

Although zeolites can be used to sieve metals in the water, they lack affinity to anionic species which hinders their ability to remove metals such as fluoride in the water. This is due to their alumina framework which has a net negative charge (Jia et al., 2022). This net negative is balanced by cations giving the zeolite its cation exchange capability (Aloulou et al., 2021). Hence cations such as lanthanum, iron, lithium, magnesium, and zirconium are used to improve the fluoride removal efficiency of the zeolite (Zendehdel et al., 2020, Jia et al., 2022). This phenomenon is achievable owing to the attraction of cations towards anions.

Various studies have incorporated zeolitic materials with multiple metal oxides for the simultaneous removal of multiple contaminants in water. A study by Cheng et al. (2018) modified zeolite with magnesium-aluminum-titanium to remove fluoride ions and reported 72%, 80%, and 95% defluoridation efficiency respectively. Gao et al. (2021) modified zirconium zeolite and reported a defluoridation efficiency of 95%. Furthermore, Cui et al. (2019a) investigated zeolite functionalized with silver-copper-zinc metal oxides against *E. coli* and *S. aureus* and reported a zone of inhibition of 9.75 and 7.68 respectively. Also, silver ion functionalized zeolites were investigated in the removal of pathogens such as *E. coli, P. aeruginosa, V. cholerae, and V. parahaemolyticus* and results indicated that the silver functionalized zeolite inhibited the growth of these pathogens (Krishnani et al., 2012, Sánchez et al., 2017).

To the author's knowledge, little has been done on the modification of zeolite materials with zirconium and silver metal oxides for the removal of fluoride and pathogens in groundwater. In this study, zeolite was modified with zirconium (Zr^{+4}) and silver (Ag^{+}) metal oxides for the simultaneous removal of fluoride and pathogens in water. Obtained samples were characterized and fluoride adsorption studies were performed to investigate the efficiency of the Zr4+/Ag+ modified zeolite. Additionally, an analysis of adsorption kinetics and isotherm models was conducted to assess the adsorption mechanisms. The antimicrobial efficacy of the modified zeolite was investigated using the well-assay diffusion method.

5.2 Methodology

5.2.1 Materials

Raw bentonite clay was supplied by ECCA Holdings (Pty) Ltd, Cape Bentonite Mine (Cape Town, South Africa). Chemicals of analytical grade such as sodium hydroxide (NaOH) 98% and silver nitrate ($AgNO_3$) 99.9% used in this study were obtained from Rochelle Chemicals and Lab Equipment CC, South Africa Ltd. The *E. coli* strain, MacConkey agar, Mueller Hinton agar and broth, zirconium chloride ($ZrCl_4$), silver nitrate ($AgNO_3$), and TISAB (III) solution were obtained from Sigma Aldrich, South Africa. No purification of reagents was conducted, and hence the reagents were used as they were.

5.2.2 Preparation of Zr^{4+}/Ag^{+} modified zeolite

The modification of zeolite with Zr^{4+}/Ag^{+} metal oxides was conducted following the procedures described by Ojumu et al. (2016), Lin et al. (2018), and Amin et al. (2021) with slight modification. Briefly, 10 g of calcined bentonite clay were added to 2.5 M NaOH solution. In the same solution, zirconium chloride ($ZrCl_4$) and silver nitrate ($AgNO_3$) metal oxides were added at varying molar concentrations as indicated in Table 1. The obtained mixture was subjected to sonication in the up 400s Heilscher probe ultrasound for 2 hours at an amplitude of 100% and cycle of 0.5. After sonication, the obtained mixture was subjected to hydrothermal treatment for crystallization of the material following optimum conditions described in the zeolite synthesis report. In this procedure, 20 mL of the sonicated mixture was added into a 45 mL capacity Teflon Parr autoclave reactor. The Teflon Parr autoclave reactor was then placed in a 220V~50 Hz EcoTherm labotec oven for 90 minutes at 105 ºC. The obtained crystallized solution was centrifuged with the Z 366 Hermle centrifuge at 4000 rpm for 15 minutes and dried in an oven overnight at 70 ºC. The obtained samples were then stored in plastic bottles to prevent moisture and for safekeeping.

Table 5.1: Variation of zirconium and silver metal oxides molar concentration

Sample Name	Zr (Molar)	Ag (Molar)
ZZA1	0.3	0.3
ZZA2	0.5	0.1
ZZA3	0.1	0.3
ZZA4	0.1	0.5
ZZA5	0.3	0.5
ZZA6	0.5	0.5
ZZA7	0.1	0.1
ZZA8	0.3	0.1
ZZA9	0.5	0.3

5.2.3 Physiochemical characterization

The S1 TITAN 600 X-ray Fluorescence (XRF), Shimadzu SALD-2300 laser diffraction particle size analyzer, and platinum ATR Fourier Transform Infrared (FTIR) instruments were used to determine the elemental composition, particle size, and functional groups of the materials respectively. Also, TESCAN Scanning Electron Microscopy- Energy Dispersive Spectroscopy (SEM-EDS) and TriStar II 3020 Brunauer Emmett Teller (BET) were used to determine the morphology and surface area of the materials respectively.

5.2.4 Batch Fluoride Sorption Studies

Batch fluoride adsorption studies were performed to assess the defluoridation efficiency of Zr^{4+}/Ag^{+} modified zeolite against field groundwater obtained from Siloam village, Limpopo. The ORION Ion Selective Electrode (ISE, 9609BNWP) and the ACCSEN PC8 pH meter were used to analyze fluoride ions and pH levels in the samples, respectively. Fluoride analysis indicated that the field groundwater had a concentration of 6.2 mg/L with a pH of 8 ±0.5. Prior to fluoride analysis, Total Ionic Strength Adjustment Buffer (TISAB(III)) was added to the samples at a ratio of 1:10 mL to increase the ionic strength of the ions and eliminate any interfering ions. In detail, batch fluoride studies were performed by studying the effects of agitation time, pH, concentration, and temperature. The effect of agitation time was performed in a 100 mL solution of field groundwater using 0.5 grams of the adsorbent at varying times of 1, 5, 10, 20, 30, 60, 90, 180, 270, and 380 minutes (s). This experiment was carried out in a 250 mL capacity polyethylene bottle at an agitation speed of 250 rpm using the STUART SSL2 shaker. The resulting solution was filtered using a 0.45 µm filter membrane and the filtrate was analyzed for fluoride. The effect of initial pH was performed in 100 mL solutions of field groundwater with varying pH ranges of 2, 4, 6, 8, and 10 which were adjusted using 0.1 M of HCl and 1 M NaOH solution in a dropwise manner. The effect of concentration was carried out by simulating 100 ml fluoride solutions with various concentrations of 5, 10, 15, 20, 30, 40 and 50 mg/L at room temperature. Then, 0.5 g of Zr^{4+}/Ag^{+} modified zeolite was added into the 100 mL fluoride solutions and agitated at 250 rpm at optimal conditions. Also, the effect of temperature was carried out using the simulated fluoride concentrations at 35°C and 45°C. Following batch experiments, fluoride analysis proceeded with the application of similar steps. Equation 5.1 was utilized to compute the percentage removal of fluoride, with C_o representing the initial fluoride concentration and C_e representing the final fluoride concentration.

$$Percentage\ fluoride\ removal\ (\%) = \frac{C_o - C_e}{C_o} \times 100 \qquad (5.1)$$

5.2.5 Regeneration experiments

The regeneration potential of the Zr^{4+}/Ag^{+} modified zeolite was evaluated using 0.01 M of hydrochloric acid. This was conducted by mixing fluoride-rich adsorbent in 100 mL of HCl solution and agitated for 1 hour at a speed of 250 rpm for fluoride desorption. The solution was then filtered using a 0.45 µm membrane filter to obtain the fluoride-free adsorbent residues. The fluoride-free material was then analyzed for fluoride desorbed washed with deionized water and dried in an oven for 4 hours at 110 °C following procedures described in (Gitari et al., 2023). The dried adsorbent material was then reused in fluoride adsorption experiments. This cycle was repeated for five cycles.

5.2.6 Antimicrobial studies

The antimicrobial efficiency of the Zr^{4+}/Ag^{+} modified zeolite was performed using the agar well-assay diffusion method. In this procedure, the *E. Coli* and *S. aureus* strains were used as indicator bacteria. The preparation of the bacterial cultures was as follows. Agars and Broth were prepared in ultrapure water and the mixture was subjected to autoclave for 15 minutes and then transferred into plate discs. *E. coli* and *S. aureus* strains were inoculated upon prepared plate discs of MacConkey agar and incubated at 37°C for 24 hours to establish colonies. Thereafter, 3 colonies were swabbed from the agar transferred to the Mueller Hinton broth, and incubated for 2 hours at 37 °C. Subsequently, 50 µL of incubated broth was transferred into plate discs of Mueller Hinton Agar and evenly distributed using the glass cell spreader and left to cool for 30 minutes. Holes were punched upon the agar plate using the opening end of sterile pipet tips and 50 µL of the adsorbent was pipetted in the holes. The agar was then incubated overnight at 37 °C in an inverted position. Lastly, zones of inhibition were measured.

5.3. Results and discussion

5.3.1 Optimisation of Zr^{4+}/Ag^{+} modification conditions

Table 5.2 depicts the percentage composition of the resulting modified zeolites analysed via the XRF at various molar concentrations of zirconium and silver metal oxides along with the sample's adsorption capacity toward fluoride ions. Three-dimensional graphs were constructed using the design expert software version 13 to predict the optimum conditions and relationship between the variables as presented in Figure 5.1. In Figures 1A and 1B, the percentage composition of zirconium and silver in the resulting modified zeolite samples increased with the increase of molarity concentration of zirconium and silver respectively. This indicates that as the molarity concentration of zirconium and silver metal oxides increases, more zirconium and silver metals are incorporated in the zeolite matrices. Also, the incorporation of zirconium and silver in the modified zeolite matrices was verified by the EDS results in Figure 5.5. Similar observations were made in a study by Cui et al. (2019b), Barbov et al. (2023), Inglezakis et al. (2023), and Marzi et al. (2023). Thereafter, the obtained modified zeolite samples were employed to investigate the fluoride adsorption capacity of the modified samples as presented in Table 5.2 and deduce the optimum modification conditions therein. The highest fluoride adsorption capacity of 1.0 mg/g was obtained at higher sample ZZ9 modified using 0.5 M of zirconium and 0.3 molar silver concentrations. Therefore, sample ZZA9 was selected as the optimum condition for zeolite modification.

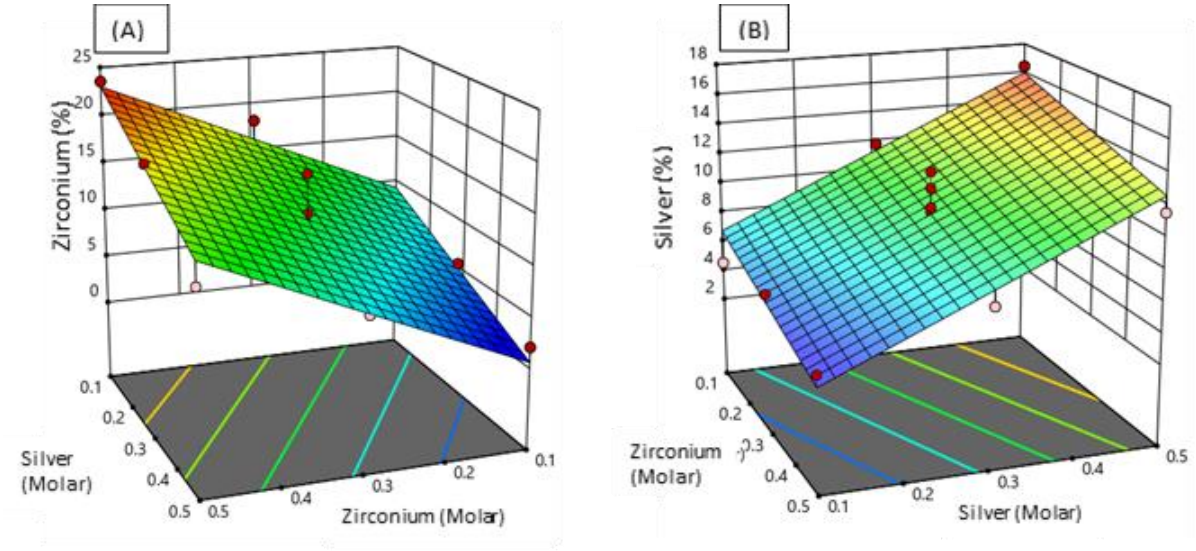

Figure 5.1: 3D surface plots of dissolution of silica (A) and aluminium (B)

Table 5.2: Preliminary fluoride removal performance of the modified zeolite samples

Sample Name	Zirconium (Molar)	Silver (Molar)	Zirconium (%)	Silver (%)	Fluoride adsorption capacity (mg/g)
ZZA1	0.3	0.3	10.94	11.37	0.13
ZZA2	0.5	0.1	23.55	4.1	0.37
ZZA3	0.1	0.3	5.49	11.82	0.20
ZZA4	0.1	0.5	2.1	16.44	0.15
ZZA5	0.3	0.5	7.28	13.96	0.12
ZZA6	0.5	0.5	11.84	11.55	0.31
ZZA7	0.1	0.1	5.78	4.52	0.40
ZZA8	0.3	0.1	18.19	5.6	0.77
ZZA9	0.5	0.3	18.88	6.94	1.00

5.3.1.1 ANOVA results

Response surface methodology (RSM) was used to optimize the molarity of zirconium and silver metal oxides for modification of zeolite. The composition content of these metal oxides was used as the response factor. The obtained Analysis of Variance (ANOVA) indicated that the linear model method is the effective and rational method for data analysis as indicated in Table 5.3. A significant p-value of 0.0001 was obtained along with a lack of fit value of

0.7322 which is higher than the threshold for statistical significance. Hence the linear model function is best fitted and adequate for this experimental data analysis.

Table 5.3: ANOVA statistics

Source	Sum of Squares	df	Mean Square	F-value	p-value	
Model	394.08	2	197.04	35.78	< 0.0001	significant
A-Zirconium	278.8	1	278.8	50.63	< 0.0001	
B-Silver	115.28	1	115.28	20.94	0.001	
Residual	55.07	10	5.51			
Lack of Fit	25.84	6	4.31	0.5894	0.7322	not significant

5.3.1.2 Actual Vs Predicted Values

The actual values of (A) zirconium and (B) silver metal oxides incorporation on zeolite were plotted against the predicted values in Figure 5.2. This data was plotted using the RSM to provide the regression coefficient of the data models. The purpose is to establish the relationship between the actual experimental data and the predicted values obtained from the RSM (Response Surface Methodology) model. The actual vs predicted values plot of zirconium incorporation in zeolite demonstrated that the regression line passes through the experimental data range. This implies that the actual and the predicted values are within the range. A similar trend was observed in the silver ions incorporation in zeolite structure. Also, the RSM indicated regression coefficients of 0.8774 and 0.8463 for zirconium and silver ions incorporation in zeolite model data, respectively. This further emphasizes that there is a correlation between the variables. Therefore, the optimization of the metal oxides incorporation in the zeolite can be predicted accurately and precisely with the RSM model function.

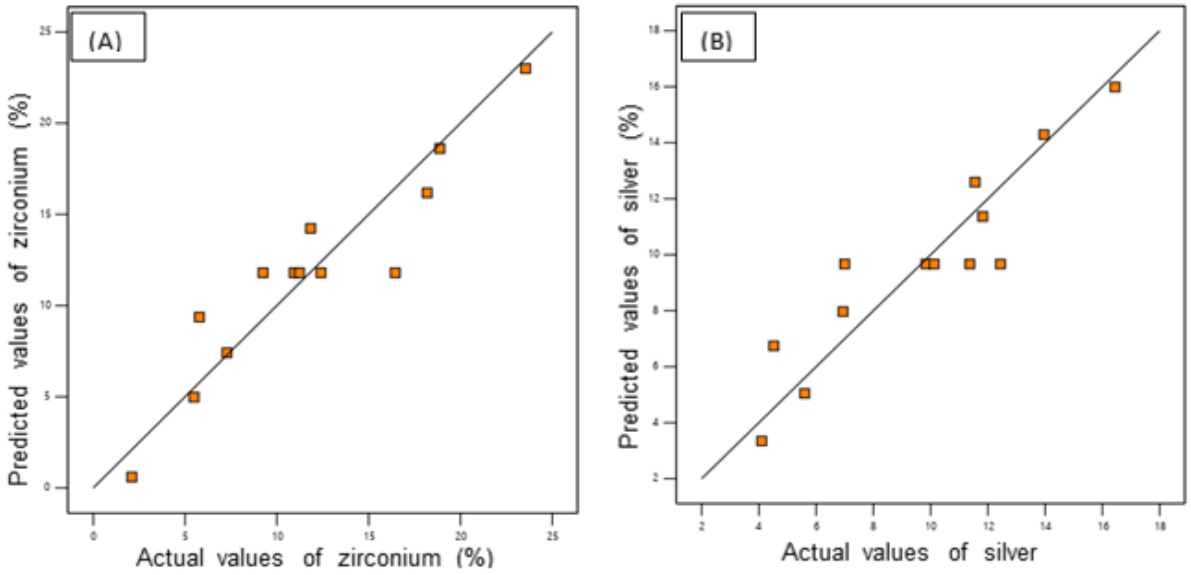

Figure 5.2: Actual vs predicted values plots of zirconium (A) and silver (B) metal oxides modification on zeolite.

5.3.2 Physiochemical characterization

5.3.2.1 XRF analysis

Table 5.4 illustrates the principal elemental compositions of both the synthesized zeolite NaP and the Zr^{4+}/Ag^{+} modified zeolite. The XRF results show that the synthesized zeolite NaP had the highest percentage of silica (SiO_2) and alumina (Al_2O_3) at 32.33% and 11.43% respectively. However, this percentage decreases after modification of the zeolite with the metal oxides. Also, the silica-to-alumina ratio of the synthesized zeolite and modified zeolite was 2.83 and 6.40 respectively. The increase in the Si/Al ratio of the Zr^{4+}/Ag^{+} modified zeolite is attributed to the sudden decrease of the aluminum composition due to sonication. It was also noted that there was a sudden increase in the zirconium (Zr) and Silver (Ag) content showing a percentage composition of 18.88% and 6.94%, respectively. This indicates that there was a modification of the zeolite matrices. Similar findings were documented in studies by Barbov et al. (2023) and Inglezakis et al. (2023)

Table 5.4: Major elemental compositions of the synthesized and modified zeolite

Name	**Chemical composition**								
	SiO_2	Al_2O_3	Fe_2O_3	MgO	K_2O	TiO_2	CaO	Zr	Ag
Zeolite NaP	32.33	11.43	2.38	0.89	0.46	0.46	1.21	0	0
Zr^{4+}/Ag^{+} modified zeolite	29.61	4.62	1.92	2.93	0.55	0.24	0.19	18.88	6.94

5.3.2.2 FTIR results

Figure 5.3 depicts the FTIR spectra of the zeolite NaP and Zr^{4+}/Ag^{+} modified zeolite. As indicated in Figure 5.3, the bands observed at =565 cm^{-1} are attributed to the Al-O bending vibrations. However, this band was absent in Zr^{4+}/Ag^{+} modified zeolite. A band at =740 cm^{-1} band was observed to contribute to the symmetric vibration of the Al-O-Si tetrahedra functional groups. An intense vibration band at 973 cm^{-1} was observed which is attributed to the Si-O asymmetric stretching in the synthesised zeolite NaP. However, in the modified zeolite, a shift in the Si-O band was observed to the =1026 cm^{-1} band position at low intensity which could be due to the dissolution process during Zr^{4+}/Ag^{+} modification. Furthermore, similar bands from the zeolite NaP and the Zr^{4+}/Ag^{+} modified zeolite samples of the -OH functional group at wavenumbers of =1600 and 3400 cm^{-1} were observed. The presence of -OH groups at =3400 cm^{-1} contributes to the absorption of water molecules absorbed by the samples. No bands associated with the Zr-O and Ag-O functional groups were observed. Studies indicate that this could be due to the strong vibrations of the zeolite matrices or the overlapping of bands (Velazquez-Peña et al., 2017, Feng et al., 2020, Yang et al., 2022). Also, Yu et al. (2021) added that zirconium could enter the zeolite cage instead of substituting the framework of the zeolite and forming new bonds hence no zirconium-related functional groups could be observed.

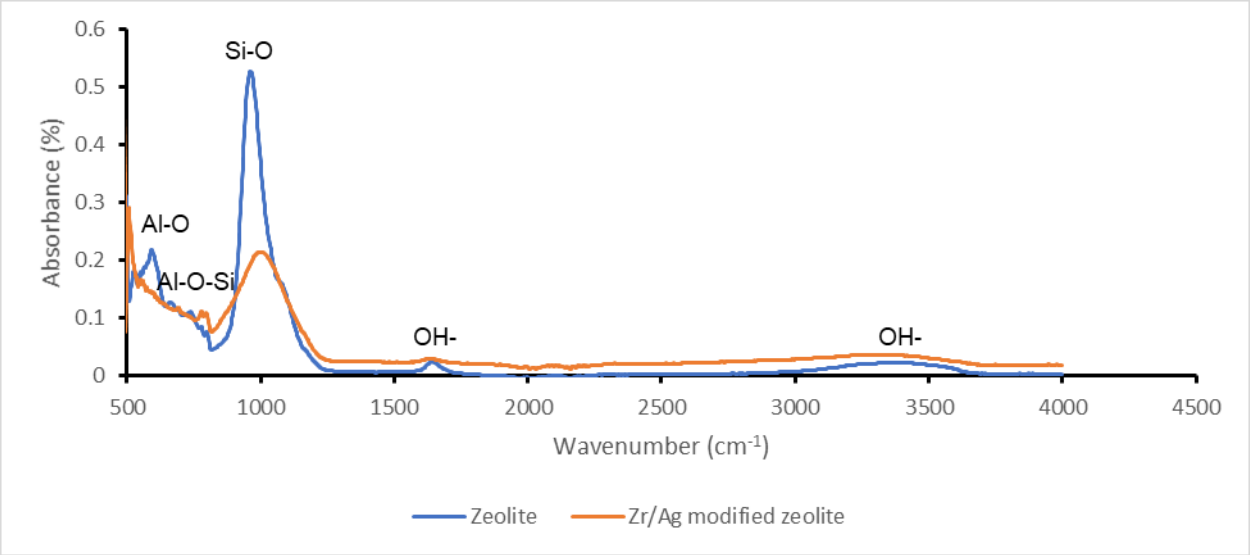

Figure 5.3: FTIR spectra of the zeolite NaP and the Zr4+/Ag+ modified zeolite.

5.3.2 3 XRD results

The XRD spectra of the zeolite NaP and Zr^{4+}/Ag^{+} modified zeolite was plotted and presented in Figure 5.4. The XRD spectral band of the zeolite NaP sample showed that the material has peaks attributed to quartz at 31.02° 2θ, zeolite NaP at 14.40°, 20.19°, 25.28°, 32.25°, and 39.05° 2θ, muscovite at 10.28° and 23.03° 2θ and zeolite SSZ-73 at 10.45° 2θ. However, the Zr^{4+}/Ag^{+} modified zeolite exhibited peaks of quartz at 50.78° 2θ and zeolite NaP phases only. The presence of quartz and zeolite NaP phases indicates that the materials are aluminosilicate in nature, and this coincides with the FTIR analysis. Conversely, no peaks attributed to zirconium and silver metal were observed. According to studies, zirconium and silver metal oxides make no significant changes to the zeolite matrices (Velazquez-Peña et al., 2017, Malek et al., 2018, Savari et al., 2020, Yang et al., 2022).

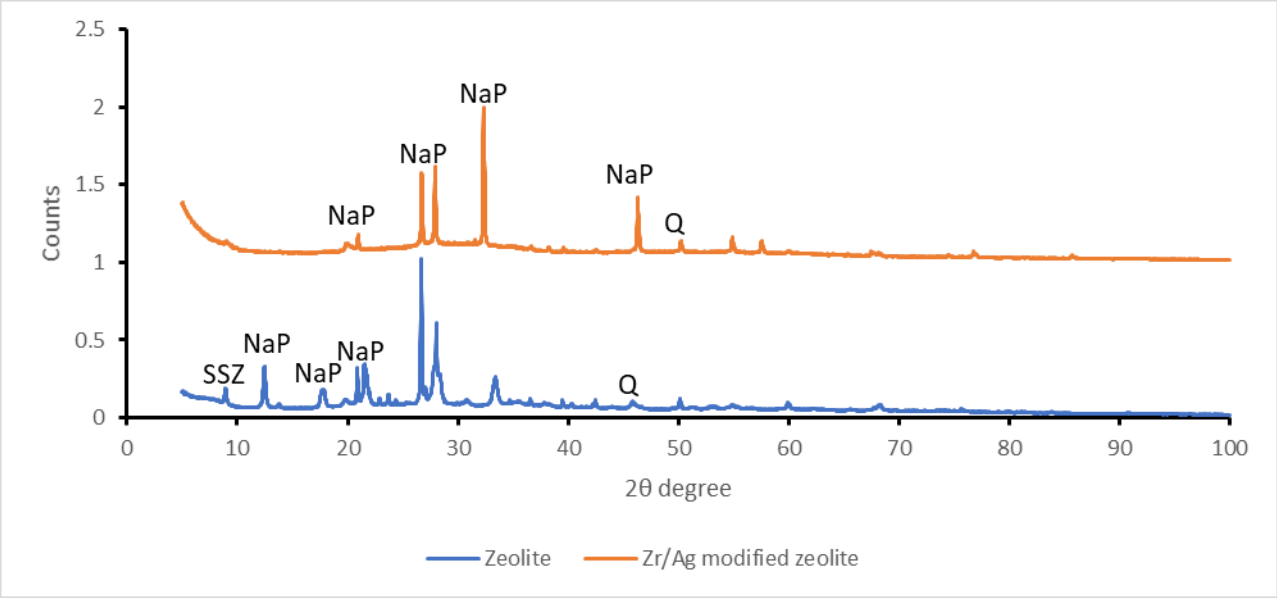

Figure 5.4: XRD spectra of synthesized zeolite NaP and Zr4+/Ag+ modified zeolite.

5.3.2.4 SEM-EDS results

The morphology of the zeolite NaP (A) and Zr^{4+}/Ag^{+} modified zeolite (B) were examined along with their corresponding EDS micrographs as shown in Figure 5.5. The observations from the morphology results indicated that the synthesized zeolite had uniform small-sized crystals along with very few irregular granules. The observed crystals of the zeolite were mellow spherical-shaped crystals. In contrast, the modified zeolite exhibited a change in morphology and a relatively flatter surface. Similar findings were documented by Savari et al. (2020) and (Salehi et al., 2020). Furthermore, the EDS micrographs of the zeolite and modified zeolite were constructed and presented in Figure 5.5. The EDS spectrum of the zeolite indicates the presence of Na, Al, O, and Si elements which are attributed to aluminosilicate minerals. This agrees with the XRF and FTIR results. However, the introduction of zirconium (Zr) and silver (Ag) elements was also observed in the Zr^{4+}/Ag^{+} modified zeolite. This underscores the successful integration of zirconium and silver metal oxides into the zeolite structure. Similar observations were made in a study by Salehi et al. (2020), Abdellaoui et al. (2021b), and Gao et al. (2021).

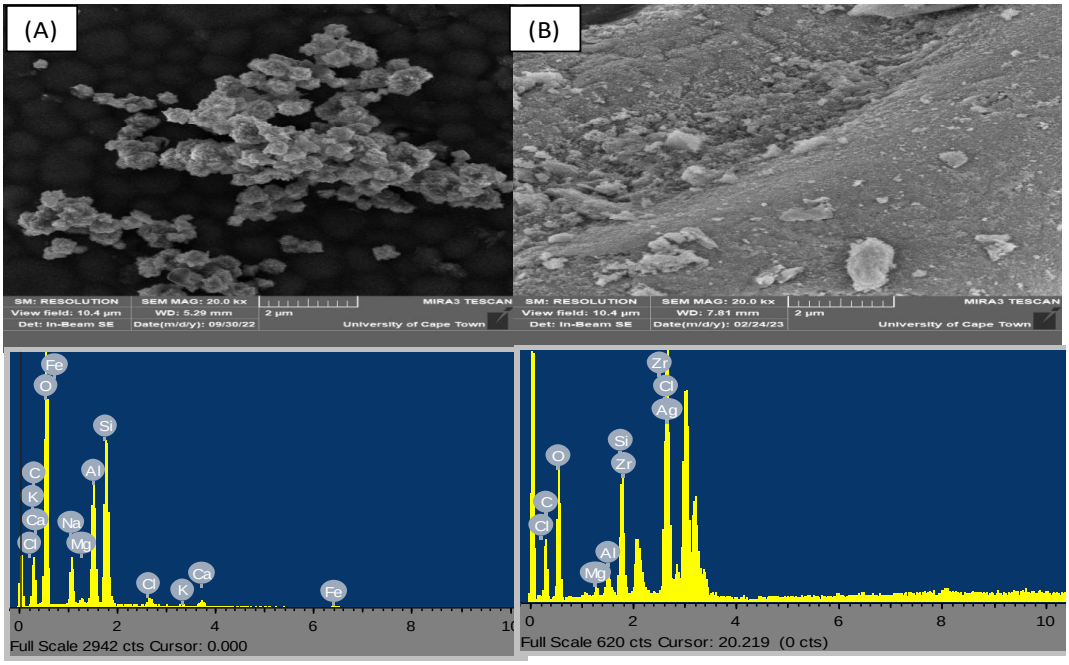

Figure 5.5: SEM-EDS morphology and micrographs of the zeolite NaP (A) and Z/Ag modified zeolite (B)

5.3.2.5 BET results

Table 5.5 showcases the BET results of the synthesized zeolite NaP and the Zr^{4+}/Ag^{+} modified zeolite samples. It was observed that the Zr^{4+}/Ag^{+} modified zeolite has a higher surface area of 174.39 m^2/g in contrast to the synthesized zeolite with a surface area of 102.18 m^2/g. The augmentation in the surface area may be ascribed to the integration of zirconium metal oxides into the zeolite matrices during the incorporation process. Studies indicated that the introduction of zirconium metal oxides in the zeolite structures results in the substitution of aluminum species causing the formation of new layers and higher porosity (Savari et al., 2020). Consequently, this leads to an increase in the surface area of the zeolite. Furthermore, the synthesised zeolite NaP exhibited a pore size of 46.65 nm whilst the Zr^{4+}/Ag^{+} modified zeolite had a higher pore size of 73.53 nm which indicates that the Zr^{4+}/Ag^{+} is composed of microporous structures. In addition, the pore volume increased from 0.12 cm^3/g to 0.32 cm^3/g. Similar observations were reported in studies by Feng et al. (2020), Abdellaoui et al. (2021b), and Gao et al. (2021).

Table 5.5: The pore size, pore volume, and surface area of the synthesized zeolite and modified zeolite

Sample	BET surface area (m^2/g)	Pore volume (cm^3/g)	Pore size (nm)
Synthesized zeolite NaP	102.18	0.12	46.65
Zr^{4+}/Ag^{+} modified zeolite	174.39	0.32	73.53

5.3.2.6 Particle Size Analysis

Figure 5.6 represents the particle analysis of the zeolite and the Zr^{4+}/Ag^{+} modified zeolite. It was observed that the particle distribution curve was unimodal for both zeolite and Zr^{4+}/Ag^{+} modified zeolite. The zeolite sample showed a particle size range of 1 µm to 320 µm while the Zr^{4+}/Ag^{+} modified zeolite exhibited a particle size range of 1 µm to 260 µm. Also, a wider distribution curve for the Zr^{4+}/Ag^{+} modified zeolite was observed. Furthermore, the mean particle sizes of 22 and 52 µm were observed for the zeolite and the Zr^{4+}/Ag^{+} modified zeolite respectively as shown in Table 5.6. Observations indicate that there was an increase in particle size distribution after the modification of the zeolite with zirconium and silver metal oxides. The increase in particle size of the Zr^{4+}/Ag^{+} modified zeolite could be due to the agglomeration of the particles.

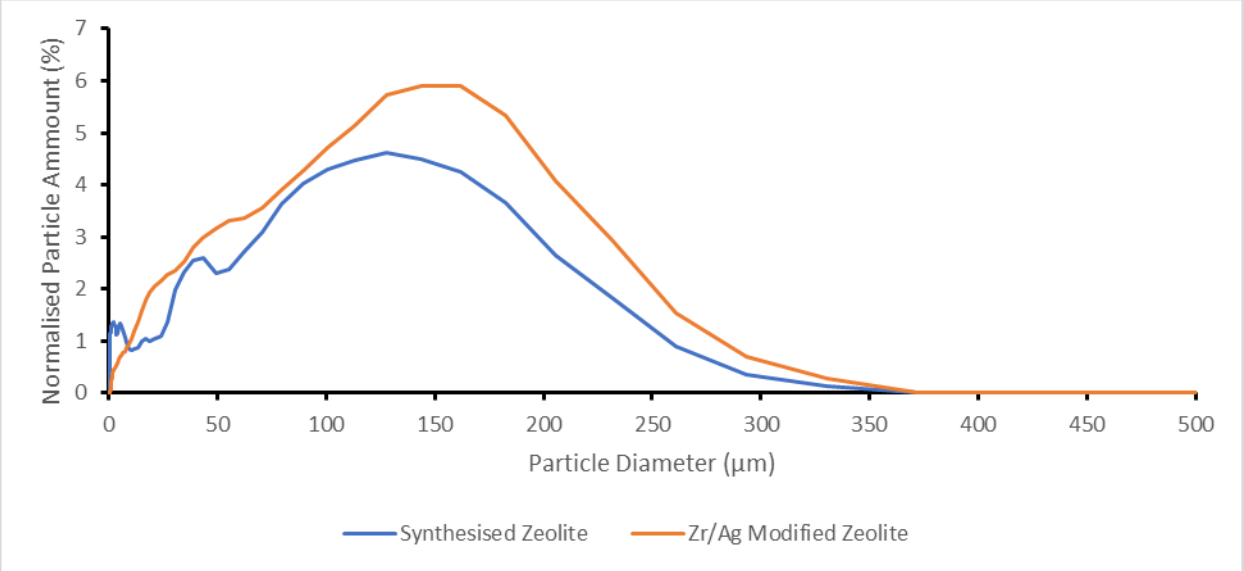

Figure 5.6: Particle distribution curves for the zeolite and the Zr4+/Ag+ modified zeolite

Table 5.6: Particle distribution size parameters of synthesized Zeolite and Zr^{4+}/Ag^{+} modified zeolite

Samples	Particle size at 90%	Mean Average
Synthesized Zeolite	160µm	22µm
Modified Zeolite	180µm	52µm

5.3.3 Batch fluoride adsorption results

5.3.3.1 Effect of pH

The effect of pH of the initial solution in fluoride uptake by the Zr^{4+}/Ag^{+} modified zeolite was evaluated, and results were presented in Figure 5.7. A graph plot depicting the relationship of fluoride percentage removal at varying pH is shown in Figure 5.7. A trend of decreasing fluoride removal percentage with increasing initial pH of the solution was observed. Research suggests that this phenomenon is governed by the surface charges of the adsorbent. Effective fluoride removal tends to occur when the surface carries a positive charge, whereas no defluoridation occurs when the surface charges are negative (Savari et al., 2020). At low pH values, the adsorbent surface is positively charged, and adsorption occurs through electrostatic attraction as negatively charged fluoride anions are attracted to the positively charged surface (Siyal et al., 2020). After a pH of 2 percent fluoride removal decreased slightly to 36% at a pH of 6 which could be due to the changes in adsorbent surface charges. According to Abdellaoui et al. (2021a), an increase in pH results in a decrease in positively charged surfaces causing a decrease in the adsorption of anions. After a pH of 6, the percentage of fluoride removal dropped sharply which corresponds to the increase of hydroxyl (-OH) ions in the solution (Yang et al., 2022). This hydroxyl (-OH) ions compete with fluoride ions for adsorption sites on the adsorbent material and an increase in alkalinity results in an increase of hydroxyl ions in the solution hence less fluoride adsorption is observed at higher pH due to repulsion forces. Consequently, a rise in the final pH of the solution was observed as the initial pH of the solution was increased. Thereafter, an optimal pH of 6 was chosen for subsequent experiments since the final solution pH was near neutral.

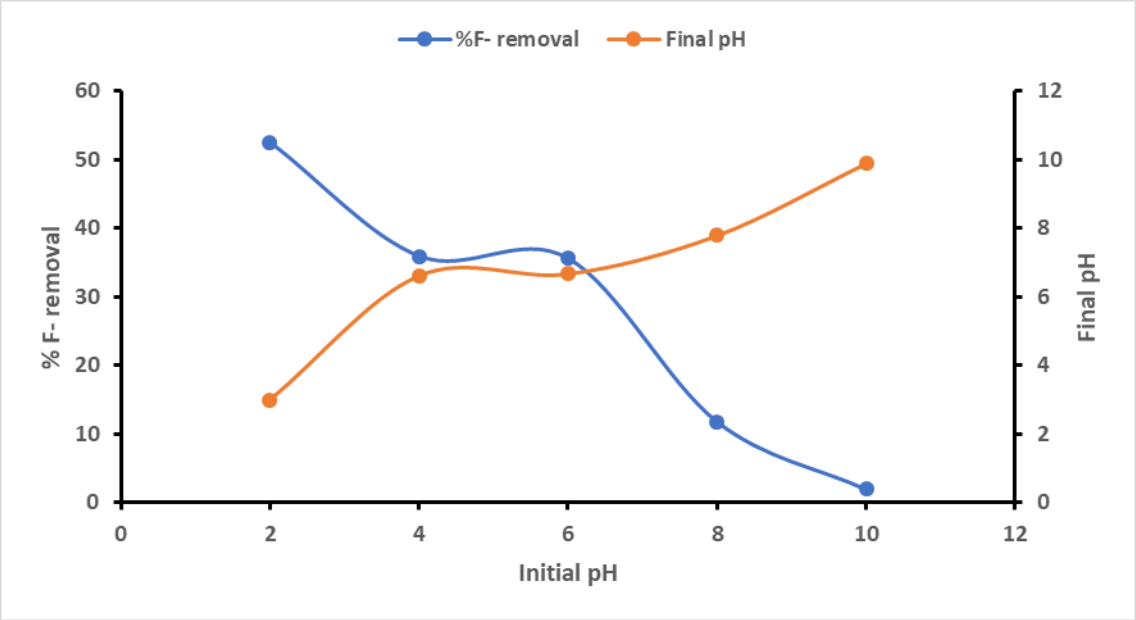

Figure 5.7: Effect of pH vs fluoride adsorption percentage (0.5 g/100 mL adsorption dosage, 270 mins contact time at 250 rpm, and initial F^- concentration of 6.2 mg/L)

5.3.3.2 Effect of Contact Time

The effect of contact time for fluoride adsorption by the Zr^{4+}/Ag^+ modified zeolite was investigated, and results are presented in Figure 5.8. Contact time was varied from 1 to 380 minutes and results of contact time against percentage fluoride removal were plotted in Figure 5.8. It was observed that the fluoride removal percentage increased with an increase in contact time from 1 to 60 minutes. This adsorption could be associated with the adsorption on the readily available active sites from the surface layers of the Zr^{4+}/Ag^+ modified zeolite causing quick adsorption of fluoride ions. Subsequently, fluoride percentage removal slowed down from 60 to 180 minutes which could be a factor of saturation of the available adsorption active sites. However, the fluoride removal percentage increased once more from 180 minutes until an equilibrium was reached at 270 minutes. This second increase in fluoride removal percentage could be due to intrapore diffusion wherein fluoride ions diffuse into the inner pores of the Zr^{4+}/Ag^+ modified zeolite as the contact time increases. A maximum percentage fluoride removal of 50.33% was observed at an optimal contact time of 270 minutes.

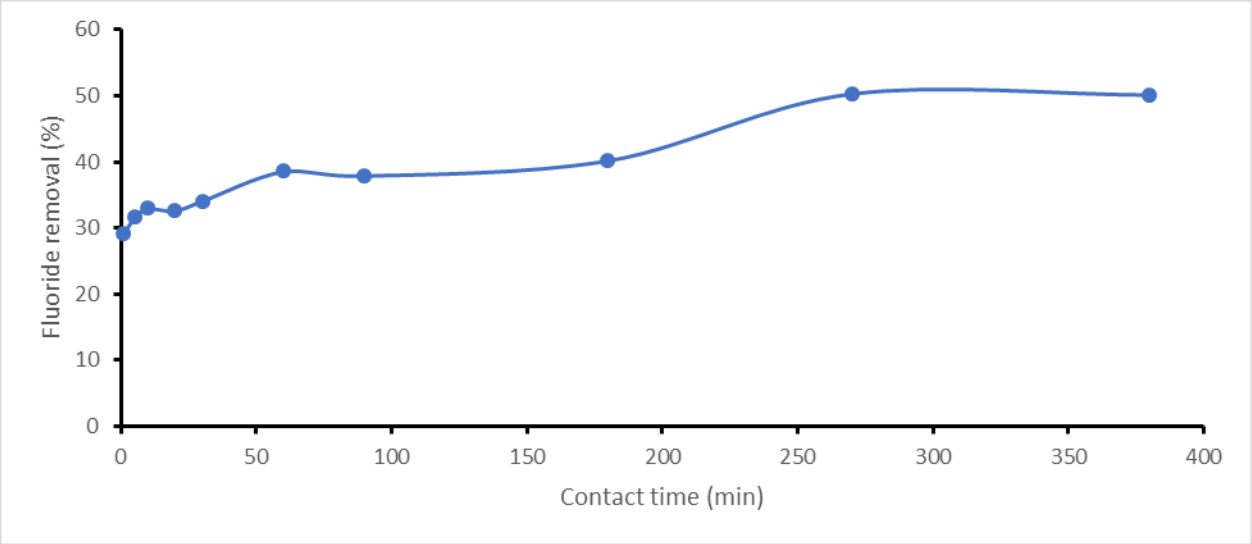

Figure 5.8: Effect of contact time vs fluoride adsorption percentage (0.5 g/100 mL adsorption dosage, agitation speed of 250 rpm, initial pH of 6, and initial F^- concentration of 6.2 mg/L)

5.3.3.3 Adsorption Kinetics

The effect of contact time adsorption data was fitted to adsorption kinetic models namely, *pseudo* first order (PFO) and *pseudo* second order (PSO) kinetic models, and the results were plotted in Figure 5.9. The models were employed to elucidate the factors controlling the adsorption rate and the underlying mechanisms involved in the process. The *pseudo*-first-order model assumes that adsorption occurs through physisorption whilst the pseudo-second-order model assumes that adsorption takes place through a chemisorption mechanism (Jasper et al., 2020, Márquez et al., 2021). The PFO and PSO linearized models are expressed by equations 5.2 and 5.3 respectively.

$$\mathrm{Log}(q_e - q_t) = logq_e - \frac{K_1}{2.303}t \qquad (5.2)$$

$$\frac{t}{q_t} = \frac{1}{K_2 q_e^2} + \frac{t}{q_e} \qquad (5.3)$$

Where q_e and q_t are the amount of adsorbate adsorbed per unit mass (mg/g) at a time t (min). K_1 (min^{-1}) and K_2 ($g.mg^{-1}/min$) represent the rate constants for the PFO and PSO respectively. The slope and intercepts of log (q_e – q_t) vs t give the value of K_1 whilst the slope and intercepts of $1/q_t$ vs t give the values of K_2. The PSO and PFO model plots are presented in Figure 5.9 and their parameters are in Table 5.7.

The correlation coefficient (R^2) value of the PSO was higher, which indicates that the PSO was better fitted with the experimental data. Also, the q_e values of the PSO model are closer to the experimental q_e value in comparison with the q_e values of the PFO. This implies that

the dominant adsorption mechanism of fluoride by the Zr^{4+}/Ag^{+} modified zeolite is chemisorption. This implies that the atoms of the adsorbent at the surface form chemical complexes with the fluoride ions (Márquez et al., 2021). Similar observations were made in a study by Feng et al. (2020), Savari et al. (2020), and Abdellaoui et al. (2021b).

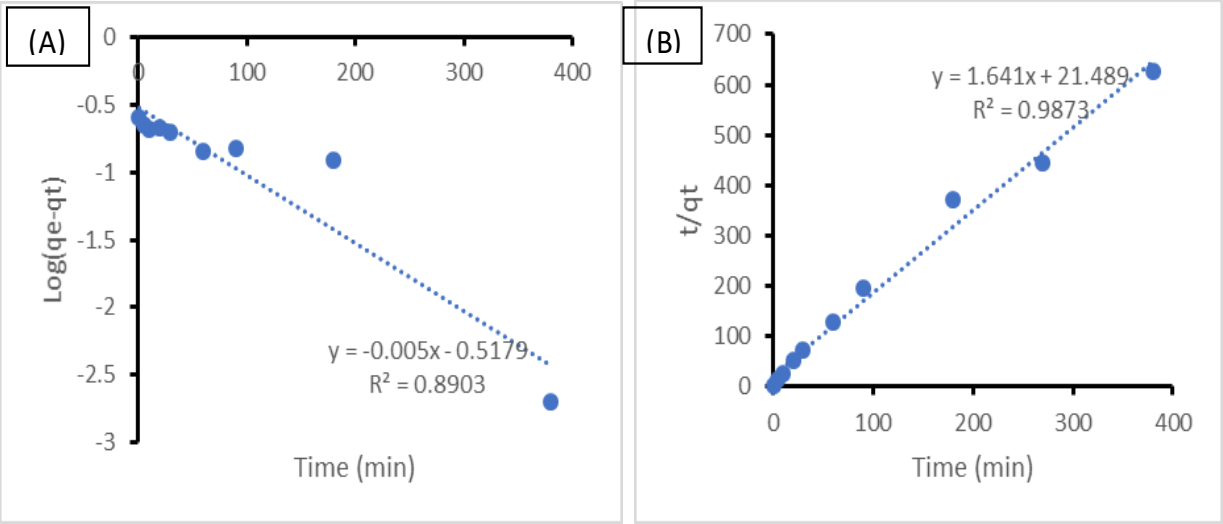

Figure 5.9: Adsorption kinetic model graphs for pseudo-first-order (A) and pseudo-second-order (B).

Table 5.7: Parameters for the *pseudo*-second-order (PSO) and *pseudo*-first-order (PFO) kinetic models.

Experimental	**Pseudo-first order (PFO)**			**Pseudo-second order (PSO)**		
Qe (mg/g)	K_1 (min^{-1})	Q_e (mg/g)	R^2	K_{2ads} ($g.mg^{-1}/min$)	Q_e (mg/g)	R^2
0.68	0.01	0.46	0.89	3.45	0.48	0.98

5.3.3.4 Effect of initial concentration and isotherms

Figure 5.10 depicts the equilibrium adsorbate concentration as a factor of adsorption capacity at varying temperatures of 25-45 °C. A simultaneous increase in adsorption capacity along with the equilibrium concentration was observed. In addition, adsorption capacity also increased with the temperature rise. To determine the mechanisms involved and the relationship between the adsorbate and the surface of the adsorbent, Langmuir and Freundlich isotherm models were fitted into the experimental data, and their graphical plots were presented in Figure 5.10. To elaborate, adsorption isotherms are mathematical equations that showcase the relationship between the number of molecules of adsorbate per unit mass as a function of equilibrium concentration in a solution at a constant temperature

(Mukherjee et al., 2018). The Langmuir isotherm model assumes that the adsorbent surface has a fixed number of adsorption active sites and adsorption takes place in each site which takes up one molecule only at a time (Mukherjee et al., 2018, Raghav and Kumar, 2018, Gitari et al., 2023). This indicates that adsorption takes place in a monolayer surface and there is no mutual interaction with the adsorbent. In contrast, the Freundlich isotherm model presumes that the adsorbent has a multinumber of adsorption active sites and adsorption takes place in a heterogeneous surface wherein there is mutual interaction of the adsorbate with the adsorbent (Mukherjee et al., 2018, Raghav and Kumar, 2018). The Langmuir and Freundlich isotherm models are given by equations 5.5 and 5.6, respectively.

$$q_e = \frac{Q_{max} K_L C_e}{1 + K_L C_e} \quad (5.4)$$

$$q_e = K_F C_e^{\frac{1}{n}} \quad (5.5)$$

Where q_e is the adsorption capacity (mg/g), C_e is the equilibrium concentration of the adsorbate (mg/L), K_L is the Langmuir constant (L/mg), K_f is the Freundlich constant (mg/g) and 1/n is the dimensionless parameter indicating the adsorption driving force's magnitude. If 1/n = 1 then adsorption is irreversible, if 1/n > 1 then adsorption is unfavourable, and if 0 < 1/n < 1 then adsorption is favourable.

The respective parameters of both Langmuir and Freundlich models for fluoride adsorption onto the Zr^{4+}/Ag^{+} modified zeolite was summarized in Table 5.8. The slope and intercept from C_e/q_e vs C_e plots determine the value of Q_{max} and K_L while the slope and intercept of log q_e vs log C_e determine the value of K_f and n.

The correlation coefficient (R^2) for the Freundlich was higher than that of the Langmuir isotherm at 25°C which indicates that adsorption occurred on a heterogeneous surface rather than a monolayer surface. Nevertheless, experiments conducted at 35°C and 45°C exhibited a better fit to the Langmuir isotherm, suggesting that adsorption took place on a monolayer surface. This indicates that there were multiple adsorption active sites at 25°C whereas there were a limited number of adsorption active sites at 35 and 45°C experiments that could only take up a single molecule of fluoride ions at a time. This could be a result of differences in surface morphology at different temperatures {Alver, 2020 #363}. These results are in agreement with a study by Feng et al. (2020), Abdellaoui et al. (2021a), and Gao et al. (2021). Moreover, the value of 1/n was between 1 and 0 which indicates that the adsorption of fluoride by Zr^{4+}/Ag^{+} modified zeolite was favourable.

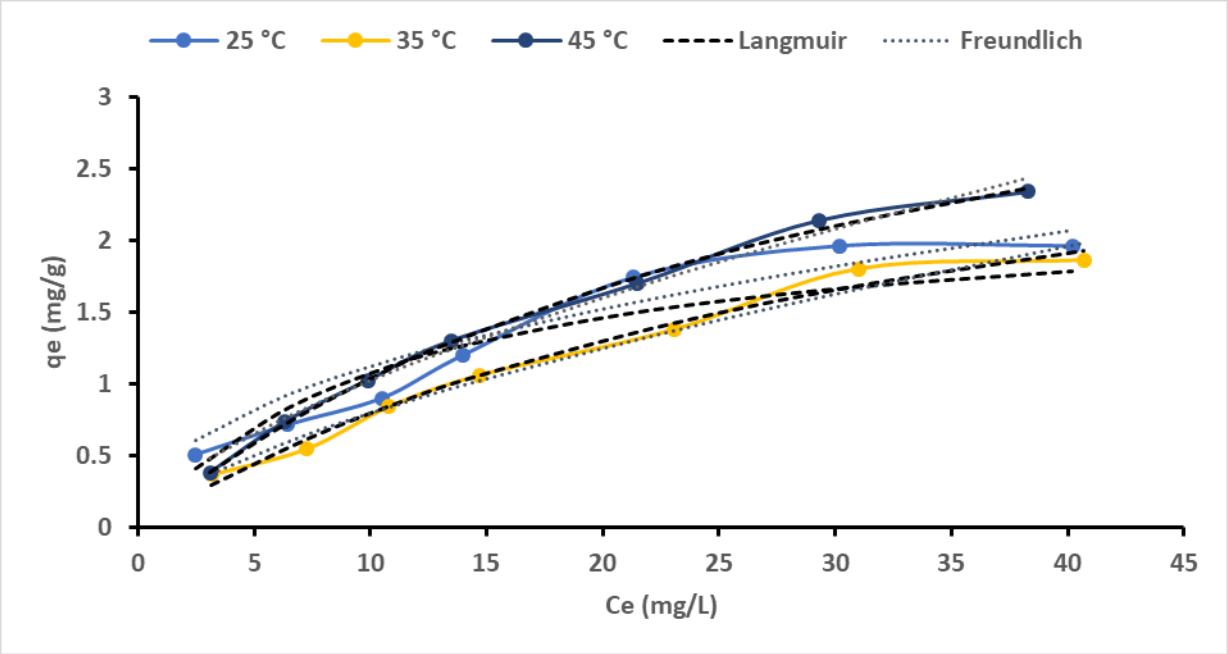

Figure 5.10: Initial concentration vs adsorption capacity at different temperatures, Langmuir and Freundlich plots for fluoride removal by Zr^{4+}/Ag^{+} modified zeolite (F)

Table 5.8: Parameters for the Langmuir and Freundlich isotherms

	Langmuir			**Freundlich**		
Experimental	Q_{max} (mg/g)	K_L (L/mg)	R^2	K_F (mg/g)/(mg/L)^n	1/n	R^2
25 ºC	2.28	0.08	0.88	0.4	0.44	0.91
35 ºC	3.58	0.02	0.98	0.17	0.64	0.97
45 ºC	4.32	0.03	0.99	0.23	0.64	0.98

5.3.3.5 Thermodynamics experiments

Thermodynamic studies were evaluated to understand the adsorption process, feasibility, and spontaneity of the sorption mechanism of fluoride. The following equations 5.6-5.8 were used to calculate the thermodynamics parameters for adsorption, standard enthalpy change (ΔH^0), Gibbs free energy change (ΔG^0), and standard entropy change (ΔS^0) (Gao et al., 2021).

$$\Delta G^{\circ} = -RT\,InK_L = \Delta H^{\circ} - T\Delta S^{\circ} \quad (5.6)$$

$$K_L = \frac{(C_0 - C_e)}{C_e \times m} = \frac{q_e}{C_e} \quad (5.7)$$

$$In\,K_L = \frac{\Delta S^{\circ}}{R} - \frac{\Delta H^{\circ}}{RT} \quad (5.8)$$

Where R represents the universal constant of 8.314 J/ (mol. K) whilst K_L is the apparent equilibrium constant. Both q_e and T are the adsorption capacity (mg/g), and absolute temperature (kelvin) respectively. C_e gives the concentration equilibrium (mg/L) while m gives the mass of the adsorbent.

Table 5.9 depicts the parameters of thermodynamics whilst Figure 5.11 shows the thermodynamic plot of the adsorption process of fluoride by Zr^{4+}/Ag^{+} modified zeolite adsorbent. It was observed that the Gibbs free energy change (ΔG^0) values were positive. This indicates that the adsorption process was non-spontaneous. The Gibbs free energy change value rises with an increase in temperature. Similar observations were made in a study by (Siyal et al., 2020). The recorded negative values for the enthalpy change (ΔH^0) suggest that the adsorption mechanism is exothermic. Exothermic reactions are conducive to both physisorption and chemisorption processes (Gabr et al., 2023). Also, the entropy change (ΔS^0) exhibited negative values which implies that the adsorption of fluoride ions was governed by decreasing randomness at the solid/liquid interface and molecules become more confined on the surface of the adsorbent. This observation aligns with findings reported in the study conducted by Hellal et al. (2023) and Amanzadeh et al. (2024).

Table 5.9: Thermodynamic parameters for fluoride adsorption by the Zr^{4+}/Ag^{+} modified zeolite

Adsorbent	**Temperature (K)**	**ΔG° (KJ/mol)**	**ΔH° (J/mol)**	**ΔS° (J/mol)**
Zr^{4+}/Ag^{+} modified zeolite	298	6.26	-39.39	-155.53
	308	10.02		
	318	9.27		

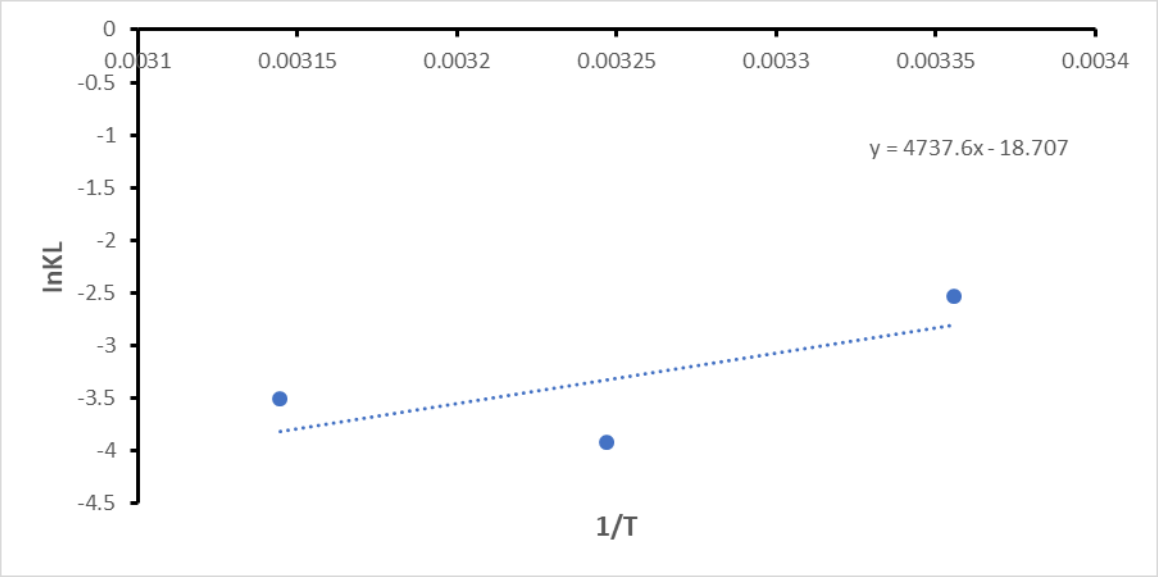

Figure 5.11: The plot of InKL against 1/T values for thermodynamics parameters

5.3.4 Regeneration studies

Regeneration and reusability of the Zr^{4+}/Ag^{+} modified zeolite adsorbent was evaluated using 0.01 M of hydrochloric acid as a regenerant to determine the practical applicability of the adsorbent. Five sequential regeneration experiments were performed, and the results are presented in Figure 5.12. It was observed that the percentage of fluoride removal slightly decreased by 1% in the fourth cycle. However, no further decrease was observed which indicates that the Zr^{4+}/Ag^{+} modified zeolite can be reused for up to five cycles which is in agreement with (Duan et al., 2017, Savari et al., 2020, Gao et al., 2021, Gupta et al., 2021). This demonstrates that the Zr^{4+}/Ag^{+} modified zeolite has potential in practical applications.

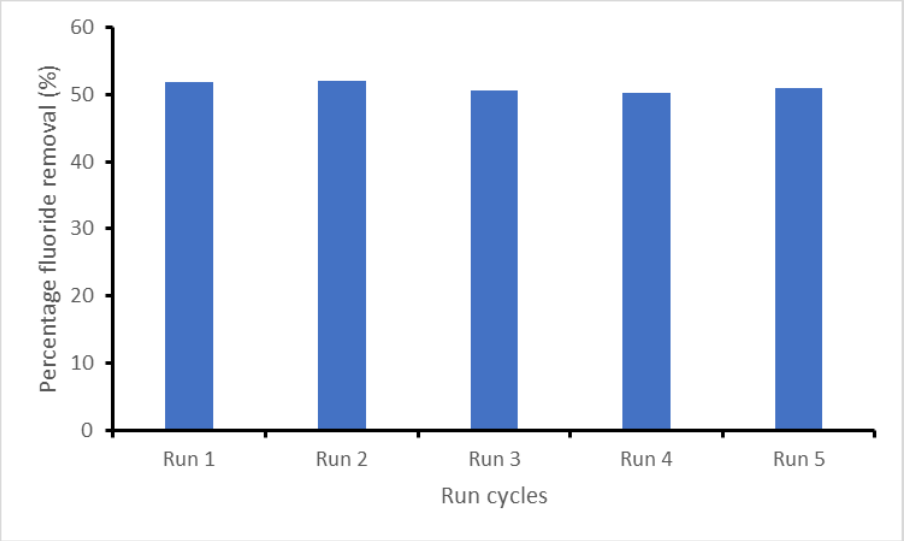

Figure 5.12: Percentage fluoride removal of cycles of regeneration for the Zr^{4+}/Ag^{+} modified zeolite using HCl as regenerant with a concentration of 0.01 (≈ Fluoride concentration=5.60, pH=6.29, agitation speed=250 rpm and agitation time=270 minutes)

5.3.5 Antimicrobial studies

5.3.5.1 Antimicrobial performance studies

The zone of inhibition results was evaluated to determine the antimicrobial potency of the Zr^{4+}/Ag^{+} modified zeolite against gram-negative *E. coli* and gram-positive *S. aureus* strains and results were presented in Figure 5.13. Both strains were subjected to adsorbent concentrations of 1, 5, 7, and 10 mg/ml wherein the *E. coli* exhibited zones of inhibition of 10, 12,13, and 15 mm whilst the *S. aureus* exhibited zones of inhibition of 10, 11.1, 11.5 and 12 mm, respectively. These results indicated that the Zr^{4+}/Ag^{+} modified zeolite has antimicrobial potency against the two investigated strains. This is due to the presence of silver metal ions in the modified zeolite which deactivate the bacterial cell activity. Several studies reported similar results due to the presence of silver ions in the zeolite material (Gupta et al., 2021, Hariram et al., 2021, Mintcheva et al., 2021, Ayinde et al., 2022).

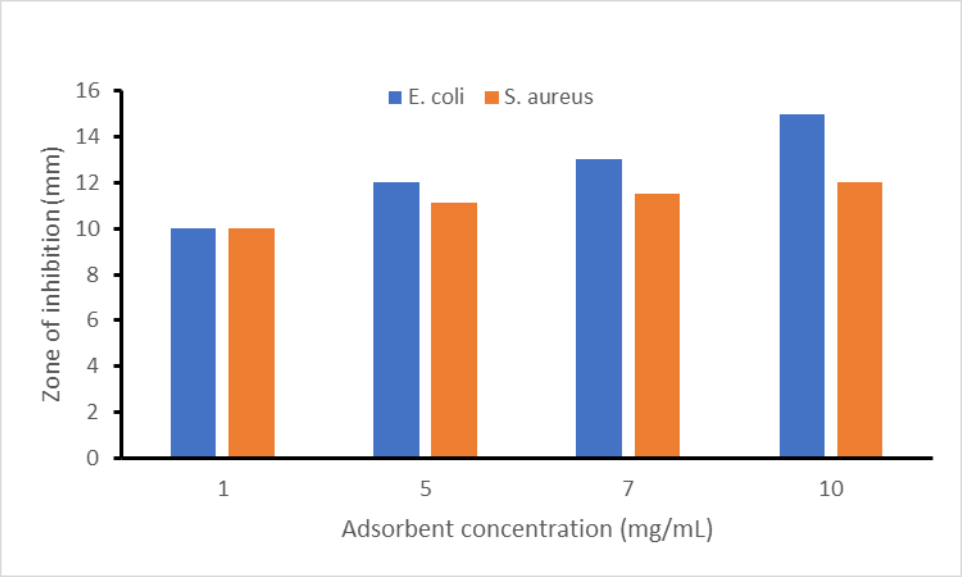

Figure 5.13: Zones of inhibition for Zr^{4+}/Ag^{+} modified zeolite against gram-negative *E. coli* and gram-positive *S. aureus* strains.

5.3.5.2 Antimicrobial mechanism

The general mechanism of antimicrobial potency involves contact of the surfactant with the bacterial cell followed by disruption of the cell activities and formation of reactive oxidative stress which leads to cell damage as shown in Figure 5.14 (Azizi et al., 2019, Rahman et al., 2019). Salim et al. (2017) described two mechanisms of microbial deactivation by metal oxides. The first mechanism involves the use of a low concentration of the surfactant which makes contact and initiates autolysis followed by denaturation of the cell structures and enzymes inside the bacteria. The second mechanism involves contact with a high concentration of surfactants which solubilize cell membrane properties into mixed micellar aggregates which then act as carboxylic groups in the bacteria. This eventually causes coagulation in the cytoplasm of the bacteria and death (Salim et al., 2017, Gupta et al., 2021, Torkian et al., 2022).

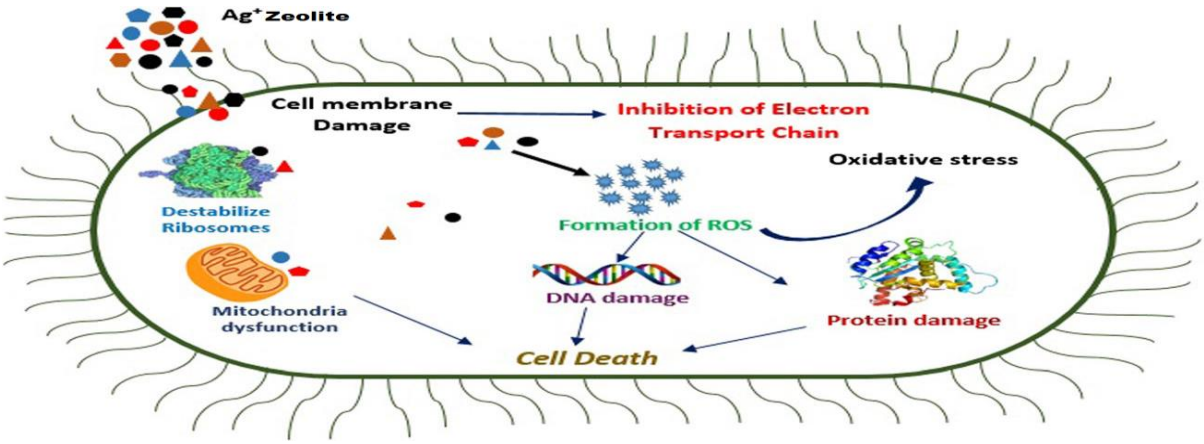

Figure 5.14: Deactivation of microbial cell functions with silver-modified zeolite (Rahman et al., 2019)

5.4. Conclusion

The aim of this study is to modify zeolite NaP and improve its fluoride sorption and antimicrobial potency. Zr^{4+}/Ag^{+} zeolite was successfully modified at optimum conditions of 0.5 and 0.3 M of zirconium and silver, respectively, 2.5 M of NaOH, 2 hours of sonication time, and hydrothermal treatment of 105 °C for 90 minutes. Maximum fluoride adsorption efficiency of 50% was achieved using a dosage 0.5g/100 mL, initial fluoride concentration of 6 mg/L, and pH of 6.2, respectively at a contact time of 270 minutes and an agitation speed of 250 rpm. Adsorption kinetics and isotherms indicated that chemisorption was the defluoridation mechanism in a monolayer surface for the modified zeolite. The thermodynamics analysis showed that the exothermic phenomenon was the dominant reaction and the adsorption process occurred non-spontaneously. Also, the Zr^{4+}/Ag^{+} modified zeolite was successfully regenerated using 0.01 M of HCl with only 1% loss of the defluoridation efficiency indicating that the modified zeolite shows practical capability. Zones of inhibition of 15 mm and 12 mm were observed against the gram-negative *E. coli* and gram-positive *S. aureus* strains respectively proving the antimicrobial potency of the Zr^{4+}/Ag^{+} modified zeolite. The obtained results in this study show that Zr^{4+}/Ag^{+} modified zeolite is a promising multifunctional adsorbent.

References

Abdellaoui, Y., Abou Oualid, H., Hsini, A., El Ibrahimi, B., Laabd, M., El Ouardi, M., Giácoman-Vallejos, G. & Gamero-Melo, P. 2021a. Synthesis of zirconium-modified merlinoite from fly ash for enhanced removal of phosphate in aqueous medium: Experimental studies supported by monte carlo/sa simulations. *Chemical Engineering Journal,* 404.

Abdellaoui, Y., El Ibrahimi, B., Abou Oualid, H., Kassab, Z., Quintal-Franco, C., Giácoman-Vallejos, G. & Gamero-Melo, P. 2021b. Iron-zirconium microwave-assisted modification of small-pore zeolite w and its alginate composites for enhanced aqueous removal of as(v) ions: Experimental and theoretical studies. *Chemical Engineering Journal,* 421.

Addison, M. J., Rivett, M. O., Phiri, O. L., Milne, N., Milne, V., Mcmahon, A. D., Macpherson, L. M. D., Bagg, J., Conway, D. I., Phiri, P., Mbalame, E., Manda, I. & Kalin, R. M. 2021. 'Hidden hot springs' as a source of groundwater fluoride and severe dental fluorosis in malawi. *Water,* 13.

Aloulou, H., Ghorbel, A., Aloulou, W., Ben Amar, R. & Khemakhem, S. 2021. Removal of fluoride ions (f(-)) from aqueous solutions using modified turkish zeolite with quaternary ammonium. *Environmental Technology,* 42**,** 1353-1365.

Amanzadeh, O., Ahmadpour, J., Shabanian, S. R. & Nikzad, M. 2024. Experimental, isotherm, kinetic and thermodynamic studies of the novel modified zeolite zsm-5 adsorbent for use in clean fuel processing. *Chemical Engineering Research and Design*.

Amin, Z., Waly, N. A. & Arshad, S. E. 2021. Biofilm inhibition and antimicrobial properties of silver-ion-exchanged zeolite a against vibrio spp marine pathogens. *Applied Sciences,* 11.

Ayinde, W. B., Gitari, M. W., Smith, J. A. & Samie, A. 2022. Sorption of fluoride and bacterial disinfection property of biosynthesized nanofibrous cellulose decorated ag-mgo-nanohydroxyapatite composite for household water treatment. *Polymers (Basel),* 14.

Azizi, L. M., Ehsani, A., Divband, B. & Alizadeh, S. M. 2019. Antimicrobial activity of titanium dioxide and zinc oxide nanoparticles supported in 4a zeolite and evaluation the morphological characteristic. *Scientific Reports,* 9**,** 17439.

Barbov, B., Zaharieva, K., Karakashkova, P., Penchev, H., Tsvetanova, L. & Dimova, S. 2023. Preparation and catalytic study of mn-nax, cu-nax and ag-/agnps-nax zeolites. *European Congress Of Psychology 2023.*

Cui, J., Yeasmin, R., Shao, Y., Zhang, H., Zhang, H. & Zhu, J. 2019a. Fabrication of ag+, cu2+, and zn2+ ternary ion-exchanged zeolite as an antimicrobial agent in powder coating. *Industrial & Engineering Chemistry Research,* 59**,** 751-762.

Cui, Q., Wang, S., Wei, Q., Mu, L., Yu, G., Zhang, T. & Zhou, Y. 2019b. Synthesis and characterization of zr incorporated small crystal size y zeolite supported niw catalysts for hydrocracking of vacuum gas oil. *Fuel,* 237**,** 597-605.

Duan, Z., Li, G., Zhou, L., Gui, H., Tan, W., Jegatheesan, V., Li, S., Wang, H. & Yang, M. 2017. Preparation of zeolite-based zirconium functional materials (ze-zr) with the aid of response surface methodology. *Process Safety and Environmental Protection,* 112**,** 353-361.

Edokpayi, J. N., Rogawski, E. T., Kahler, D. M., Hill, C. L., Reynolds, C., Nyathi, E., Smith, J. A., Odiyo, J. O., Samie, A., Bessong, P. & Dillingham, R. 2018. Challenges to sustainable safe drinking water: A case study of water quality and use across seasons in rural communities in limpopo province, south africa. *Water (Basel),* 10.

Feng, J., Jiang, L., Yuan, B., Zhang, L. & Zhang, A. 2020. Enhanced removal of aqueous phosphorus by zr–fe-, mn–fe-, and mn–zr–fe-modified natural zeolites: Comparison studies and adsorption mechanism. *Environmental Engineering Science,* 37**,** 572-584.

Gabr, S. S., Mubarak, M. F., Keshawy, M., El Sayed, I. E. T. & Abdel Moghny, T. 2023. Linear and nonlinear regression analysis of phenol and p-nitrophenol adsorption on a hybrid nanocarbon of actf: Kinetics, isotherm, and thermodynamic modeling. *Applied Water Science,* 13.

Gao, Y., Li, M., Ru, Y. & Fu, J. 2021. Fluoride removal from water by using micron zirconia/zeolite molecular sieve: Characterization and mechanism. *Groundwater for Sustainable Development,* 13.

Gitari, W. M., Obijole, O. A. & Mudzielwana, R. 2023. Synthesis of porous hydroxysodalite from aluminosilicate rich clay soils application towards fluoride and pathogen removal.

Gupta, A. R., Ranawat, B., Singh, A., Yadav, A. & Sharma, S. 2021. Zirconium-silver nano organo-bimetallic network for scavenging hazardous ions from water and its antibacterial potentiality: An environment-friendly approach. *Journal of Environmental Chemical Engineering,* 9.

Hariram, M., Ganesan, V., Muthuramkumar, S. & Vivekanandhan, S. 2021. Functionalization of kaolin clay with silver nanoparticles by murraya koenigii fruit extract-mediated bioreduction process for antimicrobial applications. *Journal of the Australian Ceramic Society,* 57**,** 505-513.

He, J., Yang, Y., Wu, Z., Xie, C., Zhang, K., Kong, L. & Liu, J. 2020. Review of fluoride removal from water environment by adsorption. *Journal of Environmental Chemical Engineering,* 8.

Hellal, M. S., Rashad, A. M., Kadimpati, K. K., Attia, S. K. & Fawzy, M. E. 2023. Adsorption characteristics of nickel (ii) from aqueous solutions by zeolite scony mobile-5 (zsm-5) incorporated in sodium alginate beads. *Scientific Reports,* 13**,** 19601.

Inglezakis, V. J., Kudarova, A., Guney, A., Kinayat, N. & Tauanov, Z. 2023. Efficient mercury removal from water by using modified natural zeolites and comparison to commercial adsorbents. *Sustainable Chemistry and Pharmacy,* 32.

Jasper, E. E., Ajibola, V. O. & Onwuka, J. C. 2020. Nonlinear regression analysis of the sorption of crystal violet and methylene blue from aqueous solutions onto an agro-waste derived activated carbon. *Applied Water Science,* 10.

Jia, C., Fan, Y., Jiang, R., Su, P., Liu, S., Zhang, X. & Wang, J. 2022. Preparation of la(iii), fe(iii) modified zeolite molecular sieves for the removal of fluorine from water. *Water,* 14.

Khabo-Mmekoa, C. M., Genthe, B. & Momba, M. N. B. 2022. Enteric pathogens risk factors associated with household drinking water: A case study in ugu district kwa-zulu natal province, south africa. *International Journal of Environmental Research and Public Health,* 19.

Krishnani, K. K., Zhang, Y., Xiong, L., Yan, Y., Boopathy, R. & Mulchandani, A. 2012. Bactericidal and ammonia removal activity of silver ion-exchanged zeolite. *Bioresource Technology,* 117**,** 86-91.

Lin, J., Jiang, B. & Zhan, Y. 2018. Effect of pre-treatment of bentonite with sodium and calcium ions on phosphate adsorption onto zirconium-modified bentonite. *Journal of Environmental Management,* 217**,** 183-195.

Liu, J., Yang, S., Luo, M. J., Chen, T., Ma, X. J., Tao, N., Zhao, X. & Wang, D. H. 2019. Association between dietary patterns and fluorosis in guizhou, china. *Frontiers in Nutrition,* 6**,** 189.

Malek, N., Azid, N. A., Hadi, A. A., Ishak, S. N., Asraf, M. H. & Awaluddin, M. Z. A. 2018. Antibacterial activity of copper exchanged zeolite y synthesized from rice husk ash.

Márquez, C. O., García, V. J., Guaypatin, J. R., Fernández-Martínez, F. & Ríos, A. C. 2021. Cationic and anionic dye adsorption on a natural clayey composite. *Applied Sciences,* 11.

Marzi, M., Kazemian, H. & Bradshaw, C. 2023. Study on phosphate removal from aqueous solutions using magnesium-ammonium- and zirconium-modified zeolites: Equilibrium, kinetic, and fixed-bed column study. *Environ Monit Assess,* 195**,** 826.

Mei, L., Qiao, H., Ke, F., Peng, C., Hou, R., Wan, X. & Cai, H. 2020. One-step synthesis of zirconium dioxide-biochar derived from camellia oleifera seed shell with enhanced removal capacity for fluoride from water. *Applied Surface Science,* 509.

Menya, D., Maina, S. K., Kibosia, C., Kigen, N., Oduor, M., Some, F., Chumba, D., Ayuo, P., Middleton, D. R. S., Osano, O., Abedi-Ardekani, B., Schuz, J. & Mccormack, V. A. 2019. Dental fluorosis and oral health in the african esophageal cancer corridor: Findings from the kenya esccape case-control study and a pan-african perspective. *International Journal of Cancer,* 145**,** 99-109.

Mintcheva, N., Panayotova, M., Gicheva, G., Gemishev, O. & Tyuliev, G. 2021. Effect of exchangeable ions in natural and modified zeolites on ag content, ag nanoparticle formation and their antibacterial activity. *Materials (Basel),* 14.

Mukherjee, S., Barman, S. & Halder, G. 2018. Fluoride uptake by zeolite naa synthesized from rice husk: Isotherm, kinetics, thermodynamics and cost estimation. *Groundwater for Sustainable Development,* 7**,** 39-47.

Naskar, M. K. 2020. Preparation of colloidal hydrated alumina modified naa zeolite derived from rice husk ash for effective removal of fluoride ions from water medium. *Journal of Asian Ceramic Societies,* 8**,** 437-447.

Odiyo, J. O. & Makungo, R. 2018. Chemical and microbial quality of groundwater in siloam village, implications to human health and sources of contamination. *International Journal of Environmental Research and Public Health,* 15.

Ojumu, T. V., Du Plessis, P. W. & Petrik, L. F. 2016. Synthesis of zeolite a from coal fly ash using ultrasonic treatment–a replacement for fusion step. *Ultrasonics sonochemistry,* 31**,** 342-349.

Raghav, S. & Kumar, D. 2018. Adsorption equilibrium, kinetics, and thermodynamic studies of fluoride adsorbed by tetrametallic oxide adsorbent. *Journal of Chemical & Engineering Data,* 63**,** 1682-1697.

Rahman, S., Rahman, L., Khalil, A. T., Ali, N., Zia, D., Ali, M. & Shinwari, Z. K. 2019. Endophyte-mediated synthesis of silver nanoparticles and their biological applications. *Appl Microbiol Biotechnol,* 103**,** 2551-2569.

Revelo-Mejia, I. A., Hardisson, A., Rubio, C., Gutierrez, A. J. & Paz, S. 2021. Dental fluorosis: The risk of misdiagnosis-a review. *Biological Trace Element Research,* 199**,** 1762-1770.

Salehi, S., Alijani, S. & Anbia, M. 2020. Enhanced adsorption properties of zirconium modified chitosan-zeolite nanocomposites for vanadium ion removal. *International Journal of Biological Macromolecules,* 164**,** 105-120.

Salim, M. M., Ahmad, N. & Malek, N. N. 2017. Review of modified zeolites by surfactant and silver as antibacterial agents. 1-20.

Sánchez, M. J., Mauricio, J. E., Paredes, A. R., Gamero, P. & Cortés, D. 2017. Antimicrobial properties of zsm-5 type zeolite functionalized with silver. *Materials Letters,* 191**,** 65-68.

Savari, A., Hashemi, S., Arfaeinia, H., Dobaradaran, S., Foroutan, R., Mahvi, A. H., Fouladvand, M., Sorial, G. A., Farjadfard, S. & Ramavandi, B. 2020. Physicochemical characteristics and mechanism of fluoride removal using powdered zeolite-zirconium in modes of pulsed& continuous sonication and stirring. *Advanced Powder Technology,* 31**,** 3521-3532.

Siyal, A. A., Shamsuddin, R., Low, A. & Hidayat, A. 2020. Adsorption kinetics, isotherms, and thermodynamics of removal of anionic surfactant from aqueous solution using fly ash. *Water, Air, & Soil Pollution,* 231.

Torkian, N., Bahrami, A., Hosseini-Abari, A., Momeni, M. M., Abdolkarimi-Mahabadi, M., Bayat, A., Hajipour, P., Amini Rourani, H., Abbasi, M. S., Torkian, S., Wen, Y., Yazdan Mehr, M. & Hojjati-Najafabadi, A. 2022. Synthesis and characterization of ag-ion-exchanged zeolite/tio(2) nanocomposites for antibacterial applications and photocatalytic degradation of antibiotics. *Environmental Research,* 207**,** 112157.

Velazquez-Peña, G. C., Olguín-Gutiérrez, M. T., Solache-Ríos, M. J. & Fall, C. 2017. Significance of fezr-modified natural zeolite networks on fluoride removal. *Journal of Fluorine Chemistry,* 202**,** 41-53.

Who 2011. Guidelines for drinking-water quality. *WHO chronicle,* 4**,** 104-108.

Yang, B., Jia, C., Sun, G., Quan, B., Zhang, C., Huo, Q. & Su, P. 2022. Enhancing the adsorption function of f- by iron and zirconium doped zeolite: Characterization and parameter optimization. *Environmental Engineering Research,* 28**,** 220010-0.

Yetis, A. D., Yesilnacar, M. I. & Atas, M. 2021. A machine learning approach to dental fluorosis classification. *Arabian Journal of Geosciences,* 14.

Yu, S., Yan, J., Lin, W., Zhang, J. & Long, J. 2021. Characterization and cracking performance of zirconium-modified y zeolite. *Catalysis Communications,* 148.

Zendehdel, R., Goli, F. & Hajibabaei, M. 2020. Comparing the microbial inhibition of nanofibres with multi-metal ion exchanged nano-zeolite y in air sampling. *Journal of Applied Microbiology,* 128**,** 202-208.

Chapter 6: Conclusions and recommendations

6.1 Conclusions

This study was designed with the main aim of synthesizing Zr4+/Ag+ modified zeolites from bentonite clay using ultrasonication assisted method for application in simultaneous fluoride and pathogen removal in water.

The specific objectives of this study were:

- To optimize conditions for the synthesis of zeolite from bentonite clay and further determine its physiochemical characteristics.
- To evaluate the effectiveness of the synthesized zeolite in fluoride and pathogens removal.
- To modify zeolite using Zr4+/Ag+ metal oxides and further evaluate its efficiency in fluoride and pathogen removal.
- To evaluate the regeneration potential of the modified Zr^{4+}/Ag^{+} zeolite.

The dissertation fully described the successful synthesis of Zr^{4+}/Ag^{+} modified zeolite from calcined bentonite clay via the ultrasonication-assisted hydrothermal route. Also, the obtained material was used to carry out defluoridation studies and antimicrobial tests along with the regeneration studies of the adsorbent. The following major conclusions were made:

- The calcined bentonite clay was successfully obtained at an optimal calcination temperature of 800 °C in 1 hour of calcination time.
- The dissolution of silica and aluminum was carried out at an ultrasonication time of 2 hours in a 2.5 M solution concentration of NaOH.
- The dissolved silica and aluminum extracts were hydrothermally treated at varying temperatures of 70 to 140 °C and time of 1.5 to 6 hours wherein the XRD results revealed that the crystallinity of the obtained synthesized material increased with the increase of both hydrothermal temperature and hydrothermal time.
- Furthermore, the XRD results indicated that at lower hydrothermal times and temperatures, zeolite NaP phases were dominant whilst, at higher hydrothermal times and temperatures, hydroxy sodalite phases were observed.
- Preliminary defluoridation studies showed that the adsorbent synthesized at an optimal hydrothermal temperature of 105 °C and time of 90 minutes containing

zeolite NaP phases exhibited a maximum fluoride adsorption capacity of 0.19 mg/g hence it was selected for subsequent experiments.

- The selected synthesized zeolite NaP adsorbent was then used in batch fluoride removal experiments which reported a maximum fluoride adsorption capacity of 0.32 mg/g at optimal conditions of 0.5g/100 mL for dosage,6 mg/L for initial fluoride and pH of 2 at an agitation time of 60 minutes and speed of 250 rpm.
- The kinetics and isotherm models revealed that the fluoride sorption mechanism occurred through chemisorption in a monolayered surface of the adsorbent and the zeolite NaP exhibited minimal regeneration potential.
- Antimicrobial tests were performed through the well-assay diffusion method and reported minimal antimicrobial potency against the gram-negative *E. coli* and gram-positive *S. aureus* strains.
- To improve the defluoridation, antimicrobial potency, and regeneration potential of the synthesized zeolite, zirconium and silver metal oxides were incorporated in the zeolite NaP matrices.
- The zeolite was modified by using zirconium and silver metal oxides through the ultrasonication-assisted hydrothermal method and XRF and EDS results showed the presence of these metal oxides in the adsorbent's matrices.
- The obtained modified was subjected to batch fluoride adsorption experiments and reported a maximum defluoridation efficiency of 50% achieved using dosage, initial fluoride, and initial pH of 0.5g/100ml, 6 mg/L, and 6.2 respectively at a contact time of 270 minutes and an agitation speed of 250 rpm.
- The isotherm and kinetic models showed that the adsorption occurred on a monolayered surface through a chemisorption process.
- The Zr^{4+}/Ag^{+} modified zeolite showed efficient regeneration potential after showing a slight decrease in efficiency by 1% using 0.01 M of hydrochloric acid as a regenerant in five regeneration cycles.
- In addition, antimicrobial studies showed that the Zr^{4+}/Ag^{+} modified zeolite exhibited zones of inhibition of 15 mm and 12 mm against the gram-negative *E. coli* and gram-positive *S. aureus* strains respectively proving that the adsorbent has the potential for removal of pathogens in the water.

6.2 Recommendations

- Investigation of the stability of the adsorbent.
- Further studies on modification of the zeolite are recommended to improve the properties and efficiency of fluoride and pathogens in water.
- Application of the adsorbent in a column study is also recommended.
- Real-time application in field groundwater for practicality of the adsorbent should be considered.
- The synthesized Zr^{4+}/Ag^{+} modified zeolite should be modeled and fabricated for use at the household level.